Action Mechanism and Structural Studies on the Lipopeptide Antibiotic Daptomycin

by

David Beriashvili

A thesis
presented to the University of Waterloo
in fulfillment of the
thesis requirement for the degree of
Master of Science
in
Chemistry

Waterloo, Ontario, Canada, 2019

AUTHOR'S DECLARATION

I hereby declare that I am the sole author of this thesis. This is a true copy of the thesis, including any required final revisions, as accepted by my examiners.

I understand that my thesis may be made electronically available to the public.

Abstract

Daptomycin (dap) is calcium-dependent lipopeptide antibiotic that is used clinically to treat systemic infections caused by Gram-positive pathogens. It is thought that dap brings about its antimicrobial effect by binding cytoplasmic bacterial membranes, via a calcium meditated interaction with the lipid phosphatidylglycerol (PG), and subsequent oligomerization. There is consensus that dap oligomerization is required for bactericidal activity, but the exact mechanism by which dap oligomers cause cell death is contested. Significant experimental evidence suggests that dap oligomers form cation-selective pores that cause membrane depolarization halting metabolite transport and resulting in cell death. Other proposed action modes include dap-induced non-selective membrane permeabilization, lipid extraction, and dislodgement of membrane-associated biosynthetic enzymes.

The effect of phospholipids acyl tails on dap cation-selective pore formation has not been studied. In this thesis, fluorescence spectroscopy experiments on large unilamellar vesicles were used to study the effects of phospholipid acyl tails on dap cation-selective pore formation in a systematic fashion. It was observed that dap could permeabilize membranes composed of equal parts PC and PG with myristoyl acyl tails, but not those containing palmitoyl and oleoyl acyl tails. Oleoyl lipid acyl tails were found to render membranes insusceptible to dap pore formation regardless of the headgroup they were ligated to and at low concentrations in the membrane (10 mol%). Further studies showed that inhibition of dap pore formation by phospholipid acyl tails is correlated with increased acyl tail length rather than lipid unsaturation. Oleoyl acyl tails were found to restrict dap pore formation by disrupting the final stage of oligomer assembly. Attempts to permeabilize oleoyl lipid acyl tail containing membranes by branching and increasing the length of dap's acyl tail moiety were unsuccessful. Overall, these findings suggest that lipid acyls affect dap's action mode and should be a major consideration when designing model membrane systems for future dap action mode studies.

Determining dap's membrane-bound structure at an atomic level would help resolve the debate in literature regarding its action mode and establish dap's structure-activity relationship. Previous attempts to determine the membrane-bound structure by solution-state nuclear magnetic resonance have failed because no suitable membrane mimetic existed. The latter portion of this thesis investigated the suitability of novel styrene-maleic acid (SMA) co-polymers to create membrane nanodisc suitable for determining dap's membrane-bound structure. Through dynamic light scattering, fluorescence spectroscopy, and solution-state NMR it was found that this polymer can form membrane nanodiscs,

with a diameter small enough for structural studies by solution-state NMR, in the presence of PG (50 mol%) and 3 mM calcium. Further, these PG containing nanodiscs allow for partially dap oligomerization, and are stable on the timescale of NMR experiments. Overall, while the SMA polymer used in this study did not allow for full dap oligomerization, the partial structure of membrane-bound dap could be obtained with this system by solution-state NMR.

Acknowledgements

I would like to thank my supervisor Prof. Dr. Michael Palmer for his patience and guidance over the last several years. His open-door policy has allowed for many interesting discussions about both science and the world in general. Most importantly, I thank him for giving me the opportunity work on a large variety of projects, which consequently expanded my scientific horizons.

I would also like to thank Prof. Dr. Thorsten Dieckmann and Prof. Dr. Scott Taylor for agreeing to advise me during this degree. I would like to thank Prof. Dr. Dieckmann for his support, advice, and introduction to the world of biomolecular nuclear magnetic resonance (NMR). I am also grateful to Prof. Dr. Taylor for his advice, support, and for treating myself as a member of his group. Additionally, I would like to extend my gratitude to Prof. Dr. Michael Overduin, currently at the University of Alberta, for being a gracious collaborator. I thank you and your group for the advice and polymer samples. Further, I would like to thank Dr. Dara Gilbert for advising to pursue an education and career in the field of biochemistry.

A debt of gratitude is owed to all my friends in the department of chemistry for making the last two years enjoyable – thank you: Eric Brefo-Mensah, Volition La, Michael Noden, Jeffery Palumbo, Kyle Piccolo, Klaudia Steckel, Jacob Soley, Norman Spencer, Dr. Carol Tanner, and Dr. Robert Taylor.

Lastly, I would like to thank my parents for their love, support, and advice; without you both this path would have been infinitely harder.

Dedication

To my parents.

Table of Contents

List of Figures

List of Tables

List of Abbreviations

CCCP	Carbonyl cyanide m-chlorophenyl hydrazone
CD	Circular dichroism
CL	Cardiolipin
Dap	Daptomycin
DLS	Dynamic light scattering
DMPC	1,2-dimyristoyl-sn-glycero-3-phosphocholine
DMPC Δ9-cis	1,2-dimyristoleoyl-sn-glycero-3-phosphocholine
DMPG	1,2-Dimyristoyl-sn-glycero-3-phosphoglycerol
DOPC	1,2-dioleoyl-sn-glycero-3-phosphocholine
DOPG	1,2-dioleoyl-sn-glycero-3-phospho-(1'-rac-glycerol)
DPDPC	1,2-dipentadecanoyl-sn-glycero-3-phosphocholine
DPH	1,6-Diphenyl-1,3,5-hexatriene
DPHC	1,2-diheptanoyl-sn-glycero-3-phosphocholine
FRET	Fluorescence resonance energy transfer
ITC	Isothermal calorimetry
LD_{50}	Lethal dose 50
L-form	cell wall-deficient bacteria
LUVs	Large unilamellar vesicles
Lysyl-PG	Lysyl Phosphatidylglycerol
MIC	Minimum inhibitory cocnentration
MLV	Multilamellar vesicle
MS	Mass spectrometry
NBD	7-nitro-2,1,3-benzoxadiazol
NBD-PE	1,2-dimyristoyl-sn-glycero-3-phosphoethanolamine-N-(7-nitro-2-1,3-benzoxadiazol-4-yl)
NMR	Nuclear magnetic resonance
PC	Phosphatidylcholine
PG	Phosphatidylglycerol
POPC	1-palmitoyl-2-oleoyl-sn-glycero-3-phosphocholine
POPE	1-palmitoyl-2-oleoyl-sn-glycero-3-phosphoethanolamine
POPG	1-palmitoyl-2-oleoyl-sn-glycero-3-phospho-(1'-rac-glycerol)

Pyr-PC	1-palmitoyl-2-pyrenedecanoyl phosphatidylcholine
SAR	Structure-activity relationship
SMA	Stryrene-maleic acid
T_m	Phase transition temperature
TMCL	1',3'-bis[1,2-dimyristoyl-sn-glycero-3-phospho]-glycerol
TOCL	1',3'-bis[1,2-dioleoyl-sn-glycero-3-phospho]-glycerol

Chapter 1

Introduction

The goal of this work is to further investigate the action mode of the lipopeptide antibiotic daptomycin (dap). Before discussing, in depth, the specific questions investigated, it is important to briefly discuss previous research regarding dap's action mode.

1.1 Brief History of Daptomycin

Dap is clinically used, as a drug of last resort, to treat infections caused by Gram-positive pathogens.[1] It is a calcium-dependent lipopeptide antibiotic that brings about its bactericidal effect by targeting the cytoplasmic membranes of Gram-positive pathogens such as *Staphylococcus aureus* and *Enterococcus faecalis*.[1] Dap is a part of the A21978C family of lipopeptide antibiotics that was discovered by researchers from Eli Lilly in the early 1980's. The A21978C family is biosynthesized by the soil bacterium *Streptomyces roseosporus* through the action of non-ribosomal peptide synthetases.[2]

1.2 Structure of Daptomycin and the A21978C Family

Each member of the A21978C family consists of a conserved 13 amino acid peptide moiety; the variation between members only pertains to the variable fatty acid tail attached at the N-terminus.[2] The conserved peptide portion consists of a ten amino acid macrocycle closed by an ester bond and a tri-amino acid exocyclic portion that bears the fatty acid moiety.[2] It is noteworthy that the conserved peptide moiety contains 6 non-proteogenic amino acids - 3 D-amino acids, which in Figure 1 are highlighted in blue, 3 L-amino acids which are highlighted in red, and two intrinsically fluorescent amino acids: trptophan-1 and kynurenine-13 (see Figure.1-1, Panel B). In solution, at physiological pH, the molecule has a net charge of -3 (see Figure. 1-1, Panel C).[2]

In its native environment, *Streptomyces roseosporus* produces 3 variants of the A21978C family (see Figure. 1-1 , Panel A).[2] Debono *et al.*(1988) found that while all 3 natural A21978C variants were potent antimicrobials they were also quite toxic. The remarkably low lethal dose 50 (LD_{50}) values exhibited by these compounds were a major obstacle that had to be overcome in order to make the A21978C family viable for clinical use. Upon further investigation, Debono *et al.* (1988) found that the antimicrobial activity and toxicity of the A21978C family could be controlled by altering the length and branching of the fatty acid moiety; derivatives with short acyl tails and no branching had slightly lower minimum inhibitory concentrations (MIC), but toxicity was more strongly reduced; the most favorable ratio of toxicity to antimicrobial activity was found with a decanoyl fatty acid tail. The combination of the conserved peptide moiety attached to a decanoyl fatty acid acyl tail was named daptomycin.

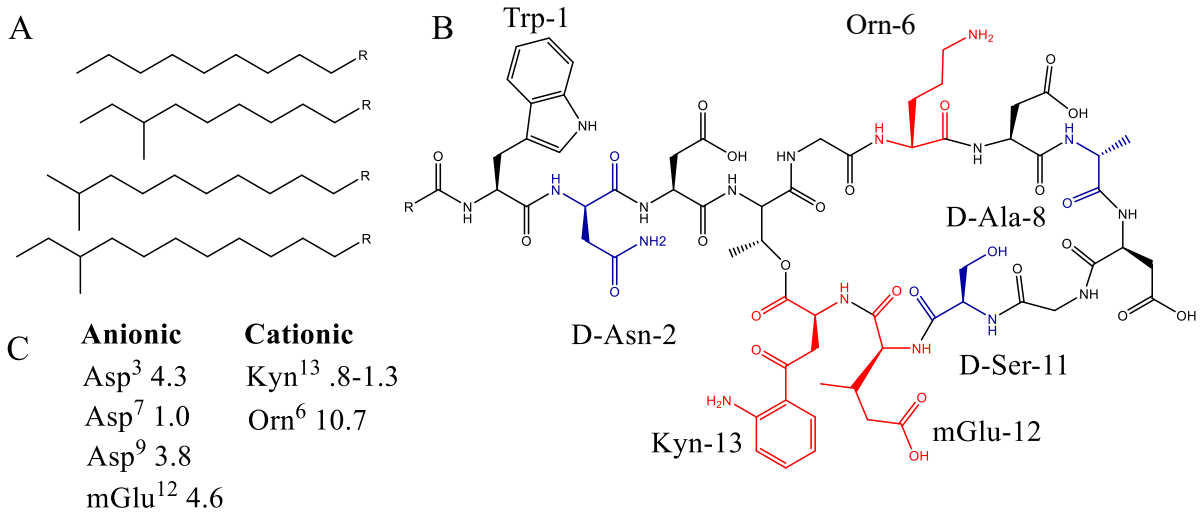

Figure 1-1. Structure of daptomycin. Panel A shows the decanoyl fatty acid moiety along the three most common analogues produced naturally by *Streptomyces roseosporus*. Panel B shows the peptide moiety shared between A21978C family members. Panel C details the pKa of the peptide moieties various ionizable side chains.

1.3 Action Mechanism of Daptomycin

Despite being discovered nearly 40 years ago and seeing extensive clinical use since 2003, the mechanism by which dap brings about its antimicrobial effect is still subject to much debate.[3–5] There is consensus that dap's antimicrobial effect is brought about by membrane-embedded oligomers that form by way of dap's calcium-mediated binding to the cytoplasmic membrane phospholipid

phosphatidylglycerol[1] (PG).[6–9] The debate surrounding dap's action mode specifically revolves around firmly establishing how exactly dap oligomers bring about microbial death.

Before discussing dap's proposed action modes in detail, a brief description of a Gram-positive bacteria's cell envelope is required. The cell envelope of Gram-positive bacteria comprises a cell wall and the cytoplasmic membrane. The cell wall consists of thick peptidoglycan layer and encapsulates the inner cytoplasmic membrane (see Figure.1-2).[10] The cytoplasmic membranes of Gram-positive bacteria, that are susceptible to daptomycin, are composed of phospholipids with phosphatidylglycerol (PG) being quite prevalent.[11,12] The acyl tails of the phospholipids are quite varied with the most abundant acyl tail being 14 carbons long with a single methylation at the 3 third position from the terminal carbon (See Appendix A Figure 5 for a detailed chart of bacterial acyl tail composition).[13]

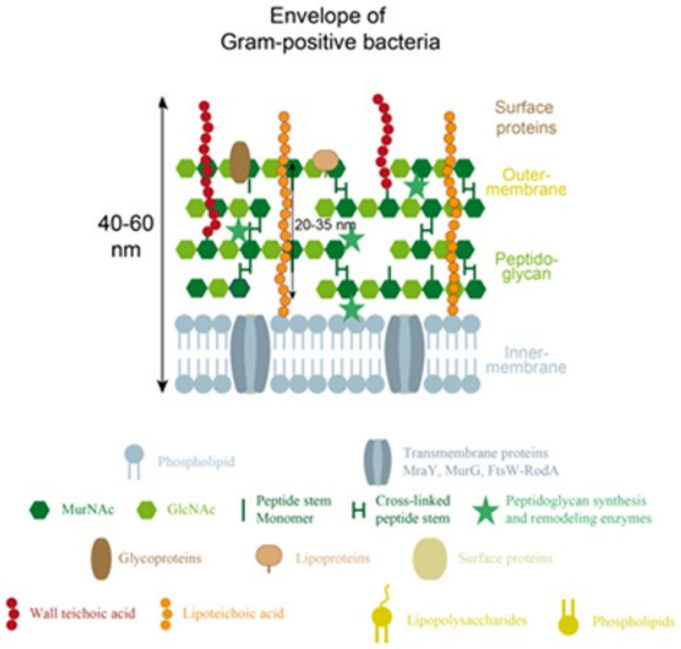

Figure 1-2. Cellular envelopes of Gram-positive and negative bacteria. This Figure shows the difference between the cellular envelopes of Gram-positive and Gram-negative bacteria.[14]

1.3.1 Daptomycin's binding to the cytoplasmic membrane

Before interacting with the cytoplasmic membrane of a Gram-positive bacterium dap must traverse the bacterium's thick murein layer. Taylor *et al.* (2017) found that dap had a lower minimum inhibitory

[1] The structures of all lipids and dap derivatives can be found in Appendix D.

concentration (.075 μg/ml vs .5 μg/ml) on Gram-positive bacterial cells lacking a cell wall (L-forms) than against intact cells of the same species.[10] These data suggest that while the cell wall does sequester some dap molecules it is not a major obstacle in dap's journey to the cytoplasmic membrane.

Once dap has reached the cytoplasmic membrane it interacts with the anionic phospholipid PG. Dap's preference for PG has been demonstrated by a variety of experiments, but the most thorough studies were conducted by Jung *et al.* (2004), who utilized circular dichroism to show that on large unilamellar vesicles (LUVs) dap's secondary structure undergoes conformational changes, indicative of membrane-binding, only in the presence of PG and physiological concentrations of calcium (≈ 1.25 mM).[6] The requirement for PG was rather surprising, considering that at physiological pH both dap and PG are anionic. Jung *et al.* (2004) rationalized the interaction by proposing that calcium mediates it by acting as an electrostatic shield. Muraih *et al.* (2011) further investigated the role of PG in dap's interaction with bacterial membranes by utilized fluorescence spectroscopy.[9] Muraih *et al.* (2011) found that dap could interact with membranes lacking PG, but at calcium concentrations 2 orders of magnitude greater than those required to observe binding of dap to PG containing membranes.[9]

1.3.2 Daptomycin brings about bacterial death by permeabilizing membranes in a cation-selective fashion

It is generally accepted that dap brings about bacterial death via cation-selective pore formation. The idea was first suggested by Alborn *et al.* (1991), who showed that *Staphylococcus aureus* cells experience membrane depolarization upon treatment with calcium and dap (recently dap-induced membrane depolarization was observed on *Bacillus subtilis* cells suggesting that cation-pore formation is likely a general action mechanism).[15,16] Several years later Silverman *et al*. (2003), confirmed this mode of action by showing that *Staphylococcus aureus* cells began to release intracellular potassium upon addition of calcium and daptomycin.[7] *In vitro* on LUVs, Zhang *et al* (2014) found that dap's pores are selective for monovalent-cations and some divalent-cations (organic cations were also transported by dap's pores, but not efficiently).[17] Most recently, the existence of dap cation-selective pores was proven empirically by Seydlová *et al.* (2018); through conductance measurements on planar lipid bilayers they observed that dap gives rise to discrete conductance events indicative of cation-selective pores.[16] They further established that dap's propensity to form said cation-selective pores and their rate of transport correlates with membrane potential.

It was Muraih *et al.* (2011) and Muraih *et al.* (2012) who made the very important discovery that dap oligomerizes on membranes. Through fluorescence resonance energy transfer (FRET) studies

conducted on LUVs, with fluorescently labelled dap derivatives, they determined that once monomeric dap binds to the membrane it forms oligomers of approximately 8 dap molecules.[9,18] Dap oligomerization was observed only on membranes containing PG.[9] Later, Zhang *et al.* in 2013 found oligomer formation to be a requirement for bactericidal activity.[19]

At the time of their studies, Muraih *et al.* (2012) speculated that the dap octamer might consist of two dap tetramers conjoining across opposing membrane leaflets. The assumption was proven true by Zhang *et al.* (2014).[20] Whilst investigating the inhibitory effects of cardiolipin on dap oligomer cation-selective pore formation, Zhang *et al.* (2014) found that dap's ability to permeabilize CL containing LUVs correlated with oligomer size.[20] They observed that on CL containing LUVs, daptomycin was restricted to the outer leaflet; oligomers still formed but consisted of 4 subunits.[20] In contrast, LUVs readily permeabilized by dap, such as those comprised of 1:1 DMPC: DMPG, had equal distribution of dap between membrane leaflets and oligomers containing 8 dap molecules. The increased subunit stoichiometry on susceptible LUVs suggested that the dap octamer is formed via a trans-membrane interaction of two tetrameric oligomers located on opposing membrane leaflets. Additionally, these data suggest that the octamer constitutes the functional cation-selective pore that is essential for antimicrobial activity.[20]

The role played by calcium in dap's binding to PG and subsequent oligomerization was investigated in depth by Taylor *et al.* (2016) and Zhang *et al*. (2016).[8,21] Taylor *et al.* (2016) utilized isothermal calorimetry (ITC) to show that formation of the membrane-embedded octamer requires each dap molecule to bind two calcium ions. The ITC results suggest that the two cations are bound in a sequential fashion by two different binding sites on dap.[8] The work with fluorescently labeled dap analogs and derivatives by Taylor *et al.* (2016) and Zhang *et al*. (2016) suggests that the first calcium binding event results in the formation of a membrane-embedded dap tetramer, and that the second calcium binding event induces the tetramer's deep insertion into the membrane, translocation of some tetramers to the inner leaflet, and subsequently octamer formation.[8,21]

1.3.3 Other proposed action modes

This section discusses alternative dap action modes, namely non-selective membrane permeabilization and dislodgement of membrane-associated proteins.[3,6,17] Before proceeding it is important to highlight that both proposed action mechanisms include the theory that dap binds to PG in a calcium-dependent fashion and dap oligomer formation is essential for bactericidal activity.

Jung *et al.* (2004) observed leakage of the fluorescent dye calcein from PG containing liposomes upon treatment with calcium and dap. Based on this observation they came to the conclusion that membrane-bound dap must bring about bacterial death by acting as detergent and permeabilizing bacterial membranes in a non-selective fashion.[6] The findings of Jung *et al*. (2004) should be taken with a grain of salt as they may not be biologically relevant; firstly, the study used non-physiologically dap concentrations – studies show that dap's free concentration in blood is 3μM, and Jung *et al*. (2004) utilized 10 μM.[22–24] Secondly, these experiments were not conducted on bacteria; when similar experiment were conducted with calcein encapsulating bacteria no dye leakage was observed upon treatment with dap (1.24 μM) and calcium (1.22 mM).[25]

Müller *et al.* (2016) propose that on *Bacillus subtilis* cells and other bacteria dap achieves antimicrobial activity by the dislodgement of membrane-bound enzymes that are crucial in the biosynthesis of the cell membrane and cell wall. Through experiments with the lipophilic fluorescent dye laurdan, whose emission spectrum shifts with changes in membrane fluidity, it was observed that dap, likely due to its bulky nature, inserts into regions of increased membrane fluidity.[3,26] They propose that dap's bulky nature restricts lipid acyl motion, which alters lipid packing and rigidifies the membrane creating cracks; these cracks are consequently filled in by migration of other fluid. As dap oligomers translocate from the outer to inner leaflet this fluid lipid sequestration and crack-filling is further propagated, thereby, increasing the rigidity of the bulk membrane; consequently, causing the expulsion of membrane-associated proteins. The membrane-associating proteins leave the rigidified membrane because they require regions of increased membrane fluidity to adopt the correct conformation and carry out key cellular functions.[3] The theory proposed by Müller *et al.* (2016) should also be taken with grain of salt because they did not correct for dap's intrinsic fluorescence; laurdan and dap's kyn-13 have overlapping excitation and emission wavelengths.[17,26,27] Therefore, without correction for kyn-13 signal it is not possible to discern if the fluorescence changes being observed are caused by laurdan or dap; as shown for example in Section 2.3.1 Figure 2-2, the fluorescence intensity of kyn-13 in membranes is quite significant. Consequently Mueller's fluorescence data is inconclusive.[27]

1.4 The Antimicrobial Crisis and its consequences

With the rising bacterial resistance to common antibiotics, it was decided that certain antimicrobial compounds would not see widespread use, but would rather be prescribed to patients only if all other treatments failed.[28] As time progressed, the ineffectiveness of common antibiotics became quite acute,

necessitating the frequent prescription of these last resort antimicrobial compounds.[28,29] The increased use of these last resort compounds provided bacteria with ample opportunity to develop resistance mechanisms, leading to the emergence so called 'super bugs', that is pathogenic bacteria whose infections cannot be treated by any antibiotics currently known to humanity.[30] The existence of superbugs is a major public healthcare crisis requiring urgent resolution; one strategy is to invent novel antibiotics that can be used to combat bacterial resistance. One method of novel antibiotic discovery, that has been successful in the past, is the production of analogs based on existing antimicrobial compounds.[31]

The creation of analogs requires finding a suitable parent compound; a viable parent molecule is an antibiotic that has good antimicrobial activity across a broad spectrum of bacteria, has little antibiotic resistance, and a well understood action mode, and structure activity relationship (SAR).[31] One such promising candidate molecule is dap; it is a potent-broad spectrum antibiotic for Gram-positive bacteria that has few reported cases of clinical resistance, but as detailed previously its action mode is not well understood.[1,3,32,33] Accordingly, gaining a better understanding of dap's action mode is of paramount importance in order to facilitate successful analog design.

1.4.1 Bacterial Resistance to Daptomycin

Although bacterial resistance to dap is infrequent there are still cases of resistance reported in clinical literature. The mechanisms discussed below are quite interesting because they relate to work presented in this thesis; they both involve bacteria altering the composition of their cytoplasmic membrane to attain dap resistance.

It has been observed that resistant strains of *Staphylococcus strains* have increased lysyl-PG content in their cytoplasmic membranes.[29] The increase in lysyl-PG content has been attributed to upregulation of multiple peptide resistance factor (mprF), a transmembrane protein with 2 domains: the first domain is a tRNA aminoacyl transferase that converts PG to lysyl-PG, and the second domain is a flippase domain the flips lysyl-PG from the inner to the outer leaflet of the cytoplasmic membrane. [29,34] The exact mechanism by which increased lysyl-PG content imparts resistance to *S. aureus* cells is not firmly established, but there two current hypotheses: overproduction of lysyl-PG simply depletes the amount of PG available for dap to bind, or the cationic nature of lysyl-PG creates a sort of electrostatic shield around the membrane limiting dap's ability to bind.[29,35,36] Recent work by Khatib *et al* (2016) suggests that lysyl-PG charge repulsion is not strong enough to totally account for the inhibitory effects of lysyl-PG.[35]

The second mechanism of resistance involves increased concentrations of CL in bacterial cytoplasmic membranes. The mechanism by which CL imparts resistance, similarly to lysyl-PG, is not established and there two hypotheses: the first involves CL's ability to restrict dap to the outer membrane leaflet, thereby disrupting cation-selective pore formation (see section 1. 3.1 for a more detailed explanation), and the second, less investigated, theory suggests that because CL is made by conjoining two PG molecules its production diminishes the PG available for binding.[20]

1.5 Research Questions

This thesis aimed to deepen the understanding of dap's action mode by investigating two specific research questions:

1. Section 1.3. 2 details various proposed action modes of dap, which were at least in part based on different effects observed on model membranes. While these model membranes typically shared the same phospholipid head groups, they differed with respect to the acyl tails.[3,6,17,32] Therefore, it is important to determine whether dap's action mode is affected by membrane phospholipid acyl tail composition.
2. As noted above, there is consensus that dap's effect involves the formation of oligomers in the cytoplasmic membrane. Elucidating the structure of these oligomers at high resolution would be important for better understanding dap's action mechanism and structure-activity relationships; however, so far, no suitable membrane model has been found that would permit the study of the dap oligomer by NMR.[37–39] This work investigates the suitability of styrene-maleic acid lipid co-polymers stabilized lipid nanodiscs, a previously untested membrane mimetic system, to determine dap's membrane-bound oligomeric structure by solution-state nuclear magnetic resonance.

Chapters 2 and 3 address the first question, whereas chapter 4 addresses the second one.

Chapter 2

Phospholipid Acyl Tails Affect Dap's Action Mode[2]

Abstract: It has been reported that dap brings about its antimicrobial effect by permeabilizing and depolarizing bacterial cell membranes in a cation-selective fashion. Recent findings on model membrane systems suggest that such is not the case consequently allowing for the proposition of alternative action modes; alternative action mechanisms suggest that dap permeabilization is either non-selective or does not occur at all. While designing the model membranes, for the alternative studies, experimenters considered the effects of lipid headgroups on dap's action mode but assumed that lipid acyl tails had a negligible effect on dap activity. In this chapter, this assumption is shown to be false. Various model membranes were studied that differed with respect to their lipid acyl tails but retained the same head group composition. It is shown that that on membranes composed of equal parts PG and phosphatidylcholine (PC), dimyristoyl lipids support membrane permeabilization, whereas dioleoyl and palmitoleyl lipids do not, even though daptomycin does bind to and from oligomers on all membrane types. These observations help reconcile some of the discrepant findings in the literature about dap's action mode.

[2] The work presented in this chapter includes data published in "Daptomycin Pore Formation is Restricted by Lipid Acyl Chain Composition," by Robert Taylor, David Beriashvili, Scott Taylor and Michael Palmer, **2017**, *ACS Infect. Dis.*, 3, 11, 797-801.

Author Contributions: Dr. Robert Taylor synthesized NBD-Dap, ran the kynurenine membrane binding assay, and the pyranine pore forming assay (replicates of the pyranine pore forming assay were run by the author of this thesis). MICs on NBD-dap were conducted by both Dr. Robert Taylor and the author of this thesis. The translocation and subunit stoichiometry assays were conducted solely by the author of this thesis. The comparison of bacterial lipid acyl tails was done by the author of this thesis, Dr. Robert Taylor, and Dr. Michael Palmer. The text in this chapter was written solely by the author of this thesis with parts adapted from the manuscript where indicated.

2.1 Introduction

An in-depth review of the literature regarding dap's action mode suggests that the divergent findings have been obtained on model membranes that had similar head group composition, but different lipid acyl tails; specifically:

- cation-selective pore formation was observed on LUVs composed of equal parts DMPC: DMPG.[17]
- non-selective membrane permeabilization was inferred from observations made on LUVs composed of equal parts POPC: POPG.[6]
- an additional proposed mechanism, which was not discussed in Chapter 1 because it was later disavowed by its authors, suggesting that dap oligomers extract membrane lipids, was inferred from results obtained on giant unilamellar vesicles (GUVs) composed of 7:3 DOPC: DOPG.[32,40]

To establish whether the variation in acyl tails could indeed account for the different findings it was decided to assay LUVs, composed of equal parts PC: PG with varying acyl tails, for dap-induced cation-selective permeabilization by fluorescence spectroscopy. A chemically defined membrane system was used because the different proposed action modes were characterized on model membrane systems composed of synthetic lipids, and additionally such systems afford total control over all experimental parameters, whereas an *in vivo* system does not.

2.2 Methods and Materials

Some sections of the materials and methods presented below are taken directly from the manuscript: Robert Taylor, David Beriashvili, Scott Taylor and Michael Palmer, **2017**, *ACS Infect. Dis*., 3, 11, 797-801.

2.2.1 Synthesis of 7-nitro2,1,3-benzoxadiazol (NBD)-labeled daptomycin

7-nitro2,1,3-benzoxadiazol dap (NBD-dap) was prepared using a modification of the procedure described before1. Daptomycin (79.4 mg, 1.0 equiv.; generously provided by Jared Silverman, formerly of Cubist, Inc.) was dissolved in water (milli-Q, 4 mL) into a dual-opening 50 mL round bottom flask. Sodium bicarbonate (NaHCO3, 12.3 mg) was added and both were stirred and brought to 55°C in an oil bath. A solution of NBD-Cl (10.75 mg, 1.1 equiv.) in methanol (HPLC grade, 4 mL) was added dropwise over 10 min. The mixture was stirred at 55oC for 1 hour under reflux. After the 1 hour was

reached, the reaction was terminated by adding 1 M HCl to a pH of ≈2-3. The reaction mixture was then evaporated to dryness and lyophilised. Analytic RP-HPLC of the mixture showed two major peaks, corresponding to native daptomycin (tr = 26 min) and NBD-daptomycin (tr = 40 min), respectively. The two products were separated on a semi-preparative column (Higgins Clipeus, C-18, 10 μm, with a linear gradient of 65% H2O (0.1% TFA)/35% acetonitrile to 55% H2O (0.1% TFA)/45% acetonitrile, over 50 minutes. The NBD-daptomycin fractions were collected and concentrated to dryness. This gave pure NBD-daptomycin, a yellow powder, after lyophilisation (8.81 mg, 10.1 % yield). The analytical RP-HPLC chromatogram (Higgins Clipeus analytical C-18 column, 5 μm, linear gradient of 65% H2O (0.1% TFA)/35% acetonitrile to 55% H2O (0.1% TFA)/45% acetonitrile (50 minutes) of the pure NBD-daptomycin showed one peak with a tr = 41 min (see Figure 1 in Appendix A). The high-resolution mass spectrometry showed three peaks that are accounted for by a single molecular species (see Figure 2 in Appendix A).

2.2.2 Antibacterial activity assay

Daptomycin and NBD-dap were tested against Bacillus subtilis ATCC 1046 at a concentration of 5 mM $CaCl_2$. Each antibiotic was tested three times in duplicate; growth and sterility controls were run in parallel. The procedure used was as described before.[10] The results were exactly as before.[9]

2.2.3 Preparation of LUVs

All lipids used to make liposomes were acquired from Avanti Polar Lipids (Alabaster, Alabama). Lipids included 1,2-dimyristoyl-sn-glycero-3-phosphocholine (DMPC), 1,2-dimyristoyl-sn-glycero-3-phospho-(1'-rac-glycerol) (sodium salt; DMPG), 1-palmitoyl-2-oleoyl-sn-glycero-3-phosphocholine (POPC), 1-palmitoyl-2-oleoyl-sn-glycero-3-phospho-(1'-rac-glycerol) (sodium salt; POPG), 1,2-dioleoyl-sn-glycero-3-phosphocholine (DOPC), and dioleoyl-sn-glycero-3-phospho-(1'-rac-glycerol) (sodium salt; DOPG). LUVs were prepared as described before.[9] Briefly, the requisite amounts of lipids – equimolar mixtures of PC and PG were used in each case – dissolved in chloroform/methanol (3:1) and dried under N_2 in a round-bottom flask. After removal of chloroform, the lipid film was resuspended in the appropriate buffer, and the resulting lipid suspension extruded repeatedly through a 100 nm polycarbonate filter. Liposomes were used at a final total concentration of 250 μM total lipid in the various assays unless stated otherwise.

2.2.4 Monitoring daptomycin-membrane interactions by kynurenine fluorescence

The assay was conducted as follows: DMPC/DMPG, DOPC/DOPG or POPC/POPG liposomes were mixed with daptomycin (3 μM) and calcium chloride (0 to 100 mM final concentration, as stated in the Results section) in HEPES-buffered saline (20 mM HEPES, 150 mM NaCl, pH 7.4). Each sample was incubated for 3 minutes. Excitation spectra (emission wavelength: 445 nm) and emission spectra (excitation wavelength: 365 nm) were acquired on a PTI QuantaMaster 4 instrument. All trials were run in triplicates at 37ºC.

2.2.4.1 Using kynurenine signal to monitor daptomycin's interaction with membranes

Assaying dap-membrane interactions by kyn-13 fluorescence was first done by Lakey *et al*. (1988), who observed that kyn is an intrinsic polarity-sensitive fluorophore; as kyn enters further into a hydrophobic environment, like a membrane bilayer, its emission signal increases and blue-shifts from 465 nm to 445 nm.[27] Consequently, through monitoring kyn's signal intensity at 445 nm it is possible to observe dap's insertion into the bilayer as a function of calcium concentration.[27]

2.2.5 Daptomycin membrane permeabilization monitored by pyranine fluorescence

The assay was conducted as follows: DMPC/DMPG, DOPC/DOPG or POPC/POPG liposomes were prepared in 5 mM MES, 5 mM Tricine, 5 mM NaCl, 250 mM sucrose (MTS), pH 6.0 with 1 mM pyranine (Sigma-Aldrich). The resulting pyranine-containing LUVs were passed through a size exclusion column (Bio-Rad P-6DG, Bio-Rad, Richmond, CA, USA) using MTS pH 6.0 without pyranine to remove the excess non-entrapped dye. The size exclusion resin was degassed, and the column poured 1 hour before passing the sample down the column. Daptomycin (2 μM), the proton carrier carbonyl cyanide m-chlorophenyl hydrazone (CCCP, 5 nM), and calcium chloride (concentrations as stated in Results) were added into MTS buffer with 100 mM NaCl and at pH 8.0. At time 0, pyranine-loaded LUVs were added to a final concentration of 250 μM total lipid. Fluorescence (excitation S3 wavelength, 460 nm; emission wavelength, 510 nm) was monitored for 300 s. Triton X100 (Biorad, Richmond, CA, USA) (0.1% final concentration) was then added to solubilize the LUVs. The fluorescence intensity after Triton X-100 solubilization was used to normalize the entire curve. All experiments were run at 30ºC.

2.2.5.1 History and rationale of the pyranine assay

The feasibility of using pyranine to detect antimicrobial peptide induced cation-selective permeabilization of membranes was first demonstrated by Clement *et al.* (1981).[41] The assay was later adapted by Zhang *et al.* (2014) to show that dap oligomers form cation-selective pores.

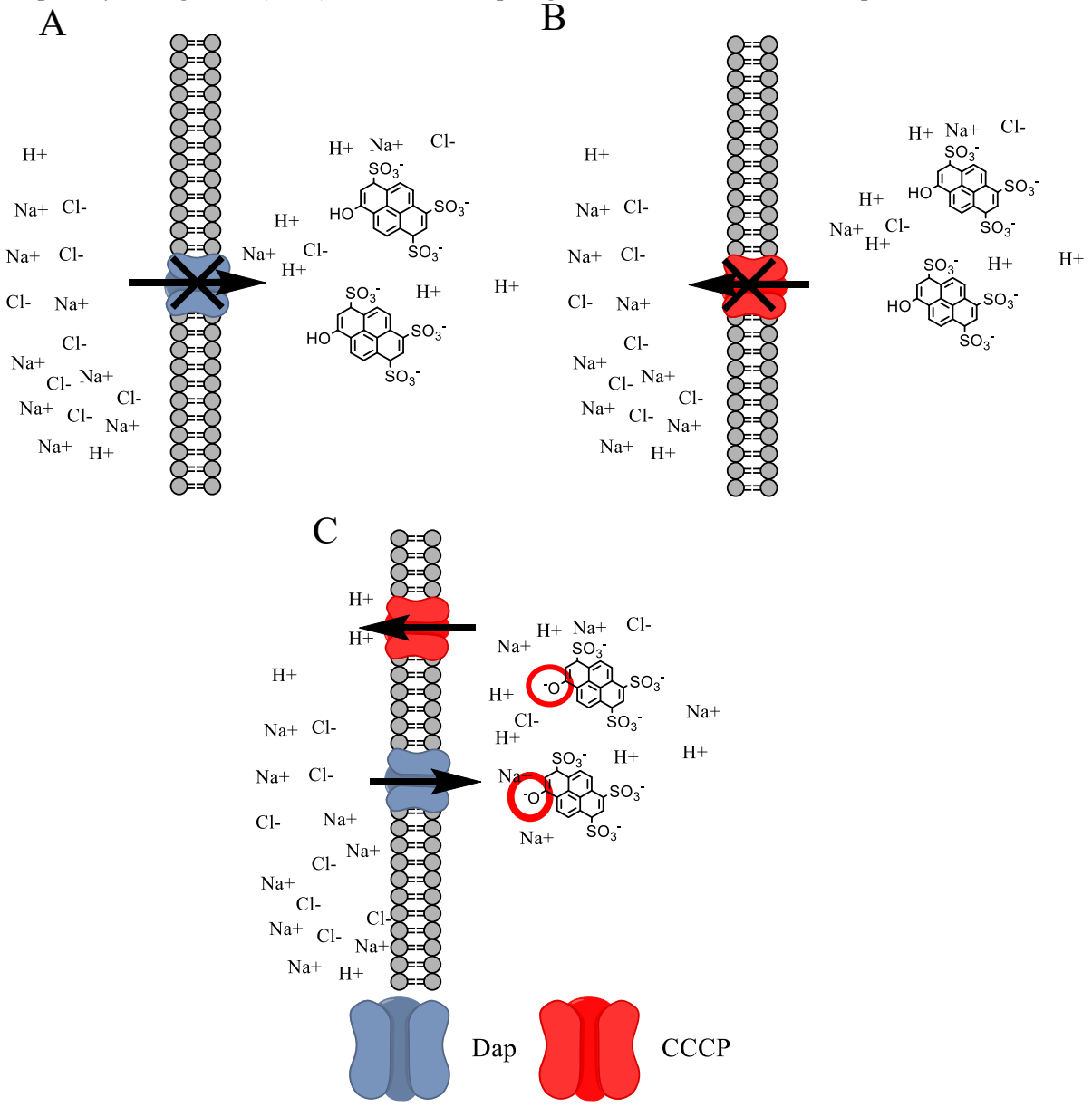

Figure 2-1. Pyranine-based pore formation assay. Panel A and B show that treating pyranine containing LUVs with CCCP or dap alone will not result in pyranine signal change as the transport of cations or protons will not be electroneutral. Panel C shows that treatment of LUVs with both CCCP and dap will cause electroneutral cation-proton exchange, and thus cause pyranine to emit as strong signal at 510 nm. The red circle highlights the deprotonation of pyranine's hydroxy group.

Briefly, pyranine is a poly-anionic fluorescent dye that is excited at 460 nm. Its emission at 510 nm is pH-dependent; at pH <7 pyranine has a low signal intensity at 510 nm because its hydroxy group is protonated and is not a good donor of electron density into the conjugated system. At pH >7 the hydroxy becomes deprotonated forming an oxyanion that readily donates electron density into the conjugated cyclic system giving rise to a strong signal at 510 nm.[41]

The rationale behind the assay is as follows: the assay couples, by way of the membrane potential, the transport of salt cations to the counter-transport of protons, which is detected by pyranine fluorescence. Practically, this is achieved as follows: pyranine is dissolved in a pH 6 low salt buffer and encapsulated into LUVs via the extrusion method. The extruded solution is passed through a size exclusion column to separate the pyranine containing LUVs from the non-encapsulated pyranine. The LUVs are then added to a cuvette, which contains a high salt, pH 8, and sucrose rich buffer (external buffer). A change in pyranine's signal requires increasing intra-LUV pH by exchanging extra-LUV cations for intra-LUV protons. This is done by treating the pyranine-containing LUVs with both dap and the proton ionophore CCCP. The presence of both dap and CCCP (Figure 2-1 Panels A,B, and C) is required because the exchange of cations can only occur if the process is electroneutral.[41,42]

2.2.6 Daptomycin membrane translocation assay

This was adapted from Zhang *et al.* (2014).[20] LUVs composed of phospholipids with varying acyl tails were treated with 1μM 2:1 NBD-dap: dap and 25 mM calcium containing HEPES-buffered saline (20 mM HEPES, 150 mM NaCl, pH 7.4). After a 4-minute period of incubation to allow dap to bind to the membranes 1 mM dithionite (Sigma-Aldrich) was added to the mixture. Data collection was begun 50 seconds before this addition to establish the unquenched base line. The NBD signal was recorded for 400 seconds, after which Triton X-100 (Biorad, Richmond, CA, USA) (0.1% final concentration) was added to solubilize the LUVs and signal recorded for an additional 60 seconds. The curve was normalized to the average signal intensity before addition of dithionite (from 0-50 seconds). The course spectra (excitation wavelength: 465 nm; emission wavelength, 530 nm) were acquired on a PTI QuantaMaster 4 instrument. The data presented are the average of 3 independent experiments conducted at 37ºC.

The experiments with 1,2-dimyristoyl-sn-glycero-3-phosphoethanolamine-N-(7-nitro-2-1,3-benzoxadiazol-4-yl) (ammonium salt) (NBD-PE), bought from Avanti Polar Lipids (Alabaster,

Alabama), (Figures 3 and 4 in Appendix) were conducted exactly as above except there was no use of NBD-dap or dap and the LUVs consisted of .5% mol/mol NBD-PE and equal parts PC: PG.

Note: it was noticed that there is considerable batch to- batch variation in the activity of dithionite; the batch that was used at 1 mM had been freshly purchased. When used at concentrations greater than 3-4 mM, this batch caused more extensive quenching of NBD-dap. This may be related to the introduction of sulfuric acid that forms through spontaneous chemical decay,[43] but the possibly was not systematically examined. The assay is also affected by the calcium concentration; less experimental variation occurs at 25 mM than at lower concentrations. A 1:2 ratio of NBD-dap to dap is required to mitigate NBD fluorescence self-quenching.[8,9,18] The data presented is the average with standard deviations of 3 independent experiments conducted at 37ºC.

2.2.7 Daptomycin oligomer subunit stoichiometry

Determination of dap oligomer subunit stoichiometry was conducted according to the methodology set out by Muraih *et al*.[18] Briefly, LUVs, made as described above, were treated with premixed ratios of dap: NBD-dap (4:1, 6:1, 8:1, 10:1) (final concentration of 10 μM) and 5 mM calcium. This resulting mixture was incubated for 3 minutes and a fluorescence emission spectrum recorded. After the measurement, an additional 4 μM dap was added to the sample. After 3 more minutes of incubation another fluorescence emission spectrum was recorded. The emission spectra (excitation wavelength: 365 nm; emission 400-600 nm) were acquired on a PTI QuantaMaster 4 instrument. The data presented is the average with standard deviations of 8 independent experiments conducted at 37ºC.

2.2.7.1 Daptmycin oligomer subunit stoichiometry assay rationale and analysis.

The rationale of this assay is to determine the subunit stoichiometry of dap oligomers by comparing the kynurenine signal from oligomers containing dap only to that of hybrid oligomers formed from mixtures of native dap and NBD-dap. The approach utilizes the fluorescence resonance energy transfer (FRET) that occurs, at an extremely short distance, between kynurenine and NBD.

The method is based on the following assumptions:

1. All oligomers contain the same number of subunits.
2. The formation of dap oligomers goes to completion on the time-scale of the experiment
3. The pre-mixture of NBD-dap and dap forms oligomers stochastically without segregation

4. Mixed oligomers, those composed of NBD-dap and dap, do not give rise to kynurenine emission signal because all kynurenine fluorescence within an oligomer is quenched by FRET to NBD
5. Once oligomers form, they are stable on the time scale of the experiment.

Based on assumptions 1 and 3, the fraction of native dap molecules (D) contained within native only oligomers is equal to:

$$D = \frac{d^n}{d}$$

where d is the fraction of unlabeled dap added to the NBD-dap, and d^n is the fraction of native dap only containing oligomers. Because it is impossible to determine d^n directly assumption 4 becomes vital. Assumption 4 states that all the measured kynurenine signal comes from oligomers containing native dap only and equates to the relative measured kynurenine fluorescence F_r; consequently, D could be directly determined from F_r if FRET is occurring only within oligomers. However, because FRET also occurs between adjacent oligomers a correction is required. To correct for the FRET between oligomers, a second sample of unlabeled dap is added, and it is assumed that the known quantity of donor-only oligomers formed from this sample is quenched by FRET between oligomers to the same extent as the unknown quantity formed in the first step. Subsequently it is possible to define F_r as follows:

$$F_r = \frac{d_2}{d_1}\left(\frac{I_1 - I_0}{I_2\frac{v_2}{v_1} - I_1}\right);$$

where d_1 and d_2 are the molar amounts of native dap in the premix and the second addition, I_0, I_1, and I_2 are the signal intensities at 445 nm for a LUV blank, after the initial 3 minute incubation, and 3 minutes after the second dap addition, and V_1 and V_2 are the sample volumes before and after the addition. Overall, it is then possible to replace D with F_r and then calculate the subunit stoichiometry *n* from the equation below:

$$n = 1 + log_d(F_r)$$

2.3 Results

2.3.1 Daptomycin's interactions with membranes composed either of equal parts DMPC/PG, POPC/PG, or DOPC/PG

Before conducting the pyranine-based pore forming assay, it was imperative to establish whether dap's ability to interact with membranes is affected by variation in phospholipid acyl tails. To this end, a mixture containing 250 µM LUVs, composed of equal parts either DMPC: DMPG, POPC: POPG, or DOPC: DOPG, and 3 µM dap was titrated with calcium. After each calcium addition and 3-minute incubation dap's kyn-13 emission spectrum (excitation: 365 nm; emission 400-600 nm) was acquired. As mentioned in section 2.2.4.1, kynurenine's emission signal is extremely polarity sensitive.[27] Therefore, as calcium concentration increases kyn inserts into the hydrophobic membrane interior, its emission signal concomitantly blue-shifts, from 465 nm to 445 nm, and becomes more intense.[27]

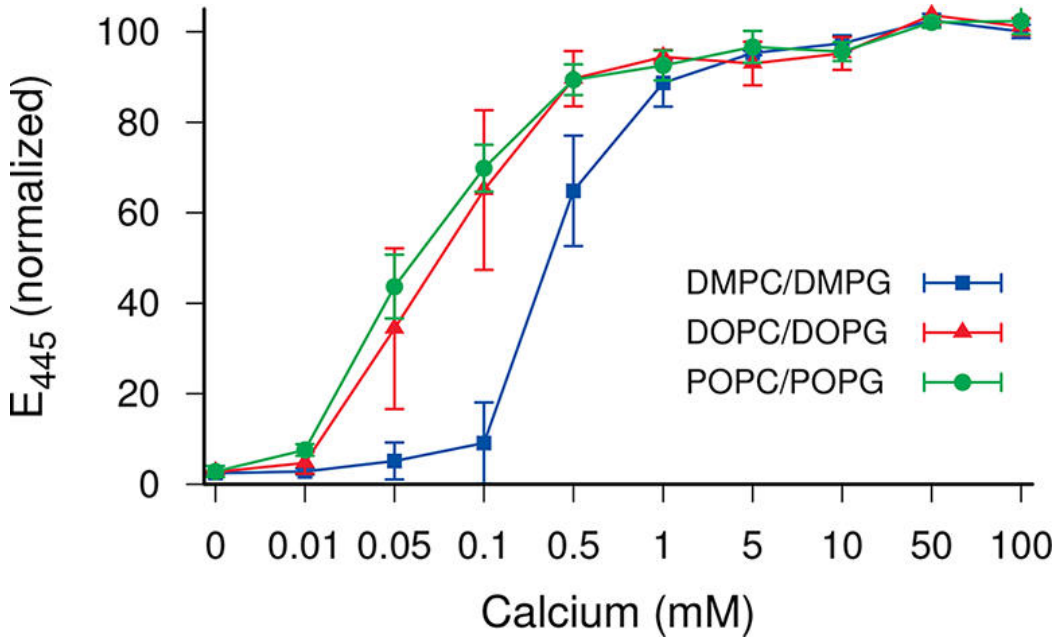

Figure 2-2. Daptomycin's interaction with LUVs composed of a conserved phospholipid headgroup composition of equal parts PC and PG and varying phospholipid acyl tails. Dap interacts with all membrane types at physiological concentrations of calcium. Dap does bind more avidly to membranes containing phospholipids with longer and unsaturated phospholipid acyl tails.

The saturation of kyn signal at 1 mM calcium for all membrane types suggests that dap readily interacts with all membranes at physiological calcium concentrations (1.25 mM). It is noteworthy that less calcium is required for dap to interact with LUVs composed of phospholipids with DO and PO acyl tails.

2.3.2 Cation-selective permeabilization of LUVs with variable phospholipid acyl tails.

Permeabilization by dap at low micromolar concentrations was observed or not observed on membranes with different acyl compositions, but also using different experimental techniques.[3,6,32,40] In this work, dap permeabilization was studied by using the same assay, but with membrane composed of different acyl tails.

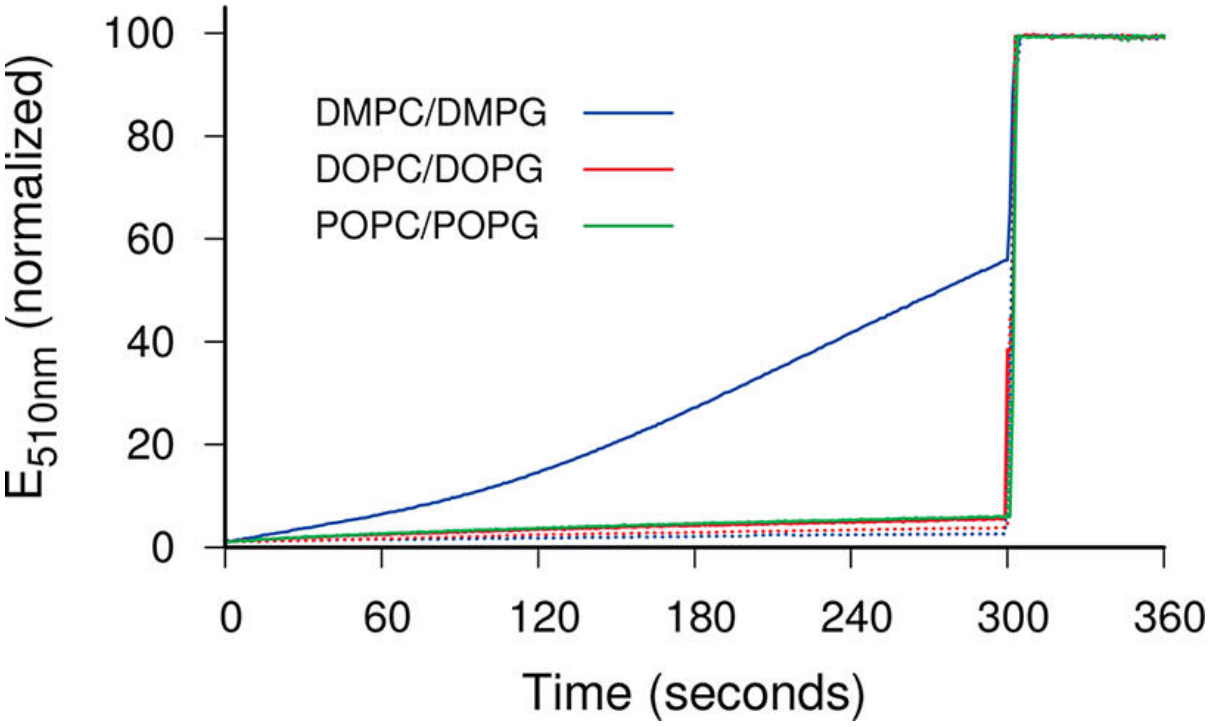

Figure 2-3. Daptomycin induced cation-selective pore formation on LUVs composed of phospholipids with conserved headgroup composition but variable fatty acid tail composition. 250 µM of either DMPC: DMPG, POPC: POPG, or DOPC: DOPG LUVs encapsulating 1 mM pyranine were used in the assay.

The data show that dap readily permeabilizes DMPC: DMPG LUVs but not POPC: POPG and DOPC: DOPG LUVs. Considering that the lipid headgroup composition was conserved amongst experiments it is possible to conclude that phospholipids with increased acyl tail length (>14 carbons) with or without unsaturation inhibit dap cation-selective permeabilization.

2.3.3 Daptomycin translocation across membranes composed of inhibitory phospholipid acyl tails

Zhang *et al.* (2014) observed that membranes containing CL are not permeabilized by dap.[20] Zhang *et al.* (2014) found that dap is not able to permeabilize CL containing membranes because on these

membranes almost all the dap is sequestered to the outer membrane leaflet. In contrast, LUVs which are readily permeabilized, those composed of equal parts DMPC: DMPG, have equal distribution of dap across the membrane leaflets.[20] Further experiments by Zhang *et al*. (2014) found that on CL containing membranes dap oligomers were composed of 4 dap molecules, whereas on DMPC: DMPG LUVs dap oligomers consisted of 8 dap molecules. Consequently, Zhang *et al*. (2014) hypothesized that cation-selective pore formation by dap requires the formation of an octameric oligomer which is composed of two conjoined tetramers located on opposing leaflets.[20] Based on Zhang *et al*. (2014) findings it was of interest to determine whether the lack of pore formation observed on POPC: POPG and DOPG: DOPC liposomes occurred via a similar mechanism.

To determine dap translocation across membrane leaflets the dithionite/NBD fluorescence quenching assay was used. LUVs containing different phospholipid acyl compositions were treated with a premix of NBD-dap, dap and calcium. After a period of incubation to allow dap-membrane binding, dithionite was added to the mixture. Dithionite instantaneously reduces NBD that resides on the outer membrane leaflet and quenches its fluorescence.

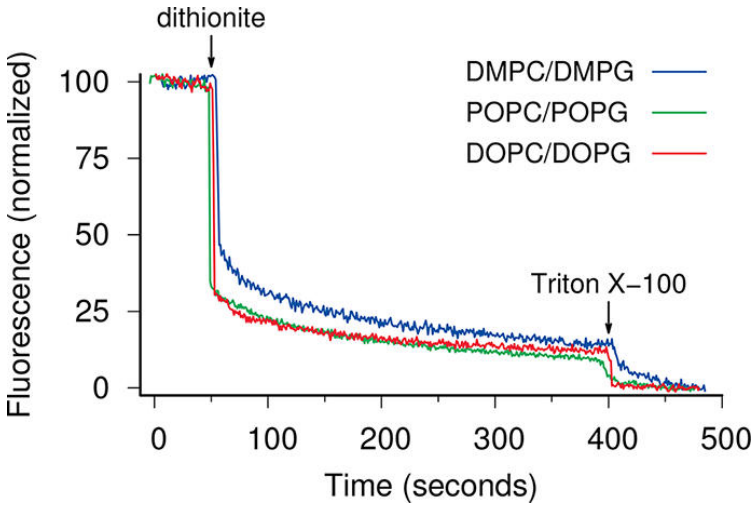

Figure 2-4. Daptomycin translocation across LUVs composed of phospholipids with acyl tails permissive and restrictive to dap cation-selective permeabilization. To make sure that dithionite could not cross the LUV membranes via dap's pore NBD-PE experiments were run; this data can be found in Appendix A - Figures 3 and 4.

Upon addition of dithionite to DMPC: DMPG liposomes the NBD signal instantaneously drops to 48 ± 6%, indicating that approximately half of all labeled daptomycin is located on the outer leaflet. The slow drop from 48% towards the baseline is due to transient flipping of dap between membrane leaflets. This result closely resembles that previously reported by Zhang *et al*. (2014), who reported that dap is

equally distributed between membrane leaflets. In contrast, on POPC: POPG and DOPC: DOPG liposomes the signal upon dithionite addition drops to 35 ± 1% and 31 ± 3% respectively. Therefore, on restrictive membranes roughly 70% of dap is located on the outer membrane leaflet. Unlike membranes which contain CL, which restricts dap to the outer leaflet, membranes composed of POPC: POPG or DOPC: DOPG allow for partially dap translocation.

2.3.4 Daptomycin oligomer subunit stoichiometry on POPC: POPG and DOPC: DOPG liposomes

Since dap is able to partially translocate across POPC: POPG and DOPC: DOPG membranes, it was of interest to see if the translocation was enough to facilitate the formation of octameric dap oligomers. The subunit stoichiometry was determined on DMPC: DMPG, POPC: POPG and DOPC: DOPG by a FRET-based assay developed by Muraih *et al.* (2012).[18]

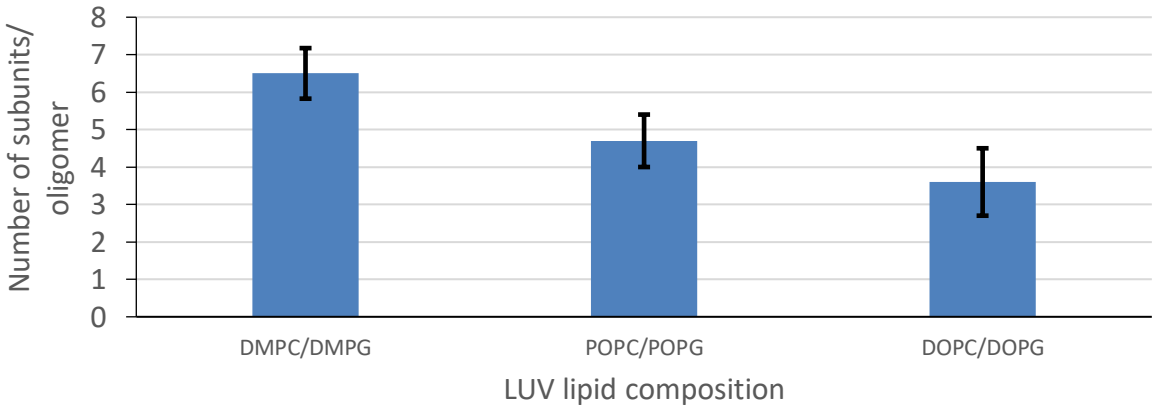

Figure 2-5. Daptomycin oligomer subunit stoichiometry on POPC: POPG and DOPC: DOPG liposomes. The subunit stoichiometry on DMPC: DMPG liposomes was 6.5 ± 0.67, on POPC: POPG liposomes 4.7 ± 0.7, and on DOPC: DOPG liposomes 3.6 ± 0.9.

Even though dap is able to partially translocate across the dap permeabilization-resistant membranes (those containing POPC: POPG and DOPC: DOPG) the octameric oligomer does not form; rather formation of a tetrameric oligomer is observed. It is important to point out the subunit stoichiometry on DMPC: DMPG is lower than 8 subunits; this is likely due to incomplete FRET within oligomers.

2.4 Discussion

The kynurenine-based membrane interaction assay shows that dap interacts with all three LUV types at physiological calcium concentrations. The more avid interaction of dap with PO and DO LUVs

maybe because these lipids have unsaturated lipid acyl tails.[44] Lipids with unsaturated acyl tails tend to be less tightly packed in a bilayer environment possibly making it easier for dap to insert.[44] For DM lipids more calcium may be required to overcome the steric hinderance that arises from tighter lipid packing.

Cation-selective pore formation is observed on liposomes composed of phospholipids with myristoyl acyl tails and not with palmitoyl and oleoyl acyl tails. Considering that the phospholipid headgroup composition was conserved amongst the LUVs it is possible to conclude that phospholipids with increased acyl tail length and/or unsaturation inhibit dap's ability to permeabilize those LUVs.

Palmitoyl and oleoyl lipids restrict dap pore formation by inhibiting octameric oligomer formation. The data suggest that dap binds to the inhibitory membranes, and forms tetramers that freely equilibrate between membrane leaflets. These tetrameric oligomers are not able to align, and form the octamer required for pore formation. Consequently the unaligned tetramers are able to continue equilibrating between leaflets with a preference to the outer leaflet ; experiments by Pogliano *et al.* (2012) show that dap has preference for membrane regions exhibiting curvature – whether it is negative or positive was not empirically determined.[5] It is likely that on DMPC: DMPG membranes dap is equally distributed between the leaflets because octamer formation is energetically favorable.

It has been proposed that dap brings about its antimicrobial effect by dislodgement of membrane-associated biosynthetic enzymes. The authors proposing this mechanism initially began their studies by attempting to determine whether *Bacillus subtilis* membranes are permeabilized by dap in a cation-selective fashion; they did not observe dap permeabilization of *Bacillus subtilis* cells (personal communication from the authors of this paper indicates that pore-forming experiments were done in the absence of calcium; thus, casting doubt on the validity of the results).[3] Based on the results from this study, it is quite possible that they did not observe cation-selective permeabilization because the phospholipid acyl tail composition of *Bacillus subtilis* cells is different from *Staphylococcus aureus* cells, on which cation-selective permeabilization has been observed, and is inhibitory to dap membrane permeabilization.[12,45–47] It is noteworthy that the proposed mechanism of membrane-protein dislodgement assumes dap's ability to translocate across membranes.[3] Dap's ability to partially translocate across membranes resistant to permeabilization suggests that on bacteria resistant to dap pore formation the antimicrobial effect maybe brought about by dap translocation.

Lastly, it is important to note that the membranes used in this study are quite different in composition from membranes found in Gram-positive bacteria. For example, PC is not commonly found in Gram-

positive bacteria, but is used because of significant precedence.[12,46] Also, liposomes lack membrane asymmetry, membrane proteins, and glycol-phospholipids all of which may affect dap's action mode in yet unknown ways. Additionally, the lipids acyl tails used in this study are not fully representative of those found in bacteria; Figure 5 in Appendix A shows that vast variation in lipid acyl tails of Gram-positive bacteria clinically treated by dap. It is important to note that the goal of this work was not to recreate the most life-like mimetic of a bacterial cytoplasmic membrane, but to reconcile discrepancies between previous studies on model membranes. Therefore, the choice of lipids was dictated by the lipids used in previous studies. Beyond the observation that lipid acyl chains can modify the activity of daptomycin, no specific inferences should be drawn from this work regarding the susceptibility of different bacterial species or strains.

Chapter 3

Mechanistic studies on the effect of membrane lipid acyl chain composition on daptomycin pore formation[3]

Abstract: Daptomycin permeabilization of membranes is dependent on their phospholipid acyl composition. In this study, liposomes were used to study the effects of phospholipids with various acyl tails on dap activity. Through the course of this work the following observations were made: oleoyl acyl tails inhibit dap's pore formation regardless of the headgroup moiety they are ligated to. This inhibition occurs even at low membrane concentrations of oleoyl lipids (10% DOPC). The inhibitory effect of acyl tails is correlated with their length rather than with their degree of unsaturation. Additionally, it was observed that dap permeabilization occurs only when octameric oligomers are formed, corroborating that the octamer constitutes the functional cationic pore. Overall, the results in this study indicate that acyl tails that inhibit daptomycin pore formation do so by disrupting the

[3] The data presented in this chapter has been published in "Mechanistic studies on the effect of membrane lipid acyl chain composition on daptomycin pore formation," David Beriashvili*, Robert Taylor*, Braden Kralt, Nooran Abu Mazen, Scott D. Taylor, and Michael Palmer, 2018 Chemistry and Physics of Lipids., 216, 73-79. *These authors contributed equally to this work.

Author Contributions: Braden Kralt and Nooran Abu Mazen synthesized and purified NBD-dap. The author of this thesis ran MICs for NBD-dap and the anteiso C_{12}-dap analog. The anteiso C_{12}-dap analog was synthesized by Braden Kralt. Dr. Robert Taylor ran MICs on C_{14}-dap. Robert Taylor ran 4 of 6 replicates for the pore forming assays presented in Figure 1 and the author of this thesis ran the remaining 2 replicates - except for the 5% DOPC liposomes which had all replicates run by Dr. Robert Taylor. The kynurenine fluorescence-based assay for monitoring membrane-dap interaction was run by the author of this thesis. All the subunit stoichiometry and translocation assays presented in this chapter and the manuscript were acquired by the author of this thesis. All fluorescence anisotropy assays for determination of membrane fluidity were run by the author of this thesis with exception of the 10% TMCL assay which was run by Dr. Robert Taylor. The pore formation assays on 10% cardiolipin LUVs, and with C_{14}-Dap were run by Dr. Robert Taylor. The pore formation assays on dap-treateded 10% DPDPC LUVs, on anetiso C_{12} dap-treated DOPC: DOPG LUVs, 20% TMCL were run by the author of this thesis. The text in this chapter was written solely by the author of this thesis with parts adapted from the manuscript where indicated.

alignment of tetramers across membrane leaflets, which on susceptible membranes gives rise to the octameric functional pore.

3.1 Introduction

In the previous chapter, it was observed that phospholipids with acyl tails longer than 14 carbons and a cis-unsaturation inhibit dap's ability to create cation-selective pores.[13] The experimental data suggest that these lipid acyl tails inhibit dap pore formation by halting oligomerization at the stage of the tetramer. The inability to form octameric oligomers likely causes the uneven distribution of dap across membrane leaflets [5,13] The work conducted in this chapter builds on findings from the previous one by answering the following questions:

- In the previous chapter, the acyl tails which caused the inhibitory effect were attached to both PC and PG. Since PG is specifically required for dap binding, do the inhibitory acyl chains have to be part of this lipid?[9]
- In chapter 2 it was confirmed that the only model membranes susceptible to dap permeabilization were those that contained dimyristoyl lipids only. The inhibitory acyl tails differ from myristic acid by both greater length and unsaturation; Consequently, can the inhibitory effect be attributed to either of these properties?
- Lastly, previous work by researchers at Eli Lily implicates dap's acyl tail moiety as a key modulator of its activity; dap analogues with longer or branched acyl tails had higher antimicrobial activity.[2] Can such analogues also restore permeabilization on membranes that are impervious to daptomycin?

3.2 Materials and Methods

Some sections of the materials and methods presented below are taken directly from the manuscript: David Beriashvili*, Robert Taylor*, Braden Kralt, Nooran Abu Mazen, Scott D. Taylor, and Michael Palmer, 2018 Chemistry and Physics of Lipids., 216, 73-79. David Beriashvili, Dr. Robert Taylor, Braden Kralt, Dr. Scott Taylor, and Dr. Michael Palmer contributed to the writing of the materials and method section. *These authors contributed equally to this work

3.2.1 Synthesis of 7-nitro2,1,3-benzoxadiazol (NBD)-labeled daptomycin

The synthesis was carried out according to Muraih *et al.*(2011) with minor modifications, as follows: Daptomycin (40.5 mg, 25 μmol), which was generously provided by Jared Silverman, formerly of

Cubist, Inc., was dissolved in a buffer (20.5 mL) containing 50 mM sodium borate and 20 mM EDTA at pH 8. To this was added a solution of 4-chloro-7-nitrobenzofurazan (NBD-Cl, 67.8 mg, 13.6 eq) in acetonitrile (13.6 mL) and the reaction was stirred at 55°C for 3 hours. Following the reaction time, the solution was brought to 0°C in an ice bath and quenched with the addition of 200 µL of acetic acid. The mixture was then purified on a Proto 200 C18 10 µm analytical column with an isocratic mobile phase of 33% acetonitrile, 67% 20 mM ammonium acetate buffered at pH 5.5, over 50 minutes. Fractions were collected and concentrated to dryness. The residue was suspended in Milli-Q water and lyophilized, giving pure NBD-daptomycin (4.4 mg, 9.8 %). The analytical RP-HPLC chromatogram (Proto 200 C18 10 µm) linear gradient of 31:69 acetonitrile / 20 mM ammonium acetate buffer (pH 5.5) to 38:62 acetonitrile / 20 mM ammonium acetate buffer (pH 5.5) over 40 minutes of the pure NBD-daptomycin showed one peak with a tr = 27 minutes (See Figure below). The single peak was collected and analyzed by ESI-MS. The molecular weight of protonated NBD-daptomycin (sum formula: C78H102N20O29) is 1783.719; the experimental value as determined by mass spectrometry is 1783.721. Typical HPLC and MS results are shown in Figures 1 and 2 in Appendix B. The MIC of the purified compound was 1.25 µg/ml (native daptomycin: 0.75 µg/ml).

3.2.2 Synthesis and characterization of C_{14}-daptomycin

The steps for this synthesis were done using the method by Gantner *et al*. (2014).[48] Myristic acid (1.31 mmol) and N, N'-dicyclohexylcarbodimide (1.57 mmol) were added to a round bottom flask in THF (2.62 mL) and stirred at room temperature for 10 minutes. N-hydroxysuccinimide (1.57 mmol in 1.41 mL THF) was added and the reaction was stirred for 22.5 hours at room temperature. The solvent was removed under reduced pressure, and dry-loaded onto a silica gel column. The product was eluted using 50:1 chloroform:methanol with an R_f =0.76. It was concentrated under reduced pressure and lyophilized to produce a white powder (221.33 mg, 51.76% yield). ^{1}H NMR (300 MHz, $CDCl_3$): δ2.83 (s, 4H), 2.60 (t, J = 7.4 Hz, 2H), 1.74 (papp, J = 6.9 Hz, 2H), 1.26 (m, 20H), 0.88 (t, J = 5.8 Hz, 3H). LRMS (ESI-MS) m/z: 326 $(M+H^+)^+$; HRMS (ESI-MS) calculated for $C_{18}H_{31}N_1O_4$ 326.2461; found 326.2359.

To a solution of Boc-deacyl-daptomycin (15.6 mg, 10 µmol; generously provided by Cubist, Inc.) in dry DMF (0.5 ml) was added myristic acid succiminidyl ester (3 mg, 6 µmol, 0.6 eq.). Triethylamine (7 µL, 50 µmol, 5 eq.) was added and the mixture stirred for three days, at room temperature. After this, trifluoroacetic acid with 0.2% thioanisole (5 mL) was added and stirred at 0oC for 20 minutes,

under argon. Analytic RP-HPLC (Higgins Clipeus, C18 column, 10 µm) utilizing a mobile phase of 0.1% trifluoroacetic acid with ultrapure water and an acetonitrile gradient from 10% to 90% over 60 minutes showed that all of the Boc-deacyl-daptomycin was consumed and a single major peak was present (tr = 44 min) as well as a native Dap peak at tr = 19 min. The solvent was removed under reduced pressure and the residue dissolved in ultrapure water and lyophilized, resulting in a white powder (17.0 mg, 98% yield). The analytical RP-HPLC chromatogram (Higgins Clipeus, C18 column, 10 µm) using a mobile phase of 0.1% trifluoroacetic acid with ultrapure water and an acetonitrile gradient from 10% to 90% over 60 minutes, gave pure C14-daptomycin showing one major peak with a tr = 17 min (Figure 5A). Mass spectrometry (ESI-MS) showed one singly charged peak with the expected molecular mass of 1676.8 (M + H+)+, as well as several accompanying most likely arising from 13C incorporation. The MIC of the purified compound was 0.5 µg/ml (native daptomycin: 0.75 µg/ml). HPLC trance and mass spectrometry analysis of C_{14}-dap can be found in Figure 3 and 4 in Appendix B respectively.

3.2.3 Synthesis and characterization of ante-daptomycin

Synthesis of 2,5-dioxopyrrolidin-1-yl 10-methyldodecanoate: To a 25 mL round-bottom flask was added 10-methyldodecanoic acid (25 mg, 0.116 mmol, 1 eq). To this was added a solution of NHS (19.8 mg, 0.172 mmol, 1.5 eq) in dry CH_2Cl_2 (5 mL) until dissolution. The reaction was cooled to 0 °C in an ice bath. To the chilled stirring solution was added EDC (37.0 mg, 0.193 mmol, 1.67 eq) and DMAP (1.4 mg, 0.012 mmol, 0.1 eq). The solution was stirred at 0 °C for 1 hr, after which the ice-bath was removed, and the mixture stirred for an additional 20 hours as monitored by TLC. Following the reaction time, the mixture was diluted with EtOAc (15 mL). The organic phase was washed with 0.1 M HCl(aq) (1x 15 mL), then washed with Sat. $NaHCO_3$ (1x 15 mL), and finally washed with brine (1x 15 mL). The organic phase was dried off with Na_2SO4, concentrated, and the residue was purified by column chromatography with a mobile phase of 1:1 EtOAc-hexane, to yield the desired product as a white solid (36 mg, quant). ^{1}H-NMR (300 MHz, $CDCl_3$) δ: 2.81 (4H, s), 2.58 (2H, t, J = 7.4 Hz), 1.72 (2H, app. quint., J = 7.2 Hz), 1.38-1.04 (16H, m), 0.85-0.81 (6H, m). ^{13}C- NMR (75 MHz, $CDCl_3$) δ: 172.1, 171.6, 39.5, 37.3, 33.8, 32.8, 32.4, 32.3, 32.0, 31.7, 29.0, 28.5, 27.4, 22.1, 14.3. HRMS (ESI^+): m/z [M+H+]+ calculated for $C_{17}H_{29}NO_4$: 312.21693, found 312.21668.

Synthesis of ante C_{12}-daptomycin: To a 7 mL glass vial was added Boc-Deacyl-Dap (10 mg, 6.4 µmol, 1 eq). The vial was equipped with a stir bar, and dry DMF (200 µL) was added. To this was added triethylamine (9 µL, 0.065 mmol, 10 eq) and 2,5-dioxopyrrolidin-1-yl 10-methyldodecanoate

(2.9 mg, 9.6 μmol, 1.5 eq) and the suspension was stirred for 72 hours. The reaction was concentrated on a high-vacuum rotary evaporator and re-dissolved in water followed by lyophilization. Then, the crude product was stirred in a solution of TFA (1 mL) containing thioanisole (2% v/v) for 25 minutes in an ice-bath. The solution was concentrated *in vacuo*, and the residue re-dissolved in dry DMF, with the solvent being removed once more. The oily residue was dissolved in water and lyophilized before purification by preparative HPLC using a Clipeus C18 10 μm column employing a linear gradient of 57:43 H_2O (+0.1 % TFA) / acetonitrile to 54:46 H_2O (+0.1 % TFA) / acetonitrile. Fractions containing the desired compound were pooled and concentrated, suspended in water and lyophilized to obtain the desired product as a white powder (9.6% yield). HRMS (ESI+): *m/z* $[M+2H^+]^{2+}$ calc'd for $C_{75}H_{107}N_{17}O_{26}$: 831.88593, found 831.88348. The analytical HPLC trace of the purified compound and mass spectra can be found in Appendix B figures 5 and 6 respectively.

3.2.4 Antibacterial activity assay

The antimicrobial assay was completed as described in section 2.2.2. 1.25 mM $CaCl_2$ was used in the studies. All MICs were identical those reported in literature.[2]

3.2.5 Preparation of LUVs

All the lipids used in this study were acquired from Avanti Polar Lipids (Alabaster, Alabama). Lipids include: 1,2-dimyristoyl-sn-glycero3-phosphocholine (DMPC), 1,2-dimyristoyl-sn-glycero-3phospho-(1′-rac-glycerol) (sodium salt; DMPG), 1,2-dioleoyl-sn-glycero-3-phosphocholine (DOPC), dioleoyl-sn-glycero-3-phospho-(1′-rac-glycerol) (sodium salt; DOPG), 1′,3′-bis[1,2dimyristoyl-sn-glycero-3-phospho]- sn-glycerol (sodium salt; TMCL), 1′,3′-bis[1,2-dioleoyl-sn-glycero-3-phospho]-sn-glycerol (sodium salt; TOCL), 1,2-dipentadecanoyl-snglycero-3phosphocholine (DPDPC), and 1,2-dimyristoleoyl-sn-glycero3-phosphocholine (DMPC-Δ9-Cis). The lipids were dissolved into chloroform and methanol (3:1) and were used without further purification. Liposomes were prepared via the extrusion method as described in section 2.2.3. Liposomes were used at a final total concentration of 250 μM total lipid in the various assays unless stated otherwise.

3.2.6 Monitoring daptomycin-membrane interactions by kynurenine fluorescence

The assay was conducted exactly like detailed in section 2.2.4.

3.2.7 Daptomycin membrane permeabilization monitored by pyranine fluorescence

The assay was conducted as described in section 2.2.5 with the exception that 2 mM dithionite was used. The increase in dithionite was required because with time dithionite degrades.[43] All experiments were run at 30 °C, except those shown in Figure 3-5 and 3-6 and , which were run at 37 °C. The results shown are the average of 6 independent experiments each.

3.2.8 Daptomycin membrane translocation assay

The assay was conducted exactly like detailed in section 2.2.6. In the experiments involving ionomycin, 100 nM ionomycin (Millipore-Sigma), 3 μM (2:1) native: NBD daptomycin, and 25 mM $CaCl_2$ were added to equimolar DOPC/DOPG liposomes and incubated for 15 minutes. In some experiments, 10 nM of the proton carrier carbonyl cyanide m-chlorophenyl hydrazone (CCCP) were also included. These conditions were chosen after consulting Erdahl *et al.* (1994).[49]

3.2.9 Daptomycin oligomer subunit stoichiometry

The assay was conducted exactly like detailed in section 2.2.7. The sole deviation from the protocol discussed in section 2.2.7 concerns the "low daptomycin" sample in Figure 3-6, Panel D, in which 2 μM rather than 10 μM of a mixture of native daptomycin and NBD-daptomycin (molar ratio, 2:1) were added to the liposomes in the first step, and 0.9 μM of native daptomycin was added in the second step to correct for inter-oligomer. All experiments we run at 37°C.

3.2.10 Diphenylhexatriene fluorescence polarization membrane fluidity assay

The phase transition temperatures of liposomes containing tetramyristoyl-cardiolipin (TMCL) or di-pentadecanoyl-phosphatidylcholine (DPDPC) were determined using the diphenylhexatriene polarization assay introduced by Shinitzky *et al.* (1974).[50] 1,6-Diphenyl-1,3,5-hexatriene (DPH; Millipore-Sigma) dissolved in methanol was added to liposomes in a 1 mL cuvette to a final concentration of 10 μM, followed by incubation for 10 min. For fluorescence anisotropy measurements, DPH was excited at 350 nm and emission measured at 428 nm. Data were acquired on a PTI QuantaMaster 4 instrument.

3.3 Results

3.3.1 Daptomycin interaction with chimeric liposomes

In the previous chapter, it was observed that dap binds to membranes composed of DO and PO lipid acyl tails at lower calcium concentrations than dimyristyl containing membranes. The avid binding was attributed to the looser packing of lipids within such membranes. The goal of this experiment was to determine whether the avid binding is caused by the oleoyl groups attached to the PC or PG headgroup; to test this dap's kynurenine signal was used to monitor dap's interaction with chimeric liposomes composed of either equal parts DOPC: DMPG or DMPC: DOPG.

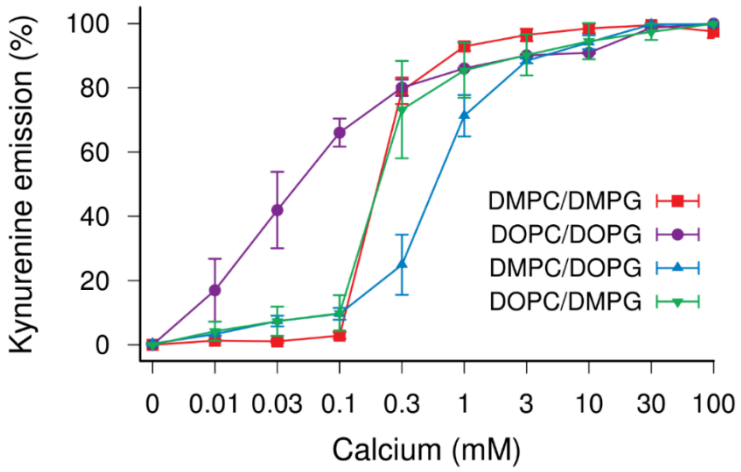

Figure 3-1. The effect of acyl tails on daptomycin binding to LUV membranes, measured by kynurenine fluorescence. The assay was conducted exactly a described in the previous chapter; samples contained 3 µM dap and 250 µM lipids (equal parts PC and PG).

Surprisingly, chimeric liposomes, those composed of equal parts DOPC: DMPG or DOPG: DMPC, require as much or more calcium for binding dap than observed with DMPC: DMPG liposomes. Overall, the data suggests that at physiological calcium concentrations dap interacts with all tested LUVs regardless of their lipid acyl tail composition. On liposomes containing mixtures of phospholipids, with bulky and non-bulky acyl tails, no preferential binding is observed.

3.3.2 Whose acyl tails are responsible for inhibition of pore formation; PC, PG, or both?

In section 2.3.2 it was reported that liposomes composed of equal parts DOPC: DOPG are not permeabilizated towards cations by dap. This raises the question whether oleoyl residues in either or

both of PC and PG are required for inhibition. To test this hypothesis, the pyranine-based pore forming assay was run on liposomes with the inhibitory oleoyl acyl tails attached to different headgroups.

As evident from Figure 3-2, the pyranine-based pore formation assay yielded the same results as reported previously; DMPC: DMPG liposomes are permeabilized by dap in a cation-selective fashion whereas liposomes composed of equal parts DOPC:DOPG are not. Interestingly, dap pore formation is inhibited regardless of whether the acyl tail is attached to PC or PG and is inhibited when as little as 10% DOPC is present in the membrane. The data suggests that the inhibition of dap pore formation by lipid acyl tails is not dependent on which lipid headgroup the inhibitory acyl tails is attached to, but inhibition simply occurs if that restrictive acyl tail is present in the membrane; it even occurs at concentrations as low as 10 mol%.

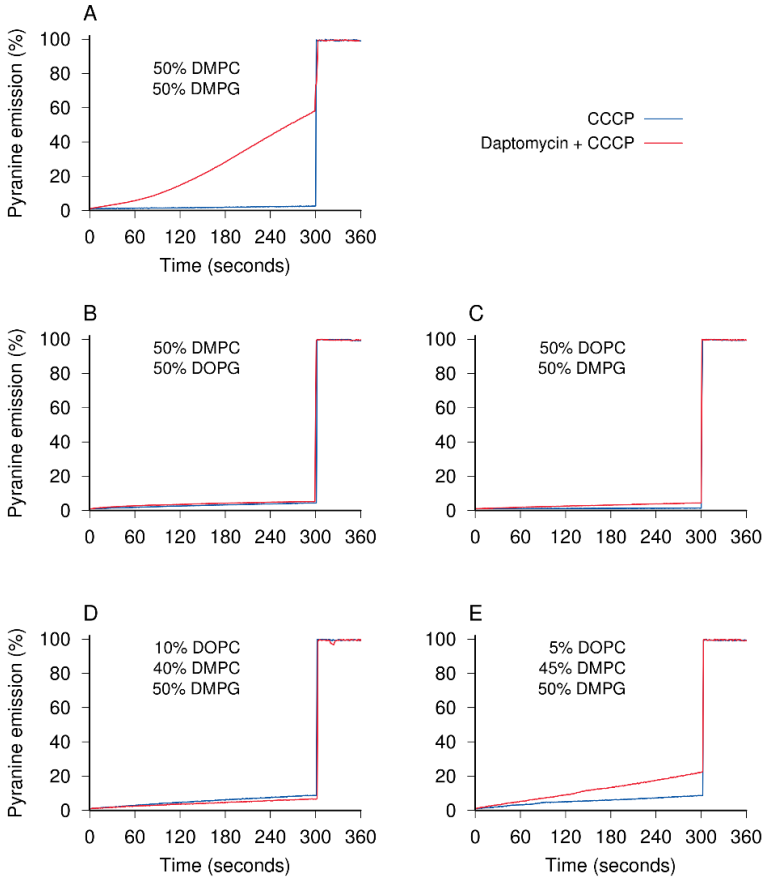

Figure 3-2. Daptomycin permeabilization of liposomes composed of varying amounts of DOPC:PG and DMPC:PG. The forming assay was completed as detailed in the previous chapter. The fluorescence signal was normalized to the average signal intensity observed after addition of Triton X-100 at 300 seconds.

3.3.3 Does inhibition of daptomycin pore-formation by 10% DOPC correlate with tetramer formation and consequently daptomycin sequestration?

In the last chapter it was proposed that phospholipid acyl tails with more than 14 carbons and unsaturation inhibit dap pore formation by not allowing octamers to form. The inability to form octamers consequently leads to asymmetric distribution of dap between the membrane leaflets. The purpose of this work was to determine whether liposomes containing 10% DOPC, 40% DMPC, and 50% DMPG inhibit pore formation via a similar mechanism, or whether they might permit formation of a complete yet functionally deficient octamer. Initially, the FRET-based stoichiometry assay was used to determine the number of dap molecules per dap oligomer formed on 10 mol% DOPC liposomes, and subsequently the dithionite-based translocation assay was run to determine dap membrane distribution.

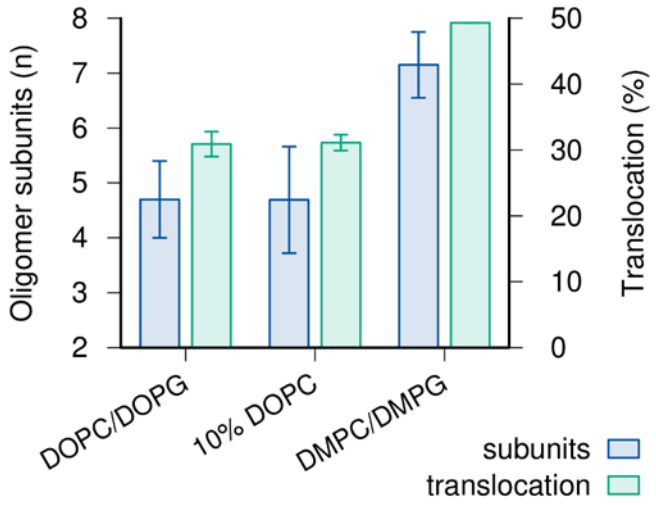

Figure 3-3. Translocation and subunit stoichiometry of daptomycin oligomers on 10% DOPC liposomes. The assays were conducted as detailed in the previous chapter. The DMPC: DMPG data were adapted from Zhang *et al*. (2014) .[20]

Figure 3-3 suggests that 10% DOPC in a background of permissive lipids (DMPC:DMPG) inhibits dap cation-selective pore formation via the same mechanism as observed with pure DOPC:DOPG liposomes; on both types of inhibitory liposomes tetramers are formed, and more than 50% of the NBD signal instantaneously disappears upon addition of dithionite. Overall, it seems that the phospholipids with increased acyl tail length and/or unsaturation do not allow for the formation of octameric dap oligomers, even if they constitute only 10% of the total lipid. The inability to form octameric oligomers

allows them to continue freely equilibrating between leaflets with a preference to the outer membrane leaflet.

Further, it was considered that the distribution of dap across the two membrane leaflets might not have reached equilibrium at the time of the measurement. To test for this possibility, the translocation assay was repeated with dap-treated liposomes that were incubated for longer than 5 minutes (15 minutes- see Figure 3-4 DOPC: DOPG) before addition of dithionite. Regardless of pre-incubation time, roughly 70% of the NBD signal disappeared upon dithionite addition suggesting that all samples, including those shown in Fig. 3-3, had indeed reached equilibrium.

3.3.4 The effect of intraliposomal calcium on daptomycin translocation

The asymmetrical distribution of dap on membranes containing phospholipids with acyl tails inhibitory to dap cation-selective pore formation could be due to the lack of intra-liposomal calcium. In all experiments with LUVs, calcium is added to the buffer only, but not contained inside the LUVs, because membrane extrusion of MLVs does not work its presence. However, dap can transport calcium ions across membrane bilayers, which means that it will be present on both sides of permissive membranes.[32,42] On the other hand, membranes containing acyl tails that inhibit dap permeabilization will likely not have calcium transported into their intraliposomal space. Consequently, it is possible that calcium stabilizes and retains daptomycin on the inner membrane leaflet on susceptible, but not on impervious membranes. Evaluating this hypothesis directly is very difficult because extrusion does not work well at high calcium concentrations. It is possible to use detergent-based methods to create calcium containing liposomes; the problem with these methods is that no matter how much time is spent removing the detergent, after liposome creation, some residue of detergent remains.[51] Considering the sensitivity of dap to its membrane environment that is not a risk worth taking.[3,13] Hence, it was decided to introduce calcium into the intraliposomal space by treating DOPC: DOPG liposomes with the calcium ionophore ionomycin.[49] After a period of incubation with ionomycin, to allow for calcium influx, NBD-dap could be added to the calcium-loaded liposomes and translocation determined. Together with ionomycin, the proton ionophore CCCP was also added to facilitate compensation of the electrogenic calcium flux.[49] It is expected that if calcium does play a role in dap's distribution between membrane leaflets, then distribution of dap on DOPC: DOPG liposomes leaflets would become less asymmetrical.

As evident from Figure 3-4 the presence of intraliposomal calcium does not seem to change the distribution of dap on equal part DOPC: DOPG membranes. This suggests that the asymmetrical distribution of dap on inhibitory membranes is not caused by a lack of calcium on the inner membrane leaflet.

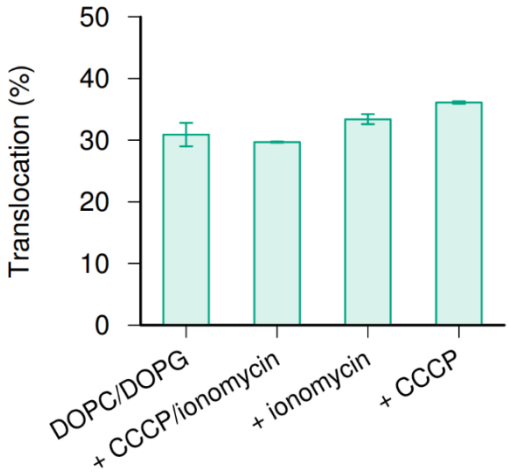

Figure 3-4. Effect of intra-liposomal calcium on daptomycin distribution on equal part DOPC: DOPG membranes. The assay utilized 250 µM DOPC: DOPG liposomes with or without the calcium ionophore ionomycin (100 nm) and/or CCCP (5nm). Controls with ionomycin and CCCP alone yield results identical to those obtained on DOPC: DOPG LUVs. Dithionite was added 15 minutes after incubation with ionomycin or addition of dap.

3.3.5 Is dap pore formation inhibition caused by lipid acyl tail unsaturation or increased acyl tail length?

In previous experiments, dap pore formation was observed on membranes containing phospholipids with myristoyl acyl tails and not observed on membranes containing phospholipids with oleoyl acyl tails. The inhibitory oleoyl acyl tails are 4 carbons longer than myristoyl acyl tails and have a cis double bond. The purpose of the following set of experiments was to determine which of the two structural distinctions between myristoyl and oleoyl acyl tails causes the inhibitory effect. To test this the pyranine-based pore formation assay was conducted on liposomes composed of 10% di-pentadecanoyl-phosphatidylcholine (DPDPC), 40% DMPC, and 50% DMPG or 10% 1,2-dimyristoleoyl-sn-glycero3-phosphocholine (DMPC-Δ9-Cis), 40% DMPC, and 50% DMPG.

Figure 3-5 shows that pyranine's emission at 510 nm increases significantly more on liposomes containing 10% DMPC-Δ9-Cis than 10% DPDPC. This suggests the inhibition of dap cation-selective

pore formation is primarily caused by increased acyl tail length (see Figure 5 Appendix B for determination of DPDPC membrane phase transition temperature). The assay with DPDPC was run for 60 seconds shorter than the other assays because the liposomes had poor stability with increasing time and the 300 second assay gave the most reproducible results. Although DPDPC is not a biologically relevant acyl tail, it was chosen instead of a biological relevant acyl tail because of its comparatively low phase transition temperature, which means that the LUVs should be in the fluid phase at the assay temperature.[13,52]

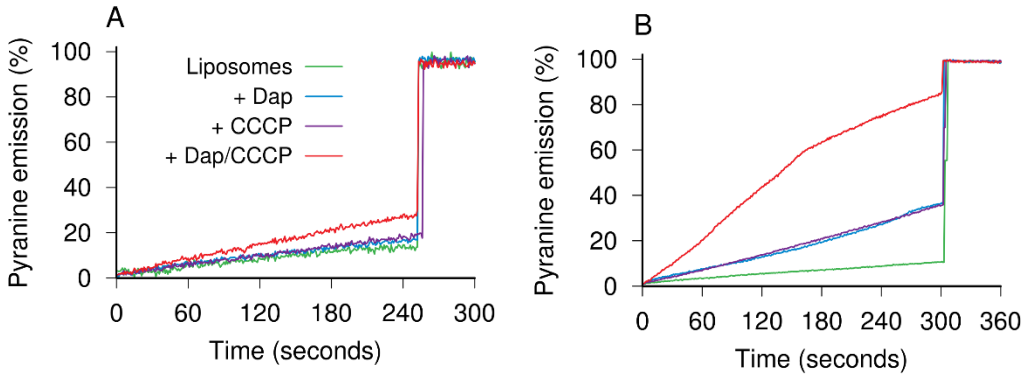

Figure 3-5. Determining whether daptomycin pore formation inhibition is caused by acyl tail length or unsaturation. The pyranine-based pore formation assays were completed as detailed in chapter 2; the results shown in panel A were obtained on 10% DPDPC, 40% DMPC, and 50% DMPG LUVs, and the results in Panel B were obtained on 10% DMPC-Δ9-Cis, 40% DMPC, and 50% DMPG LUVs.

3.3.6 Revisiting inhibition of dap pore formation on cardiolipin membranes

Zhang *et al.* (2014) showed that membranes containing as little as 10% tetra-oleoyl cardiolipin (TOCL) inhibit dap pore formation by sequestering dap to the outer membrane leaflet.[20] The issue with this finding is that Zhang *et al.* (2014) did not know, at the time, that oleoyl acyl tails are inhibitory to dap pore formation. Naturally, it is important to establish whether the inhibitory effect observed on membranes containing TOCL was caused the oleoyl lipid acyl tails or the CL headgroup moiety. To distinguish the contributions of the CL head group from that of the oleoyl side chains pyranine-based pore formation, FRET-basedsubunit stoichiometry, and dithionite/NBD-dap-based translocation assays were run on membranes containing 10% tetra-myristyl cardiolipin (TMCL), 40% DMPC, and 50% DMPG.

Before conducting any of the functional assays it was important to determine the phase transition temperature of TMCL containing membranes because model membrane composed purely of TMCL have a phase transition temperature of 47 ºC.[52] The phase transition temperature of the membranes was determined by using the fluorescent probe DPH; due to its hydrophobic nature DPH inserts into membranes and as the membrane transitions from the gel phase to the liquid crystalline the fluorescence anisotropy of DPH decreases.[53] This temperature-dependent decrease in anisotropy can then be plotted, and the phase transition temperature of the membrane discerned. Figure 3-6 Panel A shows that membranes containing 20% TMCL, 30% DMPC, and 50% DMPG are largely in the liquid crystalline phase when at 37 ºC.

Once the phase transition temperature was determined an attempt was made to run the pyranine-based pore forming assay on membranes containing 20% TMCL. Unfortunately, the 20% TMCL LUVs eluted from the size exclusion column without retaining any encapsulated pyranine; it is likely that 20% TMCL liposomes are unstable and therefore fell apart in the column because of this finding it was decided to try using 10% TMCL containing LUVs. The DPH assay showed that these LUVs were also in a liquid crystalline phase by 37 ºC. The pyranine-based pore forming assay worked quite well (Figure 3-6 Panel C); it was observed that at 2 μM dap 10% TMCL containing LUVs inhibit dap pore formation. This finding supports the conclusions of Zhang *et al.* (2014), namely that the CL heasgroup has inhibitory activty.[20] The oligomer subunit stoichiometry and translocation assays were also run in order to ascertain if 10% TMCL containing membranes inhibited dap pore formation via the same mechanism as observed on 10% TOCL membranes. The results in Figure 3-6 Panel D show that the subunit stoichiometry and translocation results obtained on 10% TMCL membranes resemble those obtained on equal part DOPC: DOPG and 10% DOPC, 40% DMPC, and 50% DMPG LUVs. This suggests that the inhibition of pore formation by 10% TMLC membranes occurs via the same mechanism as inhibition on DOPC: DOPG membranes.

Similar experiments were carried out at 10 μM dap. At this concentration, dap easily permeabilizes inhibitory membranes even without the presence of CCCP suggesting that at high concentrations dap can transport protons. The subunit stoichiometry and translocation data mirror the pyranine-based pore forming assay results as the subunit stoichiometry increases and the distribution of dap between membrane leaflets is much less asymmetrical at higher dap concentrations.

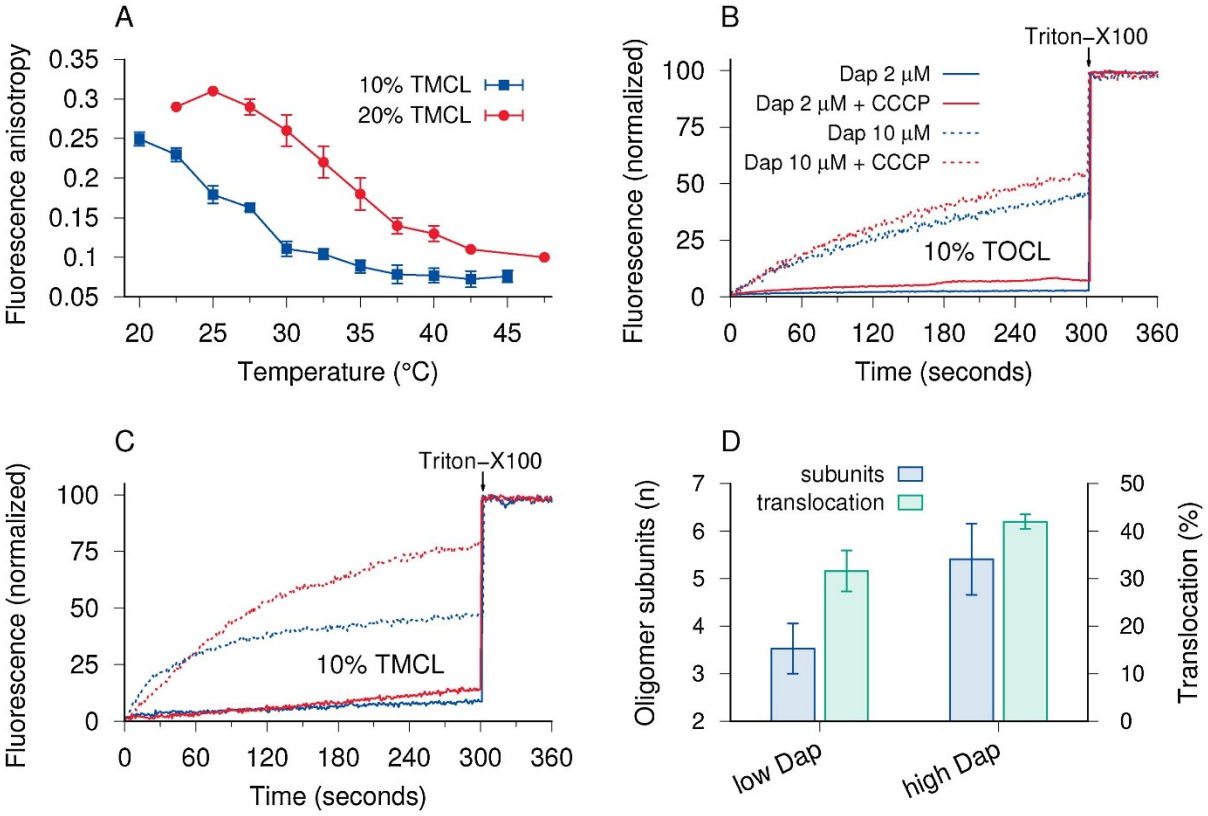

Figure 3-6. Determining the inhibitory effect of CL on daptomycin pore formation. Panel A shows the DPH assay for membrane fluidity. Panel B shows the pyranine-based pore forming assay results on 10% TOCL LUVs. Panel C shows the pyranine-based pore forming results on 10% TMCL LUVs. Panel D details the experimental results of the oligomer subunit stoichiometry and translocation assay results at different dap concentrations on 10% TMCL containing LUVs.

3.3.7 Is inhibition of dap by lipid acyl tails influenced by the nature of dap's own acyl tail?

Research by Debono *et al.* (1988) showed that dap analogs with longer and branched acyl moieties had increased antimicrobial activity. The purpose of this experimental work was to determine whether these modifications would allow to observe cation-selective pore formation on membranes that were found to be impervious to permeabilization by dap with a decanoyl moiety.

To answer this question two dap derivatives were made, and their pore forming ability was tested by the pyranine-based pore forming assay. C_{14} dap has the decanoyl fatty acid tail replaced with a myristoyl fatty acid tail and ante-dap has an ante-iso dodecanoyl acyl tail instead.

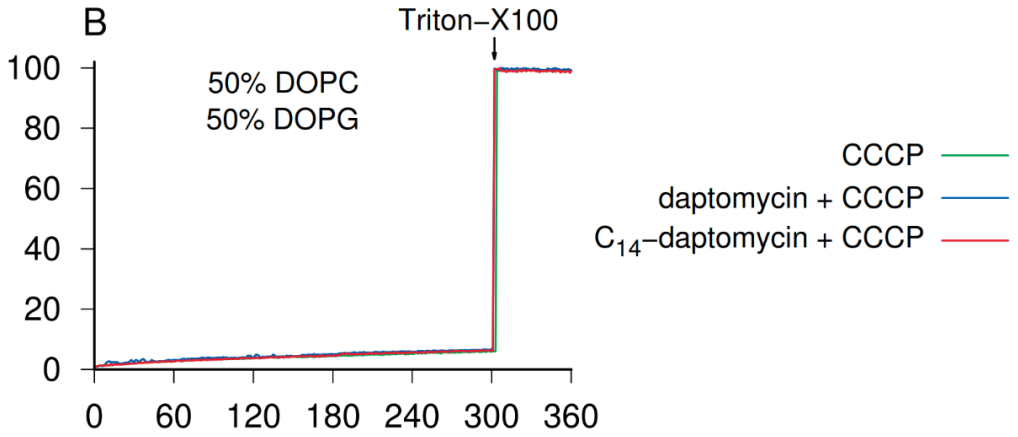

Figure 3-7. C_{14}-daptomycin permeabilization of DOPC: DOPG LUVs. The assay was completed as detailed in the previous chapter.

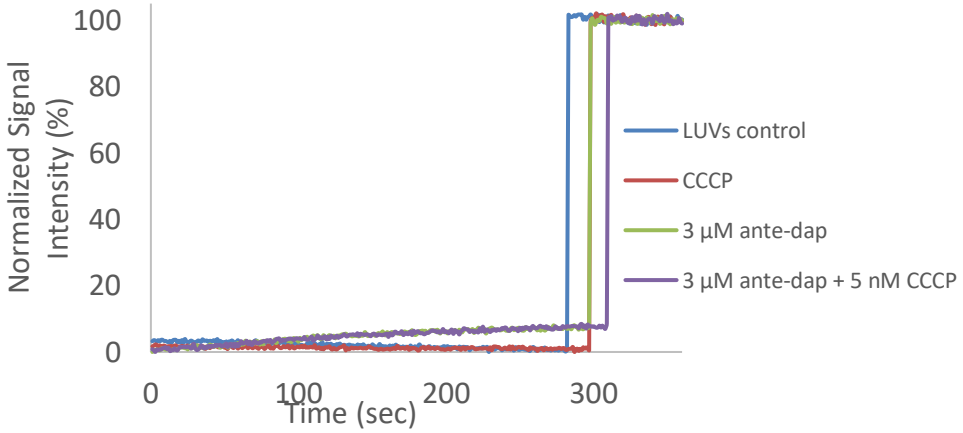

Figure 3-8. Ante-daptomycin cation-selective permeabilization of DOPC: DOPG LUVs. The assay was completed as detailed in the previous chapter. The curves are offset by 10 seconds to minimize line overlapping.

As evident from Figure 3-7 and 3-8 at low concentrations (3 µM) neither derivative of dap formed cation-selective pores on DOPC: DOPG LUVs. Overall, because this study was not exhaustive it cannot be argued that dap acyl tail moiety branching, or increased length might not overcome the inhibitory effects of DOPC: DOPG membranes.

3.4 Discussion

This chapter focused on analyzing in greater detail how the mechanism of how phospholipid acyl tails modulate dap's action mode in geater detail. Through this work it was found that:

- Oleoyl acyl tails inhibit dap pore formation regardless of the headgroup moiety they are ligated to.
- Inhibition of dap pore formation by oleoyl acyl tails is correlated with increased acyl tail length rather than lipid acyl tail unsaturation.
- Inhibition of dap cation-selective pore formation occurs on membranes with low concentrations of oleoyl acyl tails (10 mol%).
- Additionally the findings made by Zhang *et al.* (2014) regarding the ability of cardiolipin to inhibit dap cation-selective pore formation were confirmed; the CL headgroup does indeed inhibit dap's ability to permeabilize membranes.[20]
- In all the cases it was observed that phospholipid inhibition of dap cation-selective pore formation was caused the ability of oleoyl acyl tails to restrict dap octamer formation. The lack of octamer formation resulted in asymmetrical distribution of dap tetramers on membrane leaflets with most of the dap's tetramers are located on the outer membrane leaflet.

It is important to point out that the correlation between increased acyl tail length and inhibition of dap's action mode corresponds to *in vivo* findings. Both Hines *et al.* (2017) and Boudjemaa *et al.* (2018) observed, by mass spectroscopy lipidomic analysis, that clinically derived dap resistant bacteria have higher proportions of phospholipids with increased acyl tail length.[54,55] Directly comparing *in vivo* and *in vitro* results is cautioned as the model system of this study does not match the complexity of a bacterial membrane. Future experimental work could focus on corroborating the above findings on a membrane system more closely resembling a bacterial cytoplasmic membrane.

Lastly, in the first chapter of this thesis, it was mentioned that Seydlová *et al.* (2018) observed dap cation-selective pore formation to be dependent on membrane potential. Seydlová *et al.* (2018) began their conductance experiments with a membrane potential of 10 mV, and subsequently increased it by regular increments until they reached the physiological value of 150 mV; as they increased the membrane potential to 150 mV, they observed a concomitant increase in the number of dap molecules per pore, the pore diameter, and accordingly the rate of cation transport through the pore. Based on their data and subsequently its analysis, Seydlová *et al.* (2018) concluded that dap's cation-selective

pore consists of an octameric oligomer composed of two tetrameric oligomers conjoining across opposing membrane leaflets.[16] Their findings mirror those of this study, but the reader must be cautioned to not directly compare them for two reasons; firstly Seydlová *et al.* (2018) conducted their experiments on membranes composed purely of diphytanoyl-PG (PG with two saturated and highly branched acyl tails), and the observation that a membrane potential may facilitate dap pore formation on membranes that are not permeabilized in its absence is important. It seems possible that the membranes that were found to be resistant to dap under the conditions of this study would also have been permeabilized by it in the presence of a membrane potential.[16]

Chapter 4

Characterization of lipid nanodiscs as a membrane model for structural studies on membrane-bound daptomycin[4]

Abstract: Although dap itself was discovered nearly 40 years ago; its membrane-bound structure remains unknown. Several attempts have been made to determine the structure by solution-state nuclear magnetic resonance, but they failed because no membrane mimetic possessing all the required physiochemical properties could be found. This study investigates the suitability of lipid nanodiscs stabilized by styrene-maleic acid co-polymers for structural studies on dap's membrane-bound structure by solution-state NMR. Through the course of this work, it was observed that nanodiscs with a diameter small enough for solution-state NMR studies could be formed from equal DMPC: DMPG MLVs in the presence of 3 mM calcium. These nanodiscs had physiochemical properties remarkably similar to those observed on LUVs with the same phospholipid composition. Unlike a previously characterized bicelle system of similar lipid composition, the nanodiscs did not precipitate upon addition of calcium and dap (100 μM) and allowed for dap oligomerization. ^{1}H-NMR studies showed that dap, indeed, binds to the nanodiscs, and yields spectra of sufficiently high resolution for structure determination. Overall, the styrene-maleic acid co-polymer stabilized lipid nanodiscs were found to be a promising system for determining dap's membrane-bound oligomeric structure.

4.1 Introduction

Dap's action mode remains partially contested because its membrane-bound structure has yet to be solved at an atomic level of resolution. Previous attempts to determine the membrane-bound structure by solution-state NMR have either utilized membrane mimetics lacking PG or were done in the absence of calcium. It is well established that both PG and calcium are required for dap to form oligomers,

[4] The experimental work presented in this chapter was done solely by the author of this thesis. The experiments were designed by the author of this thesis, Dr. Michael Overduin, Dr. Thorsten Dieckmann, and Dr. Michael Palmer. The polymers were a gracious gift from the lab of Dr. Michael Overduin currently at the University of Alberta. Lastly, we thank Dr. Scott Taylor and his laboratory for the synthesis of NBD-dap.

which are in turn necessary for bactericidal activity, and the authors of those studies acknowledge that conducting experiments in the absence of PG and/or calcium will not yield biologically relevant structures, but they believe that some structural information is better than none.[37] They were forced to take this course of action because previous studies found that at upon mixing of dap, calcium, and a PG containing membrane mimetic at concentrations required for solution-state the spectra had significant linewidth broadening and were consequently useless for structure determination.[37] Unpublished studies by the Palmer and Dieckmann groups at the University of Waterloo, also found that at concentrations required for solution-state NMR studies, dap, calcium, and PG instantaneously precipitate.[56]

While other structural elucidation methods, like X-ray crystallography, could be used to determine the structure solution-state NMR is preferred because it is the only methodology that allows for experiments to occur at temperatures that maintain membranes in the fluid liquid crystalline phase. Determining the structure on fluid membranes is important because acquisition of the most biologically relevant data is desired. The importance of maintaining a semblance of *in vivo* conditions is underscored by the work presented in the previous two chapters, which strongly suggests that dap's membrane-bound conformation is sensitive to its surrounding membrane environment.[13,57]

Ultimately, solving dap's membrane-bound structures requires finding a membrane-mimetic that contains PG, remains soluble, and does not aggregate after formation of the dap, calcium, and PG complex. The purpose of the work presented in this chapter was to assess if lipid nanodiscs stabilized with SMA copolymers meet these requirements, and could therefore be used for the determination of dap's membrane-bound oligomeric structure, at the atomic level, by solution-state NMR.[58]

4.1.1 Membrane-associated peptide/protein structure determination by solution-state NMR

Determining the atomic level structure of almost any membrane-associating protein or peptide by solution-state NMR is an arduous task, and for two reasons: firstly solution-state NMR spectral resolution is dependent on the size of the molecule or assembly being studied, and second solution-state NMR has limited sensitivity and thus requires high sample concentrations.[59,60] Solution-state NMR spectral resolution is dependent on peak linewidth, which is inversely proportional to spin-spin relaxation time; spin-spin relaxation time (T_2) describes how fast transverse magnetization de-phases.

The rate at which dephasing occurs is inversely proportional to the rotational correlation time (τ_c) of the molecule being studied.[60,61] For proteins τ_c can approximated by treating the protein as a sphere, whose τ_c is described by Stokes-Einstein equation:

$$\tau_c = \frac{4\pi r^3 \eta}{3K_b T}$$

where r is the radius of the protein, K_B is the Boltzmann constant, T is temperature, and η is the viscosity of the solvent.[59] The equation above shows that larger proteins yield spectra with broader linewidths. The size constraint of solution-state NMR becomes an issue for highly soluble proteins with a molecular weight greater than 60 kDa, as at 60 kDa the protein's radius is too large; thus, giving rise to long τ_c and significant line broadening.[60]

Determining the structure of a 60 kDa membrane-associating protein by solution-state NMR is even more difficult. Not only is the 60 kDa membrane-associating protein itself approaching the size limit of solution-state NMR, but obtaining a biologically relevant structure requires the use of membrane bilayer.[62] Membrane bilayers, on their own without embedded protein, have diameters far too large for NMR structural studies; embedding proteins into them further increases their diameter. Since the proteins embed themselves into the bilayer their effective τ_c is now equal to τ_c of the protein-lipid complex, which is long, resulting in spectra with broadened peaks from which little information, structural or otherwise, can be gleaned.[59]

Additionally, solution-state NMR is an inherently insensitive technique. One way to overcome the lack of sensitivity is to use high protein/peptide concentrations. With membrane-associating proteins and peptides this rarely works because at high concentrations the protein-lipid complex frequently precipitates.[60]

4.1.2 Previous attempts to determine dap's membrane-bound structure

Determining dap's oligomeric structure by solution-state NMR was previously hampered because at concentrations required for solution-state NMR spectra, daptomycin, calcium, and PG formed complexes that had large diameters, which consequently yielded spectra unusable for structure determination.[37,56] To circumvent complex formation, attempts were made to determine the structure on membrane mimetics lacking PG; it was hoped that less line broadening would be occur:

For example, structure determination experiments were conducted utilizing micelles composed of 1,2-diheptanoyl-sn-glycero-3-phosphocholine (DHPC).[37] The determined structure was found to be like

that of apo-daptomycin (no calcium bound). The lack of a major conformational change in the structure suggests that these micelles do not sufficiently mimic susceptible membranes. The first issue with using exclusively DHPC containing micelles is that there is a complete lack of PG. Consider the CD studies that show daptomycin to undergo a major conformational change upon binding PG, and the experiments by Muraih *et al*. (2011), in which oligomer formation was observed to occur only in the presence of PG.[6,9] Combining the findings from these two experiments allows one to state that PG is required for dap to undergo a change in conformation, therefore, removing PG makes any structure determination experiments futile. Furthermore, DHPC has extremely short acyl tails, and consequently the monomeric membrane-bound daptomycin will still be partially in solution, and the determined structure will not be representative of dap's membrane-bound state.

Attempts were made to determine dap's structure on PG containing micelles, but at the concentrations required for solution-state NMR dap, calcium, and the PG containing micelles precipitated out of solution.[56]

4.1.3 Styrene-maleic acid co-polymers

It is evident that previous attempts to solve dap's structure failed because it was not possible to circumvent the two major obstacles of solution-state NMR: its low sensitivity and size restrictions. The low sensitivity forced experimenters to use millimolar concentrations of dap that resulted in precipitation issues on biologically relevant membranes, and the size limitations forced the use of a poor membrane mimetic, just because it was the only system with a sufficient τ_c.[37,56] Ultimately, solving dap's structure requires either increasing the sensitivity of NMR, no small task, or finding a membrane mimetic that has a short τ_c and remains soluble at concentrations of dap, calcium, and PG sufficient for solution-state NMR structural studies.

Literature about the recently developed styrene-maleic acid (SMA) co-polymer-based membrane nanodisc system suggests that it possess all the qualities required to determine dap's membrane-bound structure. The polymer converts proteo-liposomes and other membrane-protein containing membrane systems into small protein containing bilayer cylinders enveloped by SMA polymer.[63] Such nanodiscs have a diameter less than 20 nm, which is small enough to obtain legible solution-state NMR spectra. The polymer is quite promiscuous converting almost any membrane system to nanodiscs, the nanodiscs have physiochemical properties similar to natural membranes, and the protein containing nanodiscs are highly soluble at high protein concentrations; the solubility is due to the presence of numerous maleic acid moieties.[58,63]

4.1.3.1 Action mode of Styrene-maleic acid co-polymers

SMA co-polymers act as scissors by dicing up large membranes into monodisperse nano-sized circular bilayers.[63,64] The co-polymers are linear chains composed of repeating units containing styrene and maleic acid moieties; the arrangement of styrene and maleic acid within a monomeric unit is dependent on the synthesis method (see Figure 4-1, Panels A and B).[58] It is proposed that SMA co-polymers form lipid nanodiscs via a three-step mechanism [65]:

1. The polymer initially binds the membrane in a concentration-dependent fashion. The binding is driven by hydrophobic interactions between the styrene moieties of the polymer and the lipid acyl tails of the membrane. Monolayer membrane experiments show that the hydrophobic interactions are so energetically favorable that they compensate for any unfavorable electrostatic interactions between the maleic acid and anionic lipids in the membrane.[65]

2. After initial binding the polymer inserts deeper into the membrane. Optimal insertion is observed at the membrane's T_m; it is presumed that at T_m the lipids are segregated into fluid and gel patches giving rise to lipid packing irregularities. These packing irregularities are thought to facilitate polymer penetration into the bilayer. Once inserted into the bilayer the process of solubilization begins; the process is kinetically driven as it can be sped up by increasing temperature.[65]

3. The last step of the process involves the polymer completing membrane solubilization and nanodisc formation. As mentioned earlier, structural studies of SMA co-polymer stabilized lipid bilayers found that circular nanodiscs are formed (see appendix C for a schematic of a SMA stabilized nanodisc). The circular structure arises because the styrene moieties intercalate between the lipids. The intercalation of the styrene moieties into the bilayer decreases styrene electrostatic shielding on the polymer backbone; consequently Coulombic repulsion between maleic acid moieties causes the polymer to become curved.[65]

4.1.3.2 Types of Styrene-maleic acid lipid co-polymers

There are a vast variety of styrene-maleic acid co-polymers that can be used to make lipid-containing nanodiscs. For each situation, the polymers are engineered to provide optimal performance (see Figure 4-1, Panel A). Generally, polymers are produced by one of two methods: either by conventional radical polymerization or reversible addition fragmentation chain transfer. The method of synthesis has been found to regulate polymer chain length and the arrangement of styrene and maleic acid within a monomeric unit (see Figure 4-1, Panel B).[66] The optimal ratio of styrene to maleic acid moieties within a polymer is between 2:1 and 3:1; at these ratios the polymer has enough hydrophobic character to interact with the membranes while remaining soluble over a broad pH range. Additionally, the carboxylic acid side chains of maleic acid can be modified to change the pH profile in which the polymer functions, and also limit chelation of divalent cations (see Figure 4-1, Panel A).

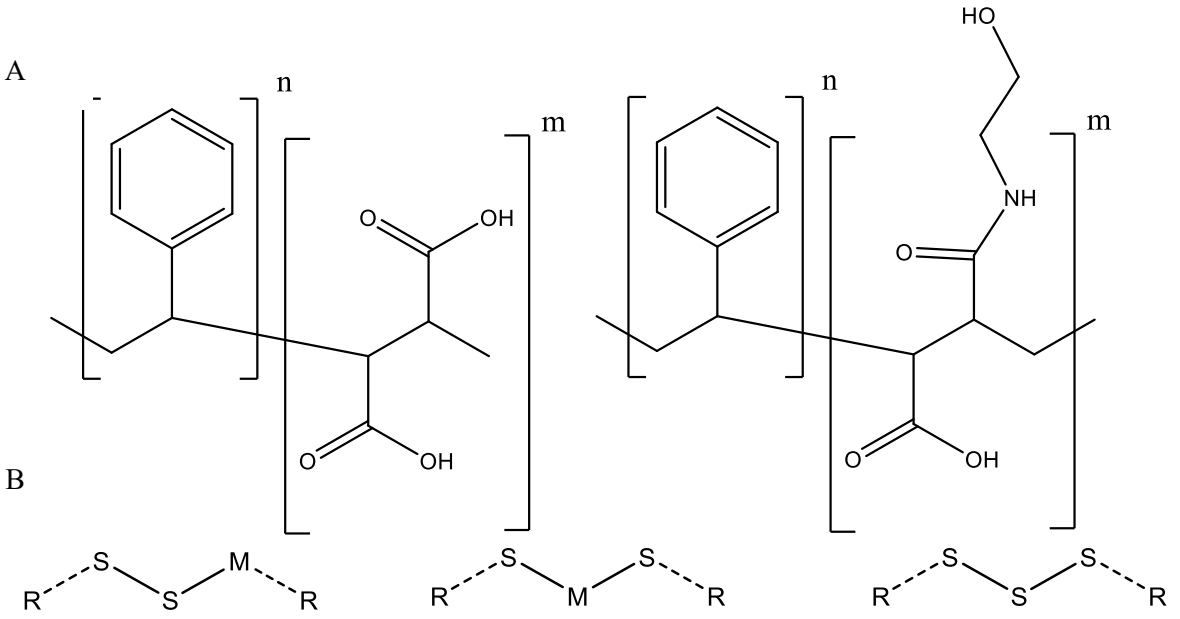

Figure 4-1. Structures of styrene-maleic acid co-polymers. Panel A shows the monomeric units of two types of SMA co-polymers: the one of the left is the generic SMA co-polymer with n usually equal to 2 and m equal to 1, and the one on the right being a low cation chelating SMA co-polymer with ethanolamine ligated to one of the two carboxylic acid side chains. Panel B shows possible arrangements of styrene (S) and maleic acid (M) within a monomeric unit of the polymer; these depend on the synthesis methodology used to create the polymer.

The next two sections discuss the factors thought to influence the formation and properties of nanodiscs. The discussion is broken into two parts; the first deals with the effects of lipid composition on nanodisc formation, and the second part details how polymer design influences nanodiscs properities. While

nanodisc formation is likely influenced by both factors at the same time, here they are discussed in isolation because their combined effects on nanodiscs formation have not be studied systemically.

4.1.3.3 Effect of lipid acyl tails on nanodisc formation

One of the first things that was done when the SMA polymers were first developed was to determine whether membrane composition influences nanodisc formation. Experiments by Arenas *et al.* (2016) studied SMA solubilization kinetics by ^{31}P solution-state NMR and nanodisc size by dynamic light scattering.[67] They found that when membranes, composed either purely of POPC or 70 mol% POPC/ 30 mol% 1-palmitoyl-2-oleoyl-sn-glycero-3-phosphoethanolamine (POPE), were treated with excess polymer the resulting nanodisc size was the same.[67] They do state that their polymers bind membranes containing lipids with smaller headgroups (30 mol% POPE) more avidly, but take longer to solubilize them into nanodiscs.[67] Their finding suggests that phospholipid headgroups do not influence nanodisc diameter. Scheidelaar *et al.* (2015) found that acyl tail length and unsaturation do not influence nanodisc size but do affect solubilization kinetics.[65]

4.1.3.4 Effect of SMA architecture on nanodisc diameter

One of the most important things when designing polymers with the intention of using the resulting nanodiscs in solution-state NMR studies is to engineer the polymer is such a fashion that the nanodiscs have a suitable diameter. Unfortunately, how SMA polymer architecture determines nanodisc diameter is not well understood; such is the situation because studies on this topic are not systematic – they are carried out on different polymers.[65]

The effect of polymer architecture on nanodisc diameter was investigated. Smith *et al.* (2017) treated membranes with excess concentrations of variable length SMA and tested the resulting nanodisc diameter by size exclusion chromatography. They observed no correlation, positive or negative, between polymer length and nanodisc size.[66] Interestingly, the number of styrene residues per unit length, and the polymer to lipid ratio can be used to control nanodisc diameter.[55,57,58] Craig *et al.* (2016) found that at similar polymer concentrations, polymers with different ratios of styrene and maleic acid per monomeric unit produced nanodiscs of various sizes.[68] Smith *et al.* (2017), conducted similar studies and propose that the conformation of the polymer in solution influences the rate at which membranes are solubilized; polymers with less hydrophobic character are not clumped in solution, which allows them to better penetrate the membrane and thus have a greater rate of solubilization.[66]

Lastly, Hall *et al.* (2018) observed that increasing the polymer to lipid ratio can be used to decrease nanodisc size.[69] Hall *et al.* (2018) suggest that as polymer concentration increases the number of nanodiscs. While they do not explain why the number of nano-discs increases concomitantly with polymer concentration, it is likely that the size/number of nanodiscs self-adjusts such that the overall collective hydrophobic surface of lipid molecules that is in contact with the polymer matches that of the polymer itself; therefore, as polymer concentration increases it can cover increasing hydrophobic area.

The mono-dispersity of nanodisc size suggests that all nanodiscs contain roughly the same numbers of lipids. It is likely that whilst forming the nanodiscs are undergoing lipid exchange through fusion and fission processes in order to reach an equilibrium distribution of lipids. In addition because the system wants to obtain the most favorable Gibbs free energy (achieved by forming more nanodiscs) the exchange of lipids between nanodiscs continues until the largest possible number of nanodiscs is formed; achieving this requires that each nanodisc contain the minimum has a decreased diameter.[69]

All the trends discussed in this section were obtained from experiments in which only the ratio of polymer to lipid was varied; pH, temperature, and buffer/salt concentration remained constant. This is highly important because pH, temperature, and buffer/salt concentrations have been shown to affect SMA activity.[58]

4.1.3.5 Effects of pH, temperature, and salt concentration on SMA solubilization activity

It is very important to consider the pH at which an SMA co-polymer will be used.[58] It has been shown that the maleic acid moieties on SMAs have their first pKa between 4 and 6 and their second pKa between 8.6 and 9; the exact values are dependent on the styrene content in the polymer.[70] Working at a low pH, where the maleic acids are not charged, will lead to polymer aggregation and precipitation. Working at too high a pH, where all the maleic acids are ionized, is also detrimental because the polymer will not bind to membranes due to electrostatic charge repulsion. Therefore, it important to fine tune the pH to obtain minimal polymer clumping whilst also not making interactions with membrane too electrostatically unfavorable.[70]

The role of temperature was alluded to earlier in section 4.1.3.1. It is generally accepted that nanodiscs form best when polymer is added to lipid bilayers at their phase transition temperature. At

this temperature, patches of fluid and gel-state bilayer coexist, and the borders between them give rise to cracks in the membrane. These cracks facilitate the polymers' insertion into the membrane.[65]

The effects of buffer and salt concentration on polymer activity have also been well studied. Generally, binding of polymers to membranes requires salt; salt reduces electrostatic repulsion between them through Debye charge screening.[70] Care must be taken when working with cations such as magnesium and calcium because the maleic moieties chelate these cations forming a hydrophobic complex that rapidly crashes out of solution.[58] There are new SMA derivatives with reduced polymer chelation; in these polymers the maleic acid carboxylic moiety is ligated to something like ethanolamine (see Figure 4-1 Panel A).[58]

4.2 Materials and Methods

4.2.1 Preparation of MLVs and nanodiscs

Lipids used to make MLVs were acquired from either Avanti Polar Lipids (Alabaster, Alabama) or Larodan (Slona, Sweden). Lipids included 1,2-dimyristoyl-sn-glycero-3-phosphocholine (DMPC), 1,2-dimyristoyl-sn-glycero-3-phospho-(1'-rac-glycerol) (sodium salt; DMPG; from Larodan), 1,2-dioleoyl-sn-glycero-3-phosphocholine (DOPC), and dioleoyl-sn-glycero-3-phospho-(1'-rac-glycerol) (sodium salt; DOPG). MLVs preparation was adopted from Skoza *et al.* (1980).[71] The requisite amounts of lipids – equimolar mixtures of PC and PG were used in each case – dissolved in chloroform/methanol (3:1) and dried under N_2 in a round-bottom flask. After removal of chloroform, the film was placed on a high vacuum overnight. The resulting lipid film was resuspended in pH 7.4, 10 mM HEPES (Biorad), and 25 mM NaCl buffer (HBS). The resulting lipid suspension was vortexed at 24ºC intermittently over a 1-hour period. MLVs were used at a final total concentration of 250 μM total lipid in the various assays unless stated otherwise.

MLVs suspended in HBS were treated with polymer; the ratio of polymer to lipid was ranged from 3:1 to 12:1 wt/wt%. The polymer was added dropwise. After polymer addition the sample was incubated at 28 ºC for 1 hour. The polymer used in these studies was a gift from the laboratory of Dr. Michael Overduin. The structure of the polymer or its name cannot be divulged at this time as the polymer is subject to a pending patent application. In this thesis, the polymer will be referred to as simply polymer. 3, 9 and 12 polymer equivalents were used because of literature precedence.[72]

4.2.2 Dynamic Light Scattering (DLS)

Dynamic light scattering measurements were conducted on a Zetasizer Nano ZS (Malvern Instruments Ltd.). Measurements were conducted in a 100 µL cuvette containing 500 µM of nanodiscs. To test the effects of calcium on nanodisc size some samples had 3 mM calcium added to the hydration buffer and upon mixing with lipid the sample rested for 10 minutes before addition of polymer. Other samples had 3 mM calcium added 10 minutes after treating the membranes with polymer. Each trace is the average of 3 experiments each consisting of 10 consecutive acquisitions. The hydrodynamic radius was determined by using CONTIN software. All data were acquired at 28ºC; the samples were incubated for 1 hour after polymer addition at 28ºC before beginning data acquisition. Various calcium concentrations were tested, but 3 mM gave the most reproducible results.

4.2.3 ^{31}P NMR measurements of nanodiscs with and without calcium

The data were acquired on 500 MHz Bruker Avance spectrometer (Bruker Biospin, Rheinstetten, Germany) with a QNP probe operating at the ^{31}P frequency of 202.5 MHz. A zg pulse, with a duration of 15 µsec at 0 db, was used to acquire 512 scans with a 2 second recycle delay. The data were analyzed on Topspin 4.0.6 where it underwent Fourier transformation and the chemical shifts were referenced to 85% H_3PO_4 dissolved in D_2O at 0 ppm. All data were acquired at 28ºC after the sample was incubated inside the spectrometer for 30 minutes. Samples consisted of 5 mM of nanodiscs (made as described in section 4.2.1) dissolved in HBS and 10% D_2O. Calcium containing samples had 3 mM calcium added 10 minutes after polymer treatment of the MLVs. 5 mM lipids were used because reproducible legible spectra could be acquired - other lipids concentrations were tested see Figure 1, Appendix D.

4.2.4 Pyrene based assay for determination of nanodisc transition temperature

4.2.4.1 Preparation of LUVs containing pyrene-PC

All lipids used to make liposomes were acquired from Avanti Polar Lipids (Alabaster, Alabama), Larodan (Slona, Sweden), and Cayman Chemicals (Ann Arbor, Michigan). Lipids included 1,2-dimyristoyl-sn-glycero-3-phosphocholine (DMPC; Avanti), 1,2-dimyristoyl-sn-glycero-3-phospho-(1'-rac-glycerol) (sodium salt; DMPG; Larodan), and 1-palmitoyl-2-pyrenedecanoyl phosphatidylcholine (pyr-pc). LUVs were prepared as described before. The requisite amounts of lipids – 0.5 mol% pyr-pc and an equimolar mixture DMPC/DMPG were dissolved in chloroform/methanol (3:1), dried under N_2 in a round-bottom flask, and placed overnight on a high vacuum. The lipid film

was then resuspended in pH 7.4, 10 mM HEPES (Biorad), and 25 mM NaCl buffer (HBS), and the resulting lipid suspension was repeatedly extruded through a 100 nm polycarbonate filter.

4.2.4.2 Preparation of MLV and nanodiscs containing pyrene-PC

MLVs and nanodiscs were made exactly as described in section 4.2.1with the exception that 0.5 mol% (1-palmitoyl-2-pyrenedecanoyl phosphatidylcholine) was added to the chloroform: methanol mixture before lipid film formation.

4.2.4.3 The experiment

250 μM of LUVs or nanodiscs suspended in HBS were placed in a disposable cuvette. The cuvette was incubated at the corresponding temperature for 10 minutes, inside the spectrometer, before acquisition of pyrene's fluorescence emission. The emission spectra (excitation wavelength: 335 nm; emission wavelength from 360 to 600 nm) were acquired on a PTI QuantaMaster 4 instrument. The data presented is the average of 3 independent experiments.

4.2.5 ^{31}P NMR determination of nanodisc phase transition temperature

The data were acquired as detailed in section 4.2.3. p1 was set at 16.1 μsec with 0 db; 512 scans were acquired with a 2 second recycle delay. The data were analyzed as detailed in section 4.2.3. The linewidths were determined by the peak-width command in Topspin 4.0.6. Samples were incubated at the appropriate temperature inside the spectrometer for 30 minutes before acquisition. Samples consisted of 5 mM of nanodiscs (made as described in section 4.2.1) dissolved in HBS and 10% D_2O.

4.2.6 Monitoring daptomycin-membrane interactions by kynurenine fluorescence

The assay was conducted as follows: 250 μM of DMPC/DMPG containing liposomes or nanodiscs were mixed with daptomycin (3 μM) and calcium chloride (0 to 10 mM final concentration) in HEPES-buffered saline (10 mM HEPES, 25 mM NaCl, pH 7.4). Each sample was incubated for 3 minutes before data acquisition. Emission spectra (excitation wavelength: 365 nm) were acquired from 400 – 600 nm on a PTI QuantaMaster 4 instrument. All trials were run in duplicate at 37ºC.

4.2.7 Synthesis of 7-nitro2,1,3-benzoxadiazol (NBD)-labeled daptomycin

The NBD-Dap used in these experiments was the same material that was used for experiments in chapter 2. The synthesis is described in section 2.2.1.

4.2.8 Daptomycin oligomer subunit stoichiometry

Dap subunit stoichiometry was determined in the same way as described in section 2.2.7 with the following exceptions: the dap: NBD-dap ratio was keep constant at 4:1, 3 mM calcium, and 10 mM HEPES, 25 mM NaCl, pH 7.4 buffer were used instead of 5 mM calcium and 20 mM Hepes and 150 mM NaCl.

4.2.9 FRET-based assay of oligomer stability

These experiments were adapted from Muraih *et al.* (2012).[18]

Sequential Samples: 250 μM equal part DMPC: DMPG 9:1 polymer to lipid wt% nanodiscs in HBS (10 mM HEPES, 25 mM NaCl, pH 7.4) were treated with 3 mM calcium and 1 μM NBD-dap. After a 3-minute incubation 4 μM dap was added to the sample and an emission spectrum was acquired. Another emission spectrum was acquired 7 minutes later. Emission spectra (excitation wavelength: 365 nm) were acquired with detection between 400 – 600 nm on a PTI QuantaMaster 4 instrument. All trials were run in duplicate at 37ºC.

Pre-mixed Samples: 250 μM equal part DMPC: DMPG 9 to 1 polymer to lipid wt% nanodiscs in HBS (10 mM HEPES, 25 mM NaCl, pH 7.4) were treated with 3 mM calcium and 5 μM mixture of 4:1 dap: NBD-dap. Emission spectra were acquired after 3-minutes of incubation and 10-minutes of incubation. Emission spectra (excitation wavelength: 365 nm) were acquired with detection between 400 – 600 nm on a PTI QuantaMaster 4 instrument. All trials were run in duplicate at 37ºC.

4.2.10 Testing for inter-oligomer FRET between nanodiscs

The dap: NBD-dap portion of the assay was done exactly at described in section 4.2.8. The dap only portion followed the same protocol as in section 4.2.8, with the exception that no NBD-dap was used; the initial addition consisted of 10 μM dap and the second addition consisted of 4 μM dap.

4.2.11 Exchange of daptomycin oligomers between nanodiscs

Initially, two samples were prepared: the first contained 5 μM Dap, 3 mM calcium, and 125 μM nanodiscs (9 polymer weight equivalents added to 1:1 DMPC:DMPG MLVs), and the second containing 5 μM NBD-Dap, 3 mM calcium, and 250 μM nanodiscs(9 polymer weight equivalents added to 1:1 DMPC:DMPG MLVs). Each sample was incubated for 3 minutes and then the fluorescence spectra were recorded. The samples were then mixed together, and fluorescence measurements were taken at regular time intervals. Emission spectra (excitation wavelength: 365 nm)

were acquired with detection between 400 – 600 nm on a PTI QuantaMaster 4 instrument. All trials were run in triplicate at 37ºC.

4.2.12 Detecting daptomycin binding nanodiscs, stabilized by nine equivalents of polymer, via ^{1}H solution state NMR

The data were acquired on 600 MHz Bruker Avance spectrometer (Bruker Biospin, Rheinstetten, Germany) operating at the ^{1}H frequency of 600 MHz. A zgesgp pulse program was used; p1 10.5 µsec, p16 1000 µsec, d16 .0005 sec, p12 2400 µsec, gpz1 31%, and gpz2 11%. 128 scans were acquired with a 1 second recycle delay. The data were analyzed on Topspin 4.0.6 where it underwent Fourier transformation. The chemical shifts were referenced to the water proton signal at 4.7 ppm. Samples were incubated at 28ºC inside the spectrometer for 30 minutes before acquisition. Nanodiscs were prepared as described above. Samples containing calcium had it added 10 minutes after addition of polymer. 10 mM Hepes, 25 mM NaCl pH 7.4 buffer was used in all samples. 10% D_2O indicates that 10% of the sample volume was D_2O. The 100% D_2O sample was prepared like all the other samples, but then lyophilized overnight and then rehydrated with only D_2O. The polymer only sample contained 9 equivalents of polymer dissolved in 90% HBS and 10% D_2O. The dap only sample consisted of dap dissolved in 10% D_2O and HBS. All samples were tested 1 hour after preparation.

4.3 Results

The polymer used in this study was recommended by Prof. Dr. Overduin after consideration of the problems previous encountered when attempting to determine dap's membrane-bound structure by solution-state NMR. This specific polymer has been engineered to have reduced cation chelation, be gentle towards non-covalent interactions between proteins or peptides and possess superior solubility. The polymer is proprietary, and the author of thesis knows neither its exact composition, nor if it would indeed work in this application.

4.3.1 Nanodisc hydrodynamic radius as determined by DLS

As mentioned previously, the polymer used in this study is novel and uncharacterized. Consequently, the first step is to determine whether the polymer can convert PG and PC containing MLVs into nanodiscs with a diameter small enough to produce legible solution-state NMR spectra.

The size of the nanodiscs was determined by DLS. DLS was chosen because it is widely used in the SMA field to characterize nanodisc size.[65,73] The idea of using DLS to determine nanodisc size was

initially worrisome to many working in the field because DLS data analysis software calculates the size of particles assuming that they are spherical; nanodiscs are not.[63,73] To determine whether this assumption yielded inaccurate data, DLS size measurements were compared to those obtained by various microscopy techniques with the comparison showing good agreement .[73]

From Figure 4-2 it is evident that the polymer can convert MLVs containing equal parts of DMPC/DMPG into nanodiscs. It seems that 3 weight equivalents of polymer to one weight equivalent of lipid is not enough to induce formation of nanodiscs with diameters less than 20 nm; 20 nm being considered the maximal diameter at which NMR spectra of sufficient quality, for structure determination, can be obtained.[74] Further the data suggests that in the presence calcium, regardless of the addition order, nanodiscs with a decreased diameter are formed.

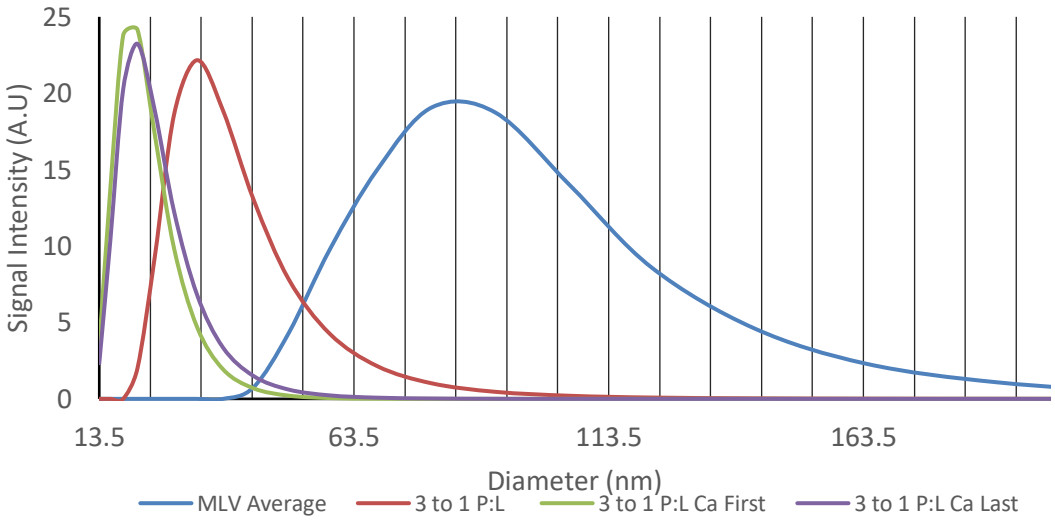

Figure 4-2: Diameter of nanodiscs containing lipid with and without calcium. Nanodiscs contained 1:1 DMPC: DMPG and polymer in three-fold total excess over the lipid by weight. The diameter of the MLVs ≈ 85 nm. In the absence of calcium, nanodiscs have a diameter ≈ 33.5 nm. When calcium is added before the polymer, the resulting nanodiscs have a diameter centered at 21 nm; if polymer is added first nanodiscs have a diameter centered at 22 nm.

As stated in the introduction, it is possible to decrease nanodisc size by increasing the polymer to lipid ratio.[66] The data in Figure 4-3 suggests that increasing polymer equivalents does decrease nanodiscs size; nanodisc diameter decreased from 33.5 nm (three-fold total excess of polymer over the lipid by weight) to 7.25 nm (nine-fold total excess of polymer over the lipid by weight). The data in Figure 4-3 shows that nanodisc diameter increases in the presence of calcium, but that the sequence of adding calcium and polymer does not affect the size. It was observed that at above 5 mM calcium the nanodisc

samples progressively became hazy and at 10 mM precipitation occurred; precipitation occurred 10 minutes after calcium (10 mM) addition to the sample. 3 mM calcium was chosen because it gave constantly reproducible nanodisc sizes and avoided precipitation.

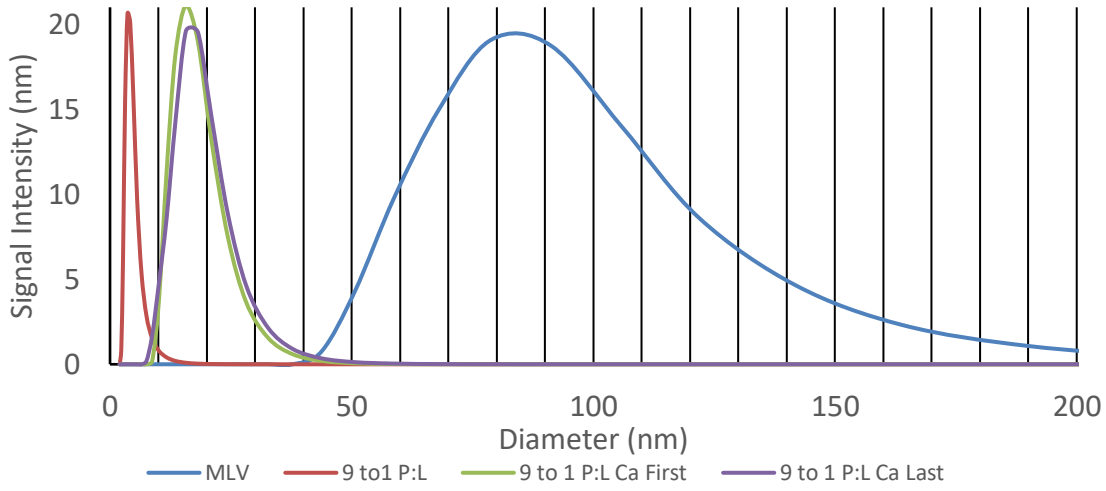

Figure 4-3. Diameter of nanodiscs with nine-fold total excess of polymer over lipid by weight with and without calcium. Nanodiscs contained 1:1 DMPC: DMPG and a nine-fold total excess of polymer over the lipid by weight. Diameter of the MLVs ≈ 85 nm. In the absence of calcium, the nanodiscs have a diameter ≈ 7.25 nm. When calcium is added first the resulting nanodiscs have a diameter centered at 15.5 nm; if polymer is added first the resulting nanodisc have a diameter centered at 16.5 nm.

4.3.2 ^{31}P NMR measurements of nanodiscs with and without calcium

The above DLS data suggests that this novel polymer can create nanodiscs containing PG that in the presence of calcium retain a diameter sufficiently small for NMR. The purpose of these experiments is to use ^{31}P NMR and see if well-resolved NMR signal can be obtained. As discussed earlier, solution-state NMR is extremely size-sensitive.[60] In the case of nanodiscs the size cut-off is around a diameter of 20 nm.[74] From the DLS results, no signal is expected for nanodisc stabilized by a three-fold total excess of polymer over the lipid by weight as they are too large. On the other hand, nanodiscs stabilized by a nine-fold total excess of polymer over lipid by weight should produce legible spectra, since their diameter is less than 20 nm.

^{31}P NMR was used to corroborate DLS results because phosphorus NMR is one of the preferred methods to study membrane systems because ^{31}P has 100% isotope abundance, it had a relatively high gyromagnetic ratio, and in samples of this nature is only present in lipids.[75,76]

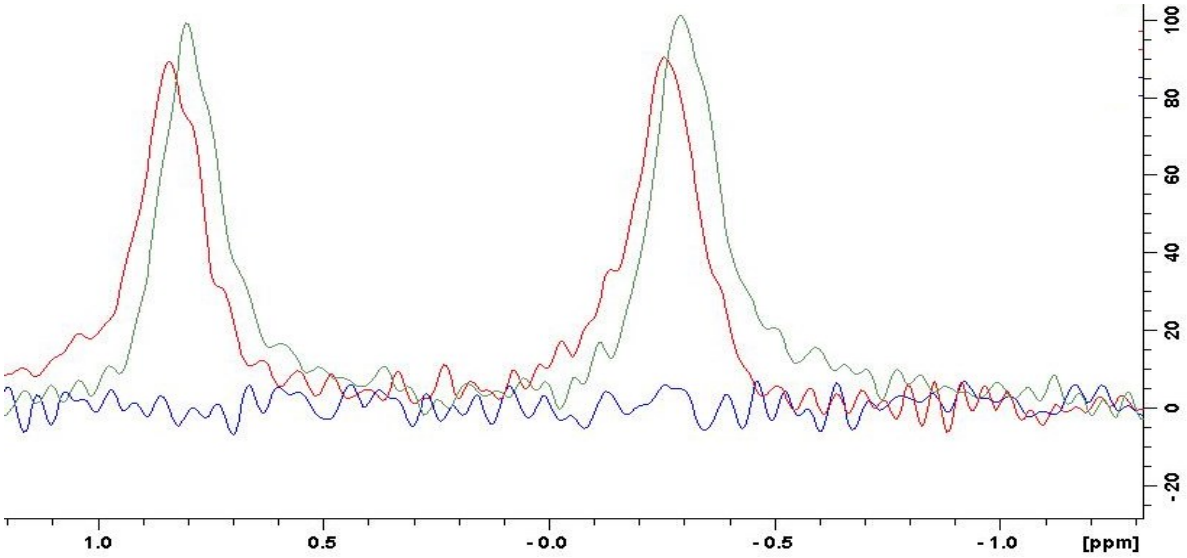

Figure 4-4. ^{31}P NMR of nanodiscs. Blue line: nanodiscs containing a three-fold total excess of polymer over the lipid by weight. Red line: nanodiscs containing a nine-fold total excess of polymer over the lipid by weight; PG peak: 0.8404 ppm; PC peak: -0.2567 ppm. Green line: nanodiscs containing a twelve-fold total excess of polymer over the lipid by weight; PG peak: 0.8002; ppm PC peak: -0. 2934.

The first set of NMR experiments focused on studying the ^{31}P signal of nanodiscs formed in the absence of calcium. The data presented in Figure 4-4 corroborates the DLS results; nanodiscs formed by the addition of 3 polymer equivalents do not give rise to a ^{31}P signal. This suggests that the nanodiscs are indeed greater than 20 nm in diameter. Nanodiscs formed by the addition of nine equivalents of polymer to lipid produce ^{31}P spectra with significant intensity suggesting that the nanodiscs are smaller than 20 nm in diameter. The phosphorus signal of nanodiscs formed by the addition of twelve equivalents of polymer was also tested. The signal intensity of these nanodiscs was slightly stronger than that nanodsics stabilized by nine-equivalents of polymer and the peaks were shifted upfield. The increase in signal intensity is likely a result of the decreased size; signal intensity is proportional to T_2, which in turn is inversely proportional to particle size.[60] The upfield shift can be attributed to chemical shift anisotropy; as the nanodiscs become smaller, more lipid molecules will directly interact with styrene group, which penetrate the lipid interface and their aromatic electrons cause shielding effects.[67]

Figure 4-5 also corroborates the results obtained by DLS; upon addition of calcium the signal intensity decreases, and the peaks are shifted upfield. These are hallmark signs of increase in nanodisc size. The decrease in signal intensity is likely caused by a short T_2. The change in chemical shift upon addition of calcium is likely due to calcium binding the lipids, which alters the chemical environment

of the phosphate phosphorus.[77] Only the sample to which calcium had been added last was tested, since DLS had shown that the order of addition does not affect nanodisc size. Additionally, nanodiscs stabilized by a three-fold excess of polymer in the presence of calcium were tested; no signal was observed, suggesting that the nanodiscs are indeed greater than 20 nm in diameter; this is in agreement with DLS measurements. Overall, the data suggests that nanodiscs stabilized with nine-equivalents of polymer have a diameter suitable for quality structural studies by solution state NMR.

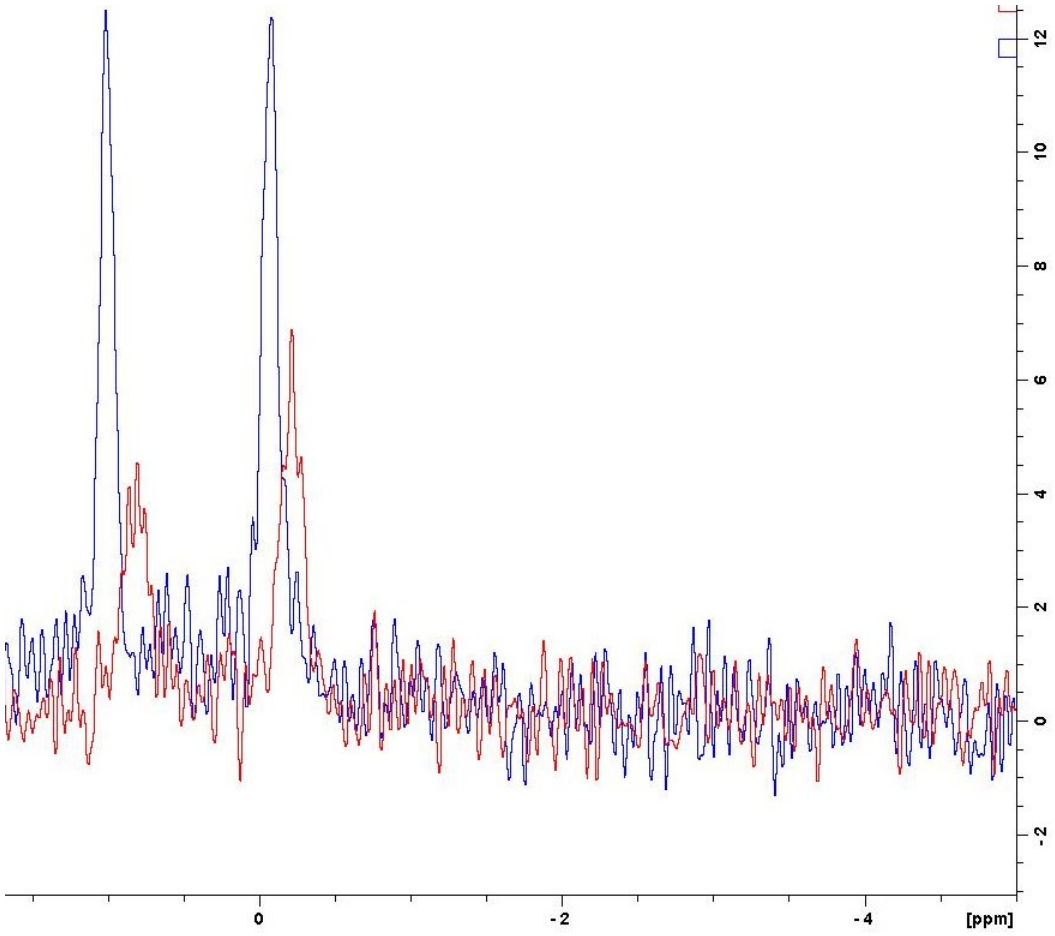

Figure 4-5. ^{31}P NMR of nanodiscs with calcium. Blue line: nanodiscs containing a nine-fold total excess of polymer over lipid by weigh; PG peak: .8404 ppm; PC peak: -.2567 ppm; Red line: nanodiscs containing a nine-fold total excess of polymer over lipid by weigh treated with 3 mM calcium added 10 minutes after polymer addition; PG peak:.7993 ppm; PC peak: -.2224 ppm.

4.3.3 Determining the lipid bilayer phase transition temperature in nanodiscs

Previous research work regarding dap's action mode shows that dap is sensitive to its surrounding membrane environment.[3,13,57] Therefore, it was important to determine whether nanodiscs have a phase transition temperature that is within a range suitable for solution-state NMR studies.

4.3.3.1 Pyrene florescence

Nanodisc phase transition temperature was determined by monitoring pyrene excimer fluorescence as a function of temperature. Pyrene is a fluorescent dye that has a long monomer lifetime allowing for efficient formation of excited dimers (excimers).[78,79] While many fluorescent dyes can form excimers, the resulting fluorescence is rarely observed because it is not clearly separated from the monomer signal; in pyrene's case the excimer signal is quite distinct.[78,79] The formation of excimers requires that pyrene molecules collide through diffusion; consequently, the change in excimer signal reports on diffusion rates.[80] In a membrane setting, since the pyrene is attached to a phospholipid acyl tail, the excimer signal reports on lipid collision frequency, which is dependent on membrane fluidity.[80]

Figure. 4-5 shows that the excimer (E) to monomer (M) ratio mid-point for LUVs is at 30 ºC. This is higher than 24 ºC, the literature reported value for the phase transition temperature of equal part DMPC: DMPG LUVs. The mid-point for nanodiscs, regardless of the amount of polymer added is slightly greater than 30 ºC. It is noteworthy that the excimer to monomer ratio is inversely related to polymer concentration; this is likely caused by several factors including styrene quenching of monomer pyrene fluorescence.[81] The meaning of this data in a broader context is considered in the discussion of this chapter.

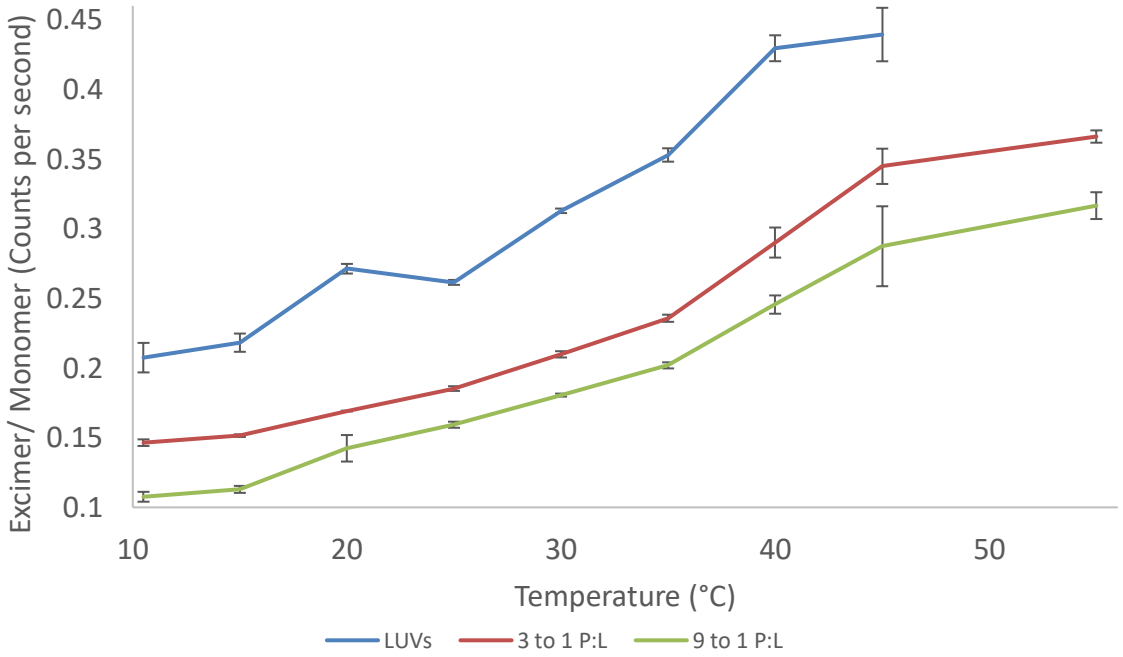

Figure 4-6. Monitoring nanodisc phase transition by pyrene excimer formation. On liposomes the phase transition temperature is 30 ºC and on nanodiscs, regardless of polymer concentration, it is slightly greater than 30 ºC.

4.3.3.2 Using ^{31}P linewidth to determine the phase transition temperature of nanodiscs

It was expected that pyrene's E/M ratio midpoint would correspond to the literature phase transition of 24 ºC but evidently this was not the case. Consequently using another method to validate the transition temperature suggested by the midpoint of the E/M ratio was required. Previous research has found that phospholipid phosphorous linewidths, at half the signal intensity, are good reporters on membrane phase transition temperature.[75,82,83] The NMR linewidth of phospholipid phosphate phosphorus atoms decreases with increasing temperature reaching a minimum at the phase transition temperature.

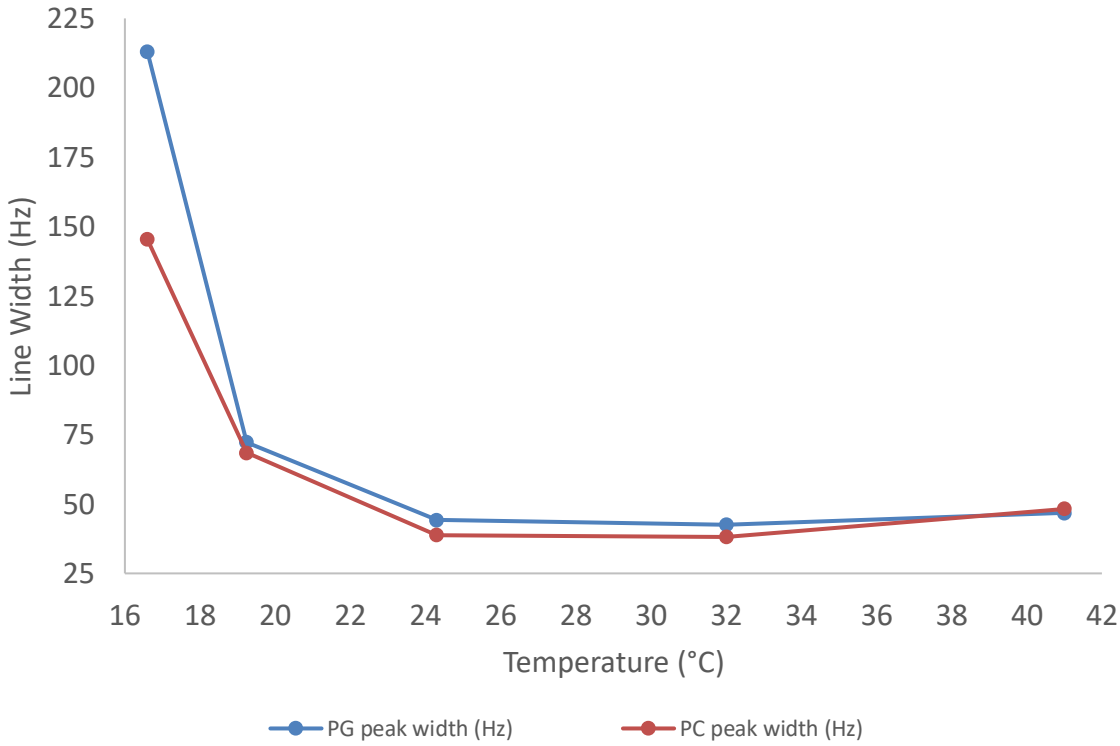

Figure 4-7. Nanodisc phase transition temperature determined by ^{31}P line width. The phase transition temperature of nanodiscs stabilized by addition of nine polymer equivalents is at 24.2 ºC.

The apparent membrane phase transition temperature determined by phosphorus NMR is 24.2 ºC. Previous experiments show that the phosphate phosphorus linewidth reaches a global minimum value at the phase transition temperature of the lipid it is a part of and does not decrease any further; consequently, because the linewidths remain constant between 24.2 ºC and 32 ºC the phase transition temperature is not greater than 24.2 ºC. Overall, the data suggests that the lipid phase transition temperature is not significantly affected by polymer. This suggest that nanodiscs have physiochemical properties like those observed on other membrane mimetics. This temperature range is sufficient for structural studies. Nanodiscs stabilized by the addition of nine weight equivalents of polymer were tested because only they are small enough to yield legible spectra.

4.3.4 Daptomycin binding to nanodiscs

Once it was determined that nanodiscs created by the addition of nine polymer equivalents were small enough to produce legible NMR spectra, and the polymer did not increase lipid phase transition temperature it was time to determine the calcium concentration required for dap to bind to nanodiscs.

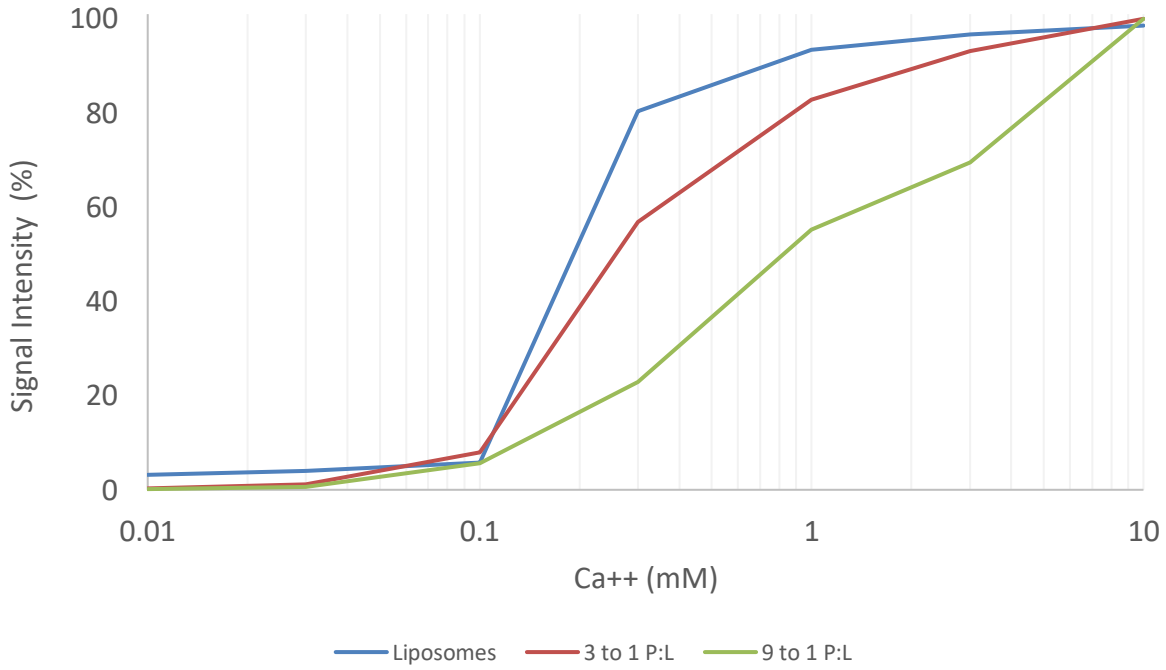

Figure 4-8. Dap binding to nanodiscs monitored by kynurenine fluorescence. With increasing polymer concentration dap requires more calcium to bind the nanodiscs. This suggests that despite being engineered for minimal chelation the polymer the polymer can still bind calcium.

Dap's binding to nanodiscs was monitored by kyn fluorescence.[27] It is evident from Figure 4-8 that with increasing polymer concentration more calcium is required to induce membrane binding; likely the polymer, despite being engineered for low calcium binding, still has affinity for calcium and consequently competes with dap for the available calcium.

4.3.5 Daptomycin oligomer subunit stoichiometry on nanodiscs

It is widely accepted that for dap to bring about is bactericidal effect it must form oligomers.[3,18] Consequently it is of the utmost importance that the membrane system used to determine the structure allows for dap oligomerization. Accordingly, the purpose of this experiment was to determine if dap could form oligomers on nanodiscs.

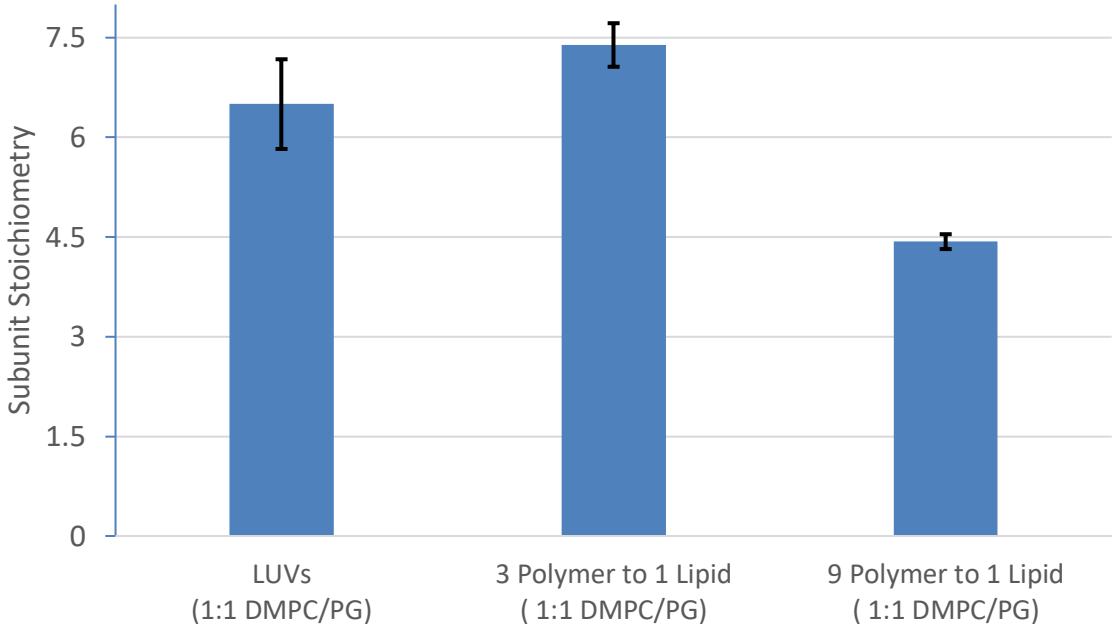

Figure 4-9. Subunit stoichiometry of daptomycin oligomers on various membrane mimetics. On LUVs the subunit stoichiometry is 6.5 ±0.68, on nanodiscs stabilized by three polymer equivalents it is 7.4 ± 0.33, and nanodiscs stabilized by nine polymer equivalents it is 4.4 ±0.11.

From Figure 4-9 it is evident that LUVs and nanodiscs stabilized by three polymer equivalents have roughly the same number of subunits; around 8 subunits (see section 2.3.4 for a discussion why the subunit stoichiometry on DM membranes ranges from 6 to 7 subunts.) – presumably 4 per leaflet. On nanodiscs stabilized by nine polymer equivalents the stoichiometry is roughly half of 8. This is not an unexpected result, because at 3 mM calcium the kynurenine signal for nanodiscs stabilized by nine polymer equivalents is only about 60% of its maximal intensity, whereas for LUVs and nanodiscs stabilized by three polymer equivalents it is nearly 100%. In the case of nanodiscs stabilized by nine polymer equivalents, the polymer is binding calcium and limiting dap's ability to undergo its second calcium binding event and subsequent octamer formation; it is highly probable that the subunit stoichiometry reflects the formation of the tetramer that is formed as a result of the first calcium binding event - as is suggested by Zhang *et al.* (2016) and Taylor et al (2016).[8,21] Overall, whilst octameric

oligomers are not observed on nanodiscs small enough for NMR studies, the conditions would allow for the study of the tetramer, which would still be of significant interest.

4.3.6 Verifying the assumptions of the subunit stoichiometry assay

To determine the subunit stoichiometry several assumptions are made; that oligomers are stable on the time scale of the experiment, and that the second addition of dap is required to account for FRET occurring between olgiomers.[18]

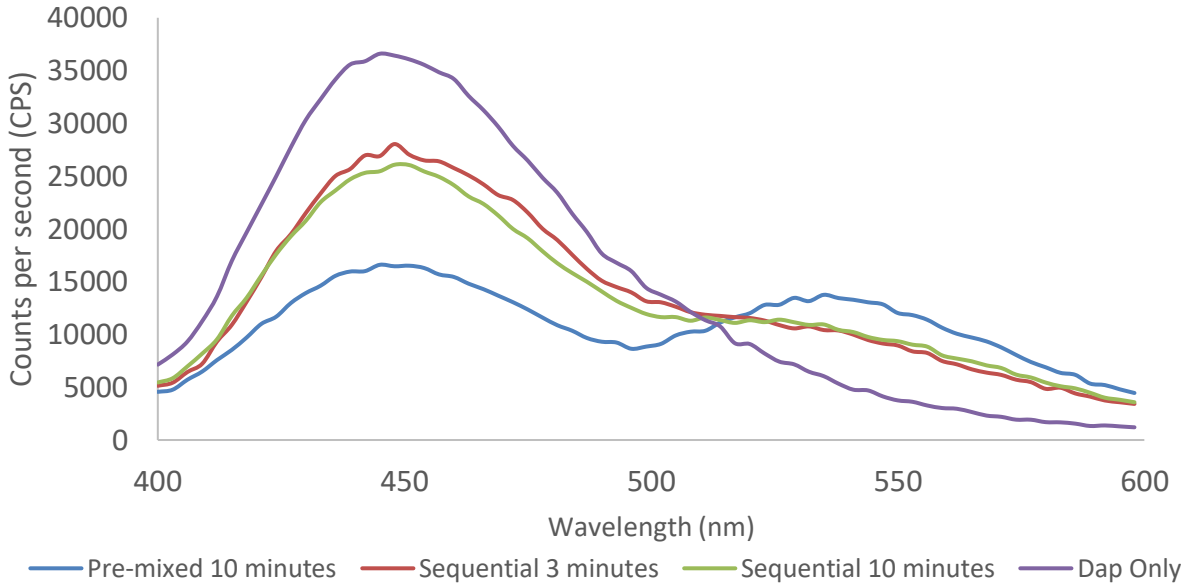

Figure 4-10. Daptomycin oligomer stability on nanodiscs stabilized by nine polymer equivalents. The dap only sample contained 4 µM dap and the spectra were acquired 10 minutes after its addition to nanodiscs (acquisitions were made at 3 and 5 minutes; they are identical to the 10 minutes trace). The premixed sample contained 1 µM NBD-dap and 4 µM dap (data acquisition was made at 3 minutes; it is identical to the 10 minutes trace). The sequential sample contained 1 µM NBD-dap and 4 µM dap added 3 minutes after.

The findings in Figure 4-10 mirror those observed by Muraih *et al.* (2012). Pre-mixing NBD-dap and dap results in a kynurenine signal that is significantly less intense than observed with the native-dap only sample. This is because dap and NBD-dap are forming hybrid oligomers in which the kynurenine fluorescence is quenched by FRET. The sequential addition of NBD-dap and dap results in increased kynurenine signal compared to the premixed sample; NBD-dap and dap form separate oligomers, and therefore the kynurenine signal is not quenched as strongly as the signal in the premixed samples. The sequential signal remains almost unchanged after 10 minutes suggesting that the two oligomer species

are stable and are not transiently exchanging dap molecules to form hybrid oligomers. As mentioned in section 2.2.7, the suppressed kynurenine fluorescence in the sequential sample compared to the dap only sample is due to kynurenine quenching occurring through FRET between oligomers. Overall, it seems that once oligomers form the comprising individual subunits do not transiently exchange.

The sequential addition experiments suggest that the second addition of dap is needed to account for FRET between oligomers. It is possible to test directly for this FRET by comparing the difference in signal between a second addition of dap to hybrid and dap only oligomers.

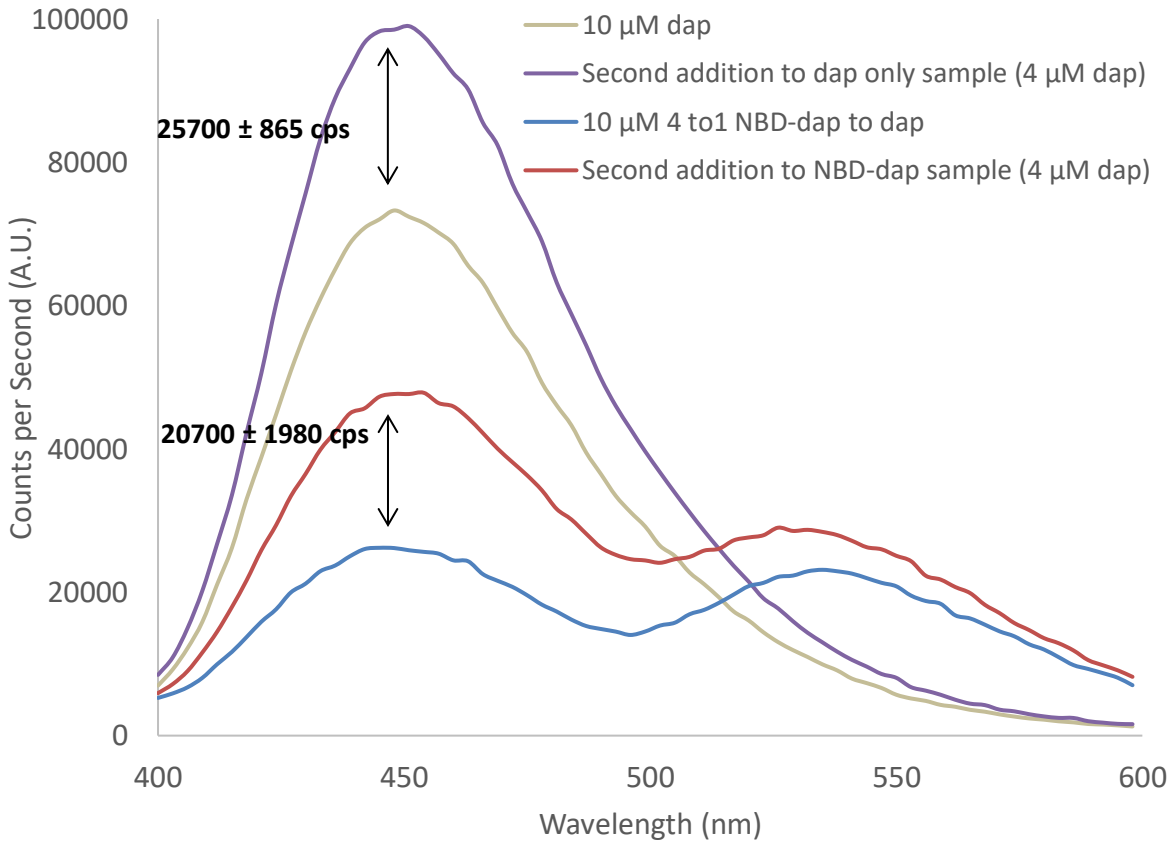

Figure 4-11. Testing for FRET between daptomycin oligomers on nanodiscs stabalized by addition of nine polymer equivalents. The assay was done exactly like described by Muraih *et al.* (2012) with the exception that 3 mM calcium and 10 mM Hepes 25 mM NaCl pH 7.4 buffer were used.

It is expected that if the difference in signal between a second addition of dap (red) to the mixed hybrid oligomers (blue) is smaller than the difference between the second addition of dap (purple) to dap only oligomers (grey), then there is FRET occurring between oligomers. If the differences between red and

blue and yellow and grey is the same, then there is no FRET between oligomers. Figure 4-11 shows that the difference between the purple and grey curves is greater than that between the red and blue curves, suggesting that there is FRET between oligomers. It is likely that the nanodiscs accommodate more than one oligomer per nanodisc; kynureinine and NBD FRET radius is too small for FRET to occur between nanodiscs.[9] Overall, both the stability and inter-oligomer FRET assumptions required for stoichiometry calculation are correct.

4.3.7 Exchange of daptomycin oligomers between nanodiscs

Previous research on nanodiscs has shown that they exchange lipids by transient fusion and fission processes. The goal of these experiments was to determine whether dap oligomers can also be exchanged between nanodiscs.

Initially, two samples are prepared: the first sample (just dap) contains nanodiscs treated with dap and calcium and the second sample (just NBD) contains nanodiscs treated with NBD-dap and calcium. Each sample is incubated, and the fluorescence spectrum is recorded. The samples are then mixed together, and fluorescence measurements are taken at regular time intervals. If the nanodiscs do not undergo fusion, then the spectra recorded after mixing should look like a linear combination of the two samples before mixing. On the other hand, if there is fusion and oligomer exchange, then the spectra recorded after sample mixing should show diminished signal intensity for kynurenine because of inter-oligomer FRET to oligomers made of only NBD-dap.

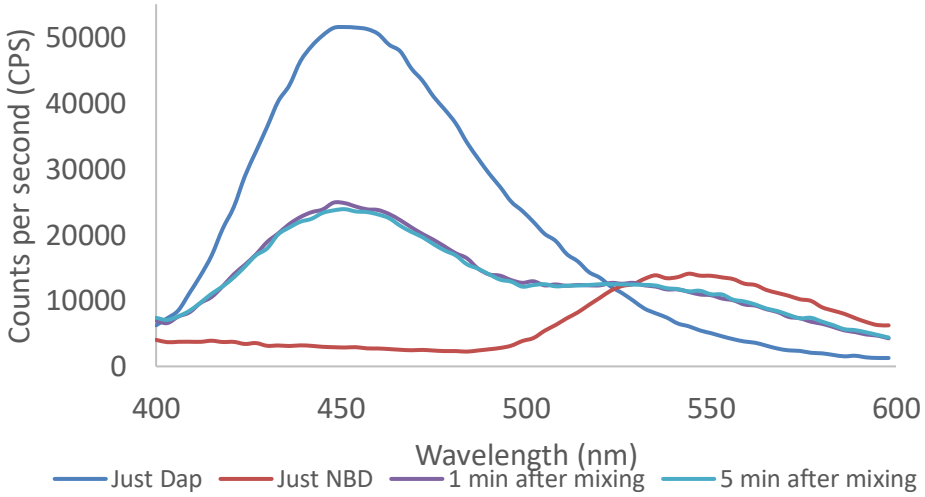

Figure 4-12. Daptomycin oligomer exchange between nanodiscs. The just dap sample contained 5 µM Dap, 3 mM calcium, and 125 µM nanodiscs. The just NBD-dap sample contained 5 µM NBD-Dap, 3 mM calcium, and 125 µM nanodiscs.

The immediate decrease in kynurenine signal intensity upon mixing of the two samples suggests that nanodiscs undergo rapid fusion and exchange oligomers. The measurements taken at different time intervals after mixing are almost identical suggesting that the process of nanodisc fusion and oligomer exchange is rapid and quickly reaches an equilibrium.

4.3.8 Observing daptomycin binding to nanodiscs, stabilized by addition of nine polymer equivalents, by ^{1}H-NMR

The goal of this experiment was to determine whether nanodiscs stabilized by 9 polymer equivalents treated with dap and calcium yield legible ^{1}H spectra.

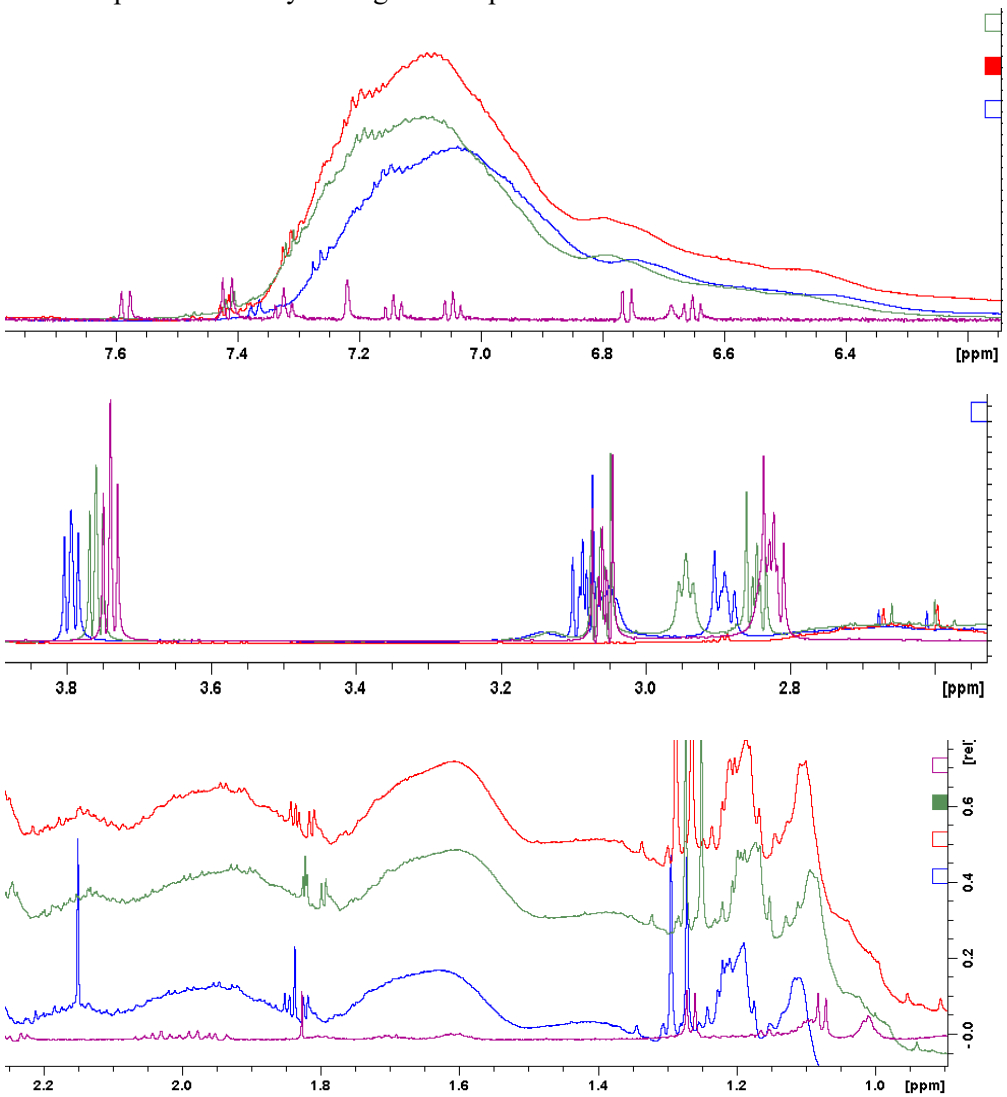

Figure 4-13. ^{1}H-NMR spectra of daptomycin interacting with nanodiscs stabilized by nine polymer equivalents. The composition of each sample is explained in table 4-1.

Table 4-1. ^{1}H-NMR sample composition

Colour	Calcium (3 mM)	Nanodiscs with lipid	D_2O	Dap (100 μM)
Blue	Yes	Yes	100%	Yes
Red	No	Polymer only	10%	No
Green	Yes	Yes	10%	Yes
Purple	Yes	No	10%	Yes

The amide region (>6 ppm) of dap (purple) is quite clear without the presence of nanodiscs (blue and green). Upon addition of nanodiscs (green) characteristic dap peaks are overshadowed by the aromatic styrene protons of the polymer (also seen in the polymer only sample; red). In the 2.8 – 3.8 ppm region of the spectrum dap peaks in the absence of nanodiscs (purple) shift. Upon addition of nanodiscs, dap peaks decrease in intensity and broaden out slightly; this is an indication of dap binding to the nanodiscs. Between 1.0 to 2.2 ppm a new peak appears at 2.15 ppm in the 100% D_2O sample, which may represent an exchangeable alcohol or amine. Overall, the ^{1}H data suggests dap is binding to the nanodiscs. While the signals obtained from nanodisc-bound dap are broadened, the extent of broadening does not render the peaks unusable for structure determination. Lastly, all the NMR samples were stored for over a week and no precipitation was observed; this result indicates that this system is very stable and is amenable to the long experimental times of NMR.

4.4 Discussion

The motivation for the work reported was to assess the suitability of using styrene-maleic acid lipid co-polymer nanodiscs to determine dap's membrane-bound structure. The study began with determining whether the polymer in question could form nanodiscs, from MLVs composed of equal parts DMPC: DMPG and in the presence of calcium and whether these discs were small enough to produce well-resolved NMR spectra. By using DLS and ^{31}P it was possible to determine that nine weight equivalents of polymer per one weight equivalent of lipid is required to create nanodiscs that are composed of DMPC: DMPG, stable in presence of calcium, and produce legible NMR spectra. The nanodisc gave the most reproducible results when 3 mM calcium was used; likely because 3 mM calcium was not enough to induce precipitation. During these studies it was observed that addition of calcium influenced nanodisc size. The effects of calcium and magnesium on SMA nanodisc size have been studied Before but with a different polymer; consequently, the results are not comparable.[84] After determining that

nanodiscs of sufficient diameter can be formed in a system that contains both calcium and PG, it was important to study their physiochemical properties. The phosphorus line width data suggests that nine weight equivalents of polymer nanodiscs containing 1:1 DMPC: DMPG have a phase transition around 24.2 °C; this is not dissimilar to values reported in literature for LUVs with the same lipid composition.[75,83]

The phosphorus NMR results further suggest that phospholipids with pyrene labeled acyl tails are reporters of lipid lateral diffusion rather than membrane phase transition temperature. On LUVs the excimer to monomer ratio begins to increase significantly only after 24.2 °C. This a surprising, until consideration is given to the process of excimer formation. It is well known that excimers can only form if two pyrene molecules are within several angstroms of each.[79] In a membrane setting the formation of excimers would involve lipids undergoing free lateral diffusion until two lipid molecules, both containing pyrene, collide so as to bring their respective pyrene's sufficiently close for excimer formation. Observation of stronger excimer signal would mean that the collision frequency between lipids is increasing. Increased collision frequency can only occur if lipids have free lateral diffusion, and free lateral diffusion can only begin in earnest when much of the membrane is in a fluid state. Much of the membrane reaches a fluid state only once the temperature of the system is significantly larger (this depends on the lipid composition of the membrane) than the phase transition temperature (T_m).[76] This is because at T_m 50% of the membrane would still in a gel-like phase; the patches of gel-like lipids can hinder free lateral diffusion by acting as physical barriers and through sequestration of lipids that could partake in collisions. In this context is not surprising that on LUVs the excimer signal rises significantly only once the temperature of the systems surpasses the NMR determined and literature phase transition of roughly 24°C.

On nanodiscs, regardless of polymer concentration, the increase in excimer signal begins at even higher temperatures than observed on LUVs. This could be because the polymers sequester pyrene-labelled lipids through pi-stacking interactions with the polymer styrene moieties; in this case the higher temperature is then required to give the pyrene lipid enough kinetic energy to disrupt this interaction and diffuse away. The decrease in excimer to monomer ratio at various temperatures between LUVs and nanodiscs can be attributed to the decreased amount of pyrene molecules per nanodisc. Each LUV, assuming a 100 nm diameter and a .7 nm^2 average lipid headgroup surface area, has 1795 pyr-PC molecules per LUV.[80] Each nanodisc stabilized by the addition of nine polymer equivalents, assuming

a 15.5 nm diameter and a .7 nm^2 average lipid headgroup surface area, has 1.4 pyr-PC molecules per nanodisc leaflet. It is likely that less pyrene molecules lower the probably of collision and therefore the excimer signal. Additionally, on some nanodiscs the pyr-pc will have no other partner pyr-PC with which to interact and will never form excimers regardless of membrane fluidity. Another consideration is that styrene has been shown to be a dynamic quencher of pyrene. Dynamic quenching implies that the lifetime of monomeric pyrene decreases; consequently, in a system that contains styrene the excited monomeric pyrene molecules will have less time to find a partner pyrene and form an excited dimer.[81] On the other hand, the first mechanism proposed here (sequestration of pyrene by styrene) should cause static quenching, and thus reduce fluorescence intensity but not lifetime. Thus, fluorescence lifetime experiments should be able to distinguish between these two mechanisms.

Once it was determined that nanodiscs stabilized by nine polymer equivalents have a phase transition temperature like LUVs with the same lipid composition, it was important to determine at what calcium concentration dap would bind the nanodiscs and whether dap oligomers would form. It was observed that dap readily oligomerizes on nanodiscs stabilized by addition of nine polymer equivalents at calcium concentrations which do not induce nanodisc precipitation. The FRET-based stoichiometry experiments showed that the oligomers formed were tetrameric and did not consist of transiently exchanging dap molecules. Dap octamers did not form, presumably because polymer and dap compete for the calcium. Additional work showed that the tetrameric oligomers transiently exchange between nanodiscs. ^{1}H-NMR studies confirmed that dap binds to nanodiscs stabilized by addition of nine polymer equivalents in the presence of 3 mM calcium without significant line broadening. Altogether, this work suggests that the SMA-X-based nanodiscs are a promising membrane mimetic that could be used to solve the membrane-bound tetrameric structure of dap by solution-state NMR.

Chapter 5

Conclusion and Future work

5.1 Conclusion

The first two chapters of this thesis present data suggesting that phospholipid acyl tails influence dap's ability to permeabilize membranes. Permeabilization was observed on membranes composed of myristoyl acyl tails, but not on those composed of phospholipids with palmitoyl or oleoyl acyl tails. Oleoyl acyl tails were found to inhibit dap membrane permeabilization regardless of the lipid headgroup they are ligated to. The gathered data indicate that oleoyl acyl tail inhibition correlates with increased acyl tail length rather than lipid unsaturation. Additionally, it was observed that oleoyl lipid acyls inhibit dap's pore formation even at small membrane concentrations (10 mol%). It seems that oleoyl acyl tails inhibit dap pore formation by disrupting the formation of dap octameric oligomers; on oleoyl membranes most of the dap is located on the outer membrane leaflet with tetrameric dap oligomers being observed. The inhibitory effect of cardiolipin observed by Zhang *et al.* (2014) was reconfirmed in this study.[20] In their experiments, Zhang *et al.* 2014) observed inhibition of dap pore formation on TOCL containing membranes; they argued that the observed inhibition was caused by the CL headgroup.[20] This argument was made because they were unaware of the inhibitory effects of oleoyl acyl tails on dap's action mode. In this study it observed that membranes containing TMCL, at concentrations used by Zhang *et al.* (2014), were also resistant to permeabilization by dap thereby confirming the finding by Zhang *et al.* (2014) that the CL headgroups does indeed inhibit dap's action mode.[20] It should be noted that TOCL membrane more strongly inhibit dap pore formation than TMCL containing membrane suggesting that the oleoyl acyl tails do contribute to the inhibitory effect.

The last chapter of this thesis investigated the use of styrene-maleic acid co-polymer membrane nanodiscs as membrane mimetics on which to determine dap's membrane-bound structure by solution-state NMR. It was observed that nanodiscs with a diameter sufficiently small to produce legible NMR spectra could be created from PG containing MLVs and in the presence of 3 mM calcium. The studies further showed that dap could bind to the nanodiscs and form partial tetrameric dap oligomers at 3 mM calcium. Additionally, the nanodiscs did not precipitate when treated with higher concentrations of calcium and dap. Overall, these findings show that while the SMA polymer used in this study does not allow for full dap oligomerization, the partial structure of membrane-bound dap could still be obtained with this system by solution-state NMR.

5.2 Future Work

5.2.1 Effects of branched acyl tails on dap membrane permeabilization

As mentioned earlier, bacterial cytoplasmic membranes have a significant number of phospholipids with branched acyl tails. Boudjemaa *et al*. (2018) found that bacteria resistant to dap not only increase the lengths of their lipid acyl tails, but also can alter the position of the branching.[55] Therefore it would be interesting to conduct the exact same experiments as in chapters 1 and 2 with LUVs containing branched phospholipid acyl tails and corroborate the finding of Boudjemaa *et al.* (2018).

5.2.2 Using a different SMA polymer to form membrane nanodiscs

One major drawback of the current nanodisc system is that the polymer used competes with dap for calcium; consequently, allowing for only partial dap oligomerization. The issue of partial oligomerization could possibly be overcome by making lipid nanodiscs with a polymer with no calcium chelation ability.

Bibliography

(1) Taylor, S. D.; Palmer, M. The Action Mechanism of Daptomycin. *Bioorg. Med. Chem.* **2016**, *24* (24), 6253–6268. https://doi.org/10.1016/j.bmc.2016.05.052.

(2) Debono, M.; Abbott, B. J.; Molloy, R. M.; Fukuda, D. S.; Hunt, A. H.; Daupert, V. M.; Counter, F. T.; Ott, J. L.; Carrell, C. B.; Howard, L. C. Enzymatic and Chemical Modifications of Lipopeptide Antibiotic A21978C: The Synthesis and Evaluation of Daptomycin (LY146032). *J. Antibiot. (Tokyo)* **1988**, *41* (8), 1093–1105.

(3) Müller, A.; Wenzel, M.; Strahl, H.; Grein, F.; Saaki, T. N. V.; Kohl, B.; Siersma, T.; Bandow, J. E.; Sahl, H.-G.; Schneider, T.; et al. Daptomycin Inhibits Cell Envelope Synthesis by Interfering with Fluid Membrane Microdomains. *Proc. Natl. Acad. Sci.* **2016**, *113* (45), E7077–E7086. https://doi.org/10.1073/pnas.1611173113.

(4) Lee, M.-T.; Yang, P.-Y.; Charron, N. E.; Hsieh, M.-H.; Chang, Y.-Y.; Huang, H. W. Comparison of the Effects of Daptomycin on Bacterial and Model Membranes. *Biochemistry* **2018**, *57* (38), 5629–5639. https://doi.org/10.1021/acs.biochem.8b00818.

(5) Pogliano, J.; Pogliano, N.; Silverman, J. A. Daptomycin-Mediated Reorganization of Membrane Architecture Causes Mislocalization of Essential Cell Division Proteins. *J. Bacteriol.* **2012**, *194* (17), 4494–4504. https://doi.org/10.1128/JB.00011-12.

(6) Jung, D.; Rozek, A.; Okon, M.; Hancock, R. E. W. Structural Transitions as Determinants of the Action of the Calcium-Dependent Antibiotic Daptomycin. *Chem. Biol.* **2004**, *11* (7), 949–957. https://doi.org/10.1016/j.chembiol.2004.04.020.

(7) Silverman, J. A.; Perlmutter, N. G.; Shapiro, H. M. Correlation of Daptomycin Bactericidal Activity and Membrane Depolarization in Staphylococcus Aureus. *Antimicrob. Agents Chemother.* **2003**, *47* (8), 2538–2544. https://doi.org/10.1128/AAC.47.8.2538-2544.2003.

(8) Taylor, R.; Butt, K.; Scott, B.; Zhang, T.; Muraih, J. K.; Mintzer, E.; Taylor, S.; Palmer, M. Two Successive Calcium-Dependent Transitions Mediate Membrane Binding and Oligomerization of Daptomycin and the Related Antibiotic A54145. *Biochim. Biophys. Acta BBA - Biomembr.* **2016**, *1858* (9), 1999–2005. https://doi.org/10.1016/j.bbamem.2016.05.020.

(9) Muraih, J. K.; Pearson, A.; Silverman, J.; Palmer, M. Oligomerization of Daptomycin on Membranes. *Biochim. Biophys. Acta BBA - Biomembr.* **2011**, *1808* (4), 1154–1160. https://doi.org/10.1016/j.bbamem.2011.01.001.

(10) Taylor, R. M.; Scott, B.; Taylor, S.; Palmer, M. An Acyl-Linked Dimer of Daptomycin Is Strongly Inhibited by the Bacterial Cell Wall. *ACS Infect. Dis.* **2017**, *3* (7), 462–466. https://doi.org/10.1021/acsinfecdis.7b00019.

(11) Hewelt-Belka, W.; Nakonieczna, J.; Belka, M.; Bączek, T.; Namieśnik, J.; Kot-Wasik, A. Comprehensive Methodology for Staphylococcus Aureus Lipidomics by Liquid Chromatography and Quadrupole Time-of-Flight Mass Spectrometry. *J. Chromatogr. A* **2014**, *1362* (Supplement C), 62–74. https://doi.org/10.1016/j.chroma.2014.08.020.

(12) White, D. C.; Frerman, F. E. Fatty Acid Composition of the Complex Lipids of Staphylococcus Aureus During the Formation of the Membrane-Bound Electron Transport System. *J. Bacteriol.* **1968**, *95* (6), 2198–2209.

(13) Taylor, R.; Beriashvili, D.; Taylor, S.; Palmer, M. Daptomycin Pore Formation Is Restricted by Lipid Acyl Chain Composition. *ACS Infect. Dis.* **2017**, *3* (11), 797–801. https://doi.org/10.1021/acsinfecdis.7b00138.

(14) GLYCOPEDIA http://glycopedia.eu/e-chapters/the-structure-of-bacterial-cell/article/the-bacterial-cell-wall (accessed May 4, 2019).

(15) Alborn, W. E.; Allen, N. E.; Preston, D. A. Daptomycin Disrupts Membrane Potential in Growing Staphylococcus Aureus. *Antimicrob. Agents Chemother.* **1991**, *35* (11), 2282–2287.
(16) Seydlová, G.; Sokol, A.; Lišková, P.; Konopásek, I.; Fišer, R. Daptomycin Pore Formation and Stoichiometry Depends on Membrane Potential of Target Membrane. *Antimicrob. Agents Chemother.* **2018**, AAC.01589-18. https://doi.org/10.1128/AAC.01589-18.
(17) Zhang, T.; Muraih, J. K.; MacCormick, B.; Silverman, J.; Palmer, M. Daptomycin Forms Cation- and Size-Selective Pores in Model Membranes. *Biochim. Biophys. Acta BBA - Biomembr.* **2014**, *1838* (10), 2425–2430. https://doi.org/10.1016/j.bbamem.2014.05.014.
(18) Muraih, J. K.; Palmer, M. Estimation of the Subunit Stoichiometry of the Membrane-Associated Daptomycin Oligomer by FRET. *Biochim. Biophys. Acta* **2012**, *1818* (7), 1642–1647. https://doi.org/10.1016/j.bbamem.2012.02.019.
(19) Zhang, T.; Muraih, J. K.; Mintzer, E.; Tishbi, N.; Desert, C.; Silverman, J.; Taylor, S.; Palmer, M. Mutual Inhibition through Hybrid Oligomer Formation of Daptomycin and the Semisynthetic Lipopeptide Antibiotic CB-182,462. *Biochim. Biophys. Acta BBA - Biomembr.* **2013**, *1828* (2), 302–308. https://doi.org/10.1016/j.bbamem.2012.10.008.
(20) Zhang, T.; Muraih, J. K.; Tishbi, N.; Herskowitz, J.; Victor, R. L.; Silverman, J.; Uwumarenogie, S.; Taylor, S. D.; Palmer, M.; Mintzer, E. Cardiolipin Prevents Membrane Translocation and Permeabilization by Daptomycin. *J. Biol. Chem.* **2014**, *289* (17), 11584–11591. https://doi.org/10.1074/jbc.M114.554444.
(21) Zhang, T.; Taylor, S. D.; Palmer, M.; Duhamel, J. Membrane Binding and Oligomerization of the Lipopeptide A54145 Studied by Pyrene Fluorescence. *Biophys. J.* **2016**, *111* (6), 1267–1277. https://doi.org/10.1016/j.bpj.2016.07.018.
(22) Woodworth, J. R.; Nyhart, E. H.; Brier, G. L.; Wolny, J. D.; Black, H. R. Single-Dose Pharmacokinetics and Antibacterial Activity of Daptomycin, a New Lipopeptide Antibiotic, in Healthy Volunteers. *Antimicrob. Agents Chemother.* **1992**, *36* (2), 318–325. https://doi.org/10.1128/AAC.36.2.318.
(23) Dvorchik, B. H.; Brazier, D.; DeBruin, M. F.; Arbeit, R. D. Daptomycin Pharmacokinetics and Safety Following Administration of Escalating Doses Once Daily to Healthy Subjects. *Antimicrob. Agents Chemother.* **2003**, *47* (4), 1318–1323. https://doi.org/10.1128/AAC.47.4.1318-1323.2003.
(24) Dvorchik, B.; Arbeit, R. D.; Chung, J.; Liu, S.; Knebel, W.; Kastrissios, H. Population Pharmacokinetics of Daptomycin. *Antimicrob. Agents Chemother.* **2004**, *48* (8), 2799–2807. https://doi.org/10.1128/AAC.48.8.2799-2807.2004.
(25) Cotroneo, N.; Harris, R.; Perlmutter, N.; Beveridge, T.; Silverman, J. A. Daptomycin Exerts Bactericidal Activity without Lysis of Staphylococcus Aureus. *Antimicrob. Agents Chemother.* **2008**, *52* (6), 2223–2225. https://doi.org/10.1128/AAC.01410-07.
(26) Sanchez, S. A.; Tricerri, M. A.; Gunther, G.; Gratton, E. Laurdan Generalized Polarization: From Cuvette to Microscope. 8.
(27) Lakey, J. H.; Ptak, M. Fluorescence Indicates a Calcium-Dependent Interaction between the Lipopeptide Antibiotic LY 146032 and Phospholipid Membranes. *Biochemistry* **1988**, *27* (13), 4639–4645. https://doi.org/10.1021/bi00413a009.
(28) Ventola, C. L. The Antibiotic Resistance Crisis. *Pharm. Ther.* **2015**, *40* (4), 277–283.
(29) Rubio, A.; Moore, J.; Varoglu, M.; Conrad, M.; Chu, M.; Shaw, W.; Silverman, J. A. LC-MS/MS Characterization of Phospholipid Content in Daptomycin-Susceptible and -Resistant Isolates of Staphylococcus Aureus with Mutations in MprF. *Mol. Membr. Biol.* **2012**, *29* (1), 1–8. https://doi.org/10.3109/09687688.2011.640948.
(30) Arias, C. A.; Murray, B. E. Antibiotic-Resistant Bugs in the 21st Century — A Clinical Super-Challenge. *N. Engl. J. Med.* **2009**, *360* (5), 439–443. https://doi.org/10.1056/NEJMp0804651.

(31) Castle, S. L. Remodeling Vancomycin Yields a Victory in the Battle against Bacteria. *Proc. Natl. Acad. Sci.* **2017**, *114* (26), 6656–6657. https://doi.org/10.1073/pnas.1707728114.
(32) Lee, M.-T.; Yang, P.-Y.; Charron, N. E.; Hsieh, M.-H.; Chang, Y.-Y.; Huang, H. W. Comparison of the Effects of Daptomycin on Bacterial and Model Membranes. *Biochemistry* **2018**, *57* (38), 5629–5639. https://doi.org/10.1021/acs.biochem.8b00818.
(33) Pokorny, A.; Khatib, T. O.; Stevenson, H. A Quantitative Model of Daptomycin Binding to Lipid Bilayers. *J. Phys. Chem. B* **2018**. https://doi.org/10.1021/acs.jpcb.8b07503.
(34) Slavetinsky, C. J.; Peschel, A.; Ernst, C. M. Alanyl-Phosphatidylglycerol and Lysyl-Phosphatidylglycerol Are Translocated by the Same MprF Flippases and Have Similar Capacities To Protect against the Antibiotic Daptomycin in Staphylococcus Aureus. *Antimicrob. Agents Chemother.* **2012**, *56* (7), 3492–3497. https://doi.org/10.1128/AAC.00370-12.
(35) Khatib, T. O.; Stevenson, H.; Yeaman, M. R.; Bayer, A. S.; Pokorny, A. Binding of Daptomycin to Anionic Lipid Vesicles Is Reduced in the Presence of Lysyl-Phosphatidylglycerol. *Antimicrob. Agents Chemother.* **2016**, *60* (8), 5051–5053. https://doi.org/10.1128/AAC.00744-16.
(36) Kilelee, E.; Pokorny, A.; Yeaman, M. R.; Bayer, A. S. Lysyl-Phosphatidylglycerol Attenuates Membrane Perturbation Rather than Surface Association of the Cationic Antimicrobial Peptide 6W-RP-1 in a Model Membrane System: Implications for Daptomycin Resistance. *Antimicrob. Agents Chemother.* **2010**, *54* (10), 4476–4479. https://doi.org/10.1128/AAC.00191-10.
(37) Scott, W. R. P.; Baek, S.-B.; Jung, D.; Hancock, R. E. W.; Straus, S. K. NMR Structural Studies of the Antibiotic Lipopeptide Daptomycin in DHPC Micelles. *Biochim. Biophys. Acta BBA - Biomembr.* **2007**, *1768* (12), 3116–3126. https://doi.org/10.1016/j.bbamem.2007.08.034.
(38) Barnawi, G.; Noden, M.; Taylor, R.; Lohani, C.; Beriashvili, D.; Palmer, M.; Taylor, S. D. An Entirely Fmoc Solid Phase Approach to the Synthesis of Daptomycin Analogs. *Pept. Sci.* **2019**, *111* (1), e23094. https://doi.org/10.1002/bip.23094.
(39) Moreira, R.; Barnawi, G.; Beriashvili, D.; Palmer, M.; Taylor, S. D. The Effect of Replacing the Ester Bond with an Amide Bond and of Overall Stereochemistry on the Activity of Daptomycin. *Bioorg. Med. Chem.* **2019**, *27* (1), 240–246. https://doi.org/10.1016/j.bmc.2018.12.004.
(40) Chen, Y.-F.; Sun, T.-L.; Sun, Y.; Huang, H. W. Interaction of Daptomycin with Lipid Bilayers: A Lipid Extracting Effect. *Biochemistry* **2014**, *53* (33), 5384–5392. https://doi.org/10.1021/bi500779g.
(41) Clement, N. R.; Gould, J. M. Pyranine (8-Hydroxy-1,3,6-Pyrenetrisulfonate) as a Probe of Internal Aqueous Hydrogen Ion Concentration in Phospholipid Vesicles. *Biochemistry* **1981**, *20* (6), 1534–1538. https://doi.org/10.1021/bi00509a019.
(42) Zhang, T.; Muraih, J. K.; MacCormick, B.; Silverman, J.; Palmer, M. Daptomycin Forms Cation- and Size-Selective Pores in Model Membranes. *Biochim. Biophys. Acta BBA - Biomembr.* **2014**, *1838* (10), 2425–2430. https://doi.org/10.1016/j.bbamem.2014.05.014.
(43) McKenna, C. E.; Gutheil, W. G.; Song, W. A Method for Preparing Analytically Pure Sodium Dithionite. Dithionite Quality and Observed Nitrogenase-Specific Activities. *Biochim. Biophys. Acta BBA - Gen. Subj.* **1991**, *1075* (1), 109–117. https://doi.org/10.1016/0304-4165(91)90082-R.
(44) Bigay, J.; Antonny, B. Curvature, Lipid Packing, and Electrostatics of Membrane Organelles: Defining Cellular Territories in Determining Specificity. *Dev. Cell* **2012**, *23* (5), 886–895. https://doi.org/10.1016/j.devcel.2012.10.009.
(45) Houtsmuller, U. M. T.; Deenen, L. L. M. van. On the Amino Acid Esters of Phosphatidyl Glycerol from Bacteria. *Biochim. Biophys. Acta BBA - Lipids Lipid Metab.* **1965**, *106* (3), 564–576. https://doi.org/10.1016/0005-2760(65)90072-X.

(46) Kaneda, T. Fatty Acids of the Genus Bacillus: An Example of Branched-Chain Preference. *Bacteriol. Rev.* **1977**, *41* (2), 391–418.
(47) den Kamp, J. A. F. O.; Redai, I.; van Deenen, L. L. M. Phospholipid Composition of Bacillus Subtilis. *J. Bacteriol.* **1969**, *99* (1), 298–303.
(48) Gantner, M.; Schwarzmann, G.; Sandhoff, K.; Kolter, T. Partial Synthesis of Ganglioside and Lysoganglioside Lipoforms as Internal Standards for MS Quantification. *J. Lipid Res.* **2014**, *55* (12), 2692–2704. https://doi.org/10.1194/jlr.D054734.
(49) Erdahl, W. L.; Chapman, C. J.; Taylor, R. W.; Pfeiffer, D. R. Ca2+ Transport Properties of Ionophores A23187, Ionomycin, and 4-BrA23187 in a Well Defined Model System. *Biophys. J.* **1994**, *66* (5), 1678–1693.
(50) Shinitzky, M.; Barenholz, Y. Dynamics of the Hydrocarbon Layer in Liposomes of Lecithin and Sphingomyelin Containing Dicetylphosphate. *J. Biol. Chem.* **1974**, *249* (8), 2652–2657.
(51) Philippot, J. R.; Schuber, F. *Liposomes as Tools in Basic Research and Industry*; CRC Press, 1994.
(52) Phase Transition Temperatures for Glycerophospholipids https://avantilipids.com/ (accessed May 4, 2019).
(53) Nelson, S. C.; Neeley, S. K.; Melonakos, E. D.; Bell, J. D.; Busath, D. D. Fluorescence Anisotropy of Diphenylhexatriene and Its Cationic Trimethylamino Derivative in Liquid Dipalmitoylphosphatidylcholine Liposomes: Opposing Responses to Isoflurane. *BMC Biophys.* **2012**, *5*, 5. https://doi.org/10.1186/2046-1682-5-5.
(54) Hines, K. M.; Waalkes, A.; Penewit, K.; Holmes, E. A.; Salipante, S. J.; Werth, B. J.; Xu, L. Characterization of the Mechanisms of Daptomycin Resistance among Gram-Positive Bacterial Pathogens by Multidimensional Lipidomics. *mSphere* **2017**, *2* (6). https://doi.org/10.1128/mSphere.00492-17.
(55) Boudjemaa, R.; Cabriel, C.; Dubois-Brissonnet, F.; Bourg, N.; Dupuis, G.; Gruss, A.; Lévêque-Fort, S.; Briandet, R.; Fontaine-Aupart, M.-P.; Steenkeste, K. Impact of Bacterial Membrane Fatty Acid Composition on the Failure of Daptomycin To Kill Staphylococcus Aureus. *Antimicrob. Agents Chemother.* **2018**, *62* (7). https://doi.org/10.1128/AAC.00023-18.
(56) Piazza, M. NMR Studies of Protein and Peptide Structure and Dynamics. **2016**.
(57) Beriashvili, D.; Taylor, R.; Kralt, B.; Abu Mazen, N.; Taylor, S. D.; Palmer, M. Mechanistic Studies on the Effect of Membrane Lipid Acyl Chain Composition on Daptomycin Pore Formation. *Chem. Phys. Lipids* **2018**, *216*, 73–79. https://doi.org/10.1016/j.chemphyslip.2018.09.015.
(58) Esmaili, M.; Overduin, M. Membrane Biology Visualized in Nanometer-Sized Discs Formed by Styrene Maleic Acid Polymers. *Biochim. Biophys. Acta BBA - Biomembr.* **2018**, *1860* (2), 257–263. https://doi.org/10.1016/j.bbamem.2017.10.019.
(59) Nucci, N. V.; Valentine, K. G.; Wand, A. J. High-Resolution NMR Spectroscopy of Encapsulated Proteins Dissolved in Low-Viscosity Fluids. *J. Magn. Reson. San Diego Calif 1997* **2014**, *241*, 137–147. https://doi.org/10.1016/j.jmr.2013.10.006.
(60) Rule, G. S.; Hitchens, T. K. *Fundamentals of Protein NMR Spectroscopy*; Focus on Structural Biology; Springer Netherlands, 2006.
(61) Keeler, J. *Understanding NMR Spectroscopy*; John Wiley & Sons, 2011.
(62) Dodevski, I.; Nucci, N. V.; Valentine, K. G.; Sidhu, G. K.; O'Brien, E. S.; Pardi, A.; Wand, A. J. Optimized Reverse Micelle Surfactant System for High-Resolution NMR Spectroscopy of Encapsulated Proteins and Nucleic Acids Dissolved in Low Viscosity Fluids. *J. Am. Chem. Soc.* **2014**, *136* (9), 3465–3474. https://doi.org/10.1021/ja410716w.
(63) Jamshad, M.; Grimard, V.; Idini, I.; Knowles, T. J.; Dowle, M. R.; Schofield, N.; Sridhar, P.; Lin, Y.; Finka, R.; Wheatley, M.; et al. Structural Analysis of a Nanoparticle Containing a Lipid

Bilayer Used for Detergent-Free Extraction of Membrane Proteins. *Nano Res.* **2015**, *8* (3), 774–789. https://doi.org/10.1007/s12274-014-0560-6.
(64) Knowles, T. J.; Finka, R.; Smith, C.; Lin, Y.-P.; Dafforn, T.; Overduin, M. Membrane Proteins Solubilized Intact in Lipid Containing Nanoparticles Bounded by Styrene Maleic Acid Copolymer. *J. Am. Chem. Soc.* **2009**, *131* (22), 7484–7485. https://doi.org/10.1021/ja810046q.
(65) Scheidelaar, S.; Koorengevel, M. C.; Pardo, J. D.; Meeldijk, J. D.; Breukink, E.; Killian, J. A. Molecular Model for the Solubilization of Membranes into Nanodisks by Styrene Maleic Acid Copolymers. *Biophys. J.* **2015**, *108* (2), 279–290. https://doi.org/10.1016/j.bpj.2014.11.3464.
(66) Smith, A. A. A.; Autzen, H. E.; Laursen, T.; Wu, V.; Yen, M.; Hall, A.; Hansen, S. D.; Cheng, Y.; Xu, T. Controlling Styrene Maleic Acid Lipid Particles through RAFT. *Biomacromolecules* **2017**, *18* (11), 3706–3713. https://doi.org/10.1021/acs.biomac.7b01136.
(67) Arenas, R. C.; Klingler, J.; Vargas, C.; Keller, S. Influence of Lipid Bilayer Properties on Nanodisc Formation Mediated by Styrene/Maleic Acid Copolymers. *Nanoscale* **2016**, *8* (32), 15016–15026. https://doi.org/10.1039/C6NR02089E.
(68) Craig, A. F.; Clark, E. E.; Sahu, I. D.; Zhang, R.; Frantz, N. D.; Al-Abdul-Wahid, M. S.; Dabney-Smith, C.; Konkolewicz, D.; Lorigan, G. A. Tuning the Size of Styrene-Maleic Acid Copolymer-Lipid Nanoparticles (SMALPs) Using RAFT Polymerization for Biophysical Studies. *Biochim. Biophys. Acta BBA - Biomembr.* **2016**, *1858* (11), 2931–2939. https://doi.org/10.1016/j.bbamem.2016.08.004.
(69) Hall, S. C. L.; Tognoloni, C.; Price, G. J.; Klumperman, B.; Edler, K. J.; Dafforn, T. R.; Arnold, T. Influence of Poly(Styrene-Co-Maleic Acid) Copolymer Structure on the Properties and Self-Assembly of SMALP Nanodiscs. *Biomacromolecules* **2018**, *19* (3), 761–772. https://doi.org/10.1021/acs.biomac.7b01539.
(70) Scheidelaar, S.; Koorengevel, M. C.; van Walree, C. A.; Dominguez, J. J.; Dörr, J. M.; Killian, J. A. Effect of Polymer Composition and PH on Membrane Solubilization by Styrene-Maleic Acid Copolymers. *Biophys. J.* **2016**, *111* (9), 1974–1986. https://doi.org/10.1016/j.bpj.2016.09.025.
(71) Szoka, F.; Papahadjopoulos, D. Comparative Properties and Methods of Preparation of Lipid Vesicles (Liposomes). *Annu. Rev. Biophys. Bioeng.* **1980**, *9* (1), 467–508. https://doi.org/10.1146/annurev.bb.09.060180.002343.
(72) Ravula, T.; Ramadugu, S. K.; Di Mauro, G.; Ramamoorthy, A. Bioinspired, Size-Tunable Self-Assembly of Polymer–Lipid Bilayer Nanodiscs. *Angew. Chem. Int. Ed.* **2017**, *56* (38), 11466–11470. https://doi.org/10.1002/anie.201705569.
(73) Paulin, S.; Jamshad, M.; Dafforn, T. R.; Garcia-Lara, J.; Foster, S. J.; Galley, N. F.; Roper, D. I.; Rosado, H.; Taylor, P. W. Surfactant-Free Purification of Membrane Protein Complexes from Bacteria: Application to the Staphylococcal Penicillin-Binding Protein Complex PBP2/PBP2a. *Nanotechnology* **2014**, *25* (28), 285101. https://doi.org/10.1088/0957-4484/25/28/285101.
(74) Puthenveetil, R.; Nguyen, K.; Vinogradova, O. Nanodiscs and Solution NMR: Preparation, Application and Challenges. *Nanotechnol. Rev.* **2017**, *6* (1), 111–126. https://doi.org/10.1515/ntrev-2016-0076.
(75) Cullis, P. R.; De Kruyff, B.; Richards, R. E. Factors Affecting the Motion of the Polar Headgroup in Phospholipid Bilayers. A 31P NMR Study of Unsonicated Phosphatidylcholine Liposomes. *Biochim. Biophys. Acta BBA - Biomembr.* **1976**, *426* (3), 433–446. https://doi.org/10.1016/0005-2736(76)90388-6.
(76) Voet, D.; Voet, J. G. *Biochemistry*; Wiley, 2004.

(77) Macdonald, P. M.; Seelig, J. Calcium Binding to Mixed Phosphatidylglycerol-Phosphatidylcholine Bilayers as Studied by Deuterium Nuclear Magnetic Resonance. *Biochemistry* **1987**, *26* (5), 1231–1240. https://doi.org/10.1021/bi00379a005.
(78) Stegmann, T.; Schoen, P.; Bron, R.; Wey, J.; Bartoldus, I.; Ortiz, A.; Nieva, J. L.; Wilschut, J. Evaluation of Viral Membrane Fusion Assays. Comparison of the Octadecylrhodamine Dequenching Assay with the Pyrene Excimer Assay. *Biochemistry* **1993**, *32* (42), 11330–11337.
(79) Hammarström, P.; Kalman, B.; Jonsson, B.-H.; Carlsson, U. Pyrene Excimer Fluorescence as a Proximity Probe for Investigation of Residual Structure in the Unfolded State of Human Carbonic Anhydrase II. *FEBS Lett.* **1997**, *420* (1), 63–68. https://doi.org/10.1016/S0014-5793(97)01488-9.
(80) Galla, H.-J.; Sackmann, E. Lateral Diffusion in the Hydrophobic Region of Membranes: Use of Pyrene Excimers as Optical Probes. *Biochim. Biophys. Acta BBA - Biomembr.* **1974**, *339* (1), 103–115. https://doi.org/10.1016/0005-2736(74)90336-8.
(81) Redpath, A. E. C.; Pekcan, Ö.; Winnik, M. A. The Quenching of Alkyl Pyrene Fluorescence by Atactic and Isotactic Polystyrene. *J. Photochem.* **1983**, *23* (2), 283–288. https://doi.org/10.1016/0047-2670(83)80070-7.
(82) McLaughlin, A. C.; Cullis, P. R.; Berden, J. A.; Richards, R. E. 31P NMR of Phospholipid Membranes: Effects of Chemical and Anisotropy at High Magnetic Field Strengths. *J. Magn. Reson. 1969* **1975**, *20* (1), 146–165. https://doi.org/10.1016/0022-2364(75)90162-6.
(83) Cullis, P. R.; de Kruyff, B. 31P NMR Studies of Unsonicated Aqueous Dispersions of Neutral and Acidic Phospholipids. Effects of Phase Transitions, P2H and Divalent Cations on the Motion in the Phosphate Region of the Polar Headgroup. *Biochim. Biophys. Acta BBA - Biomembr.* **1976**, *436* (3), 523–540. https://doi.org/10.1016/0005-2736(76)90438-7.
(84) Danielczak, B.; Meister, A.; Keller, S. Influence of Mg2+ and Ca2+ on Nanodisc Formation by Diisobutylene/Maleic Acid (DIBMA) Copolymer. *Chem. Phys. Lipids* **2019**. https://doi.org/10.1016/j.chemphyslip.2019.03.004.
(85) Mishra, N. N.; Bayer, A. S.; Tran, T. T.; Shamoo, Y.; Mileykovskaya, E.; Dowhan, W.; Guan, Z.; Arias, C. A. Daptomycin Resistance in Enterococci Is Associated with Distinct Alterations of Cell Membrane Phospholipid Content. *PloS One* **2012**, *7* (8), e43958. https://doi.org/10.1371/journal.pone.0043958.

Appendix A

Figure 1. HPLC trace of NBD-dap - section 2.2.1

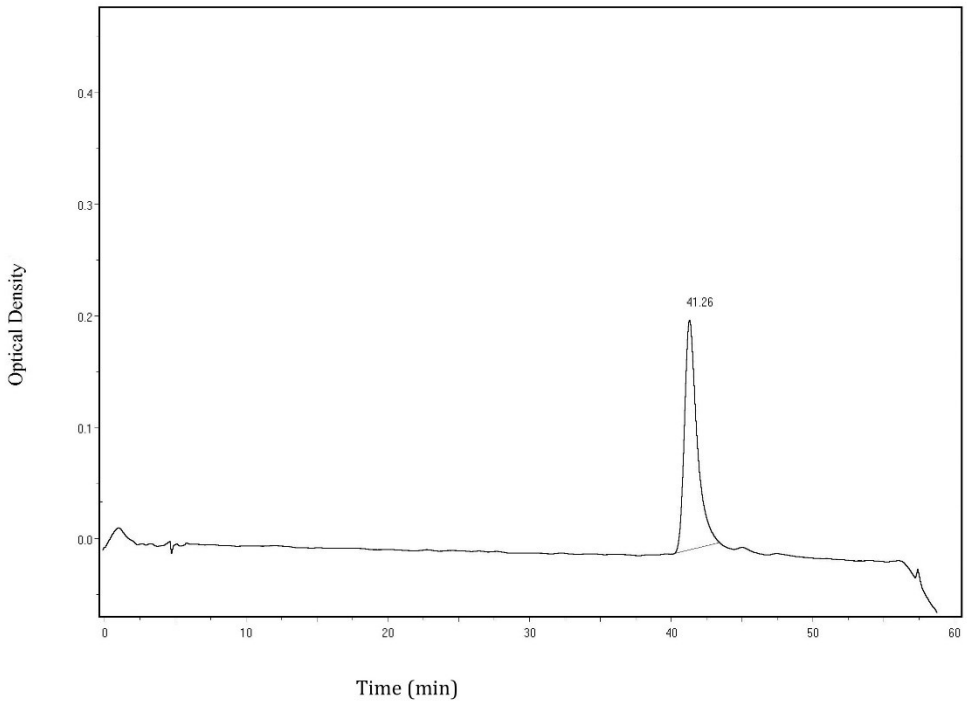

Figure 2. High resolution MS of NBD-dap -section 2.2.1

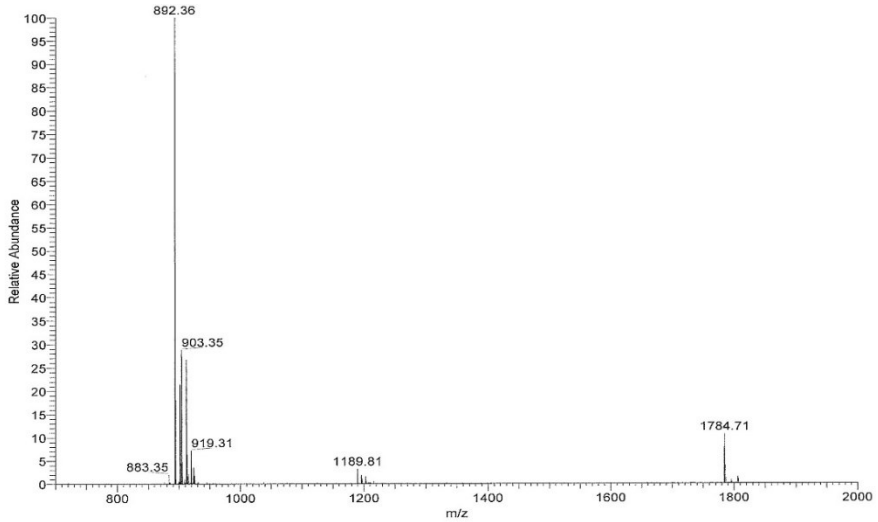

Figure 3. Dithionite quenching of NBD-PE on POPC: POPG LUVs

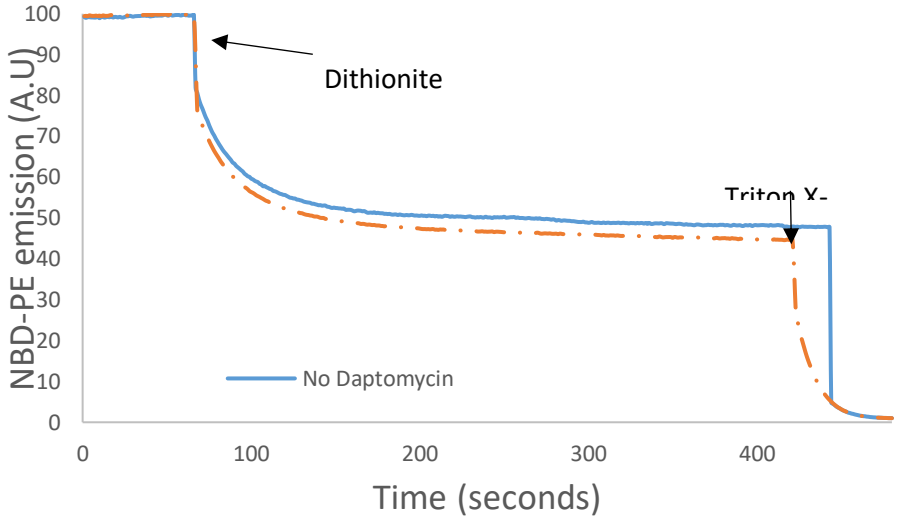

Figure 4. Dithionite quenching of NBD-PE on DOPC: DOPG LUVs

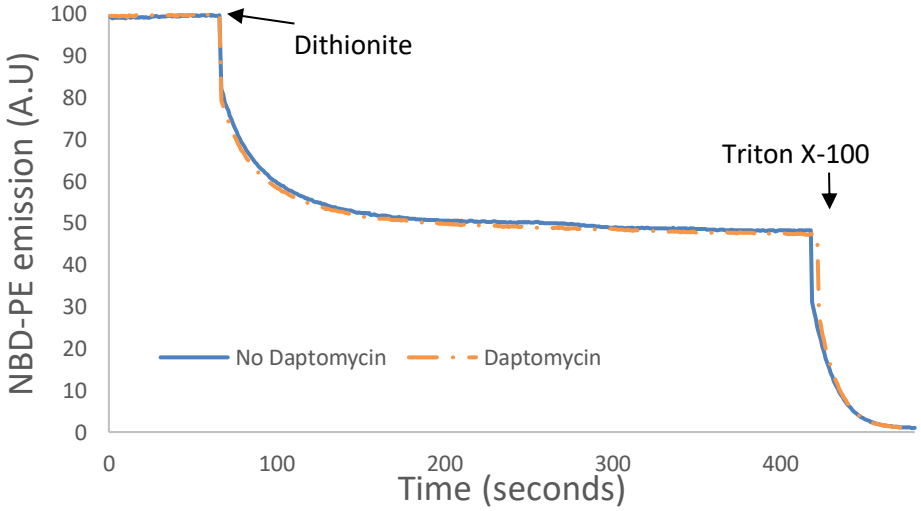

To make sure that dap could not enter the intra-LUV space via dap's pore 0.5 % mol/mol NBD-PE was incorporated into liposomes containing either equal parts POPC: POPG or DOPC: DOPG. 250 µM of one type of LUV was incubated for 3 minutes. Fluorescence acquisition of the NBD signal was at 520 nm (excitation 478 nm) was began and then dithionite (1 mM) was added. The experiment was repeated the same way for dap containing traces; in those cases, 2 µM dap and 25 mM calcium were added to the LUV sample and incubated for 3 minutes before starting data acquisition. 0.1% Triton X-100 was added to solubilize the liposomes. The experiments were done at 37ºC. Overall, dithionite does not enter the intra-LUV space of neither PO (Figure 3) and DO (Figure 4) containing liposomes. Refer to section 2.3.3.

Figure 5. Gram-positive bacteria cytoplasmic membrane composition.

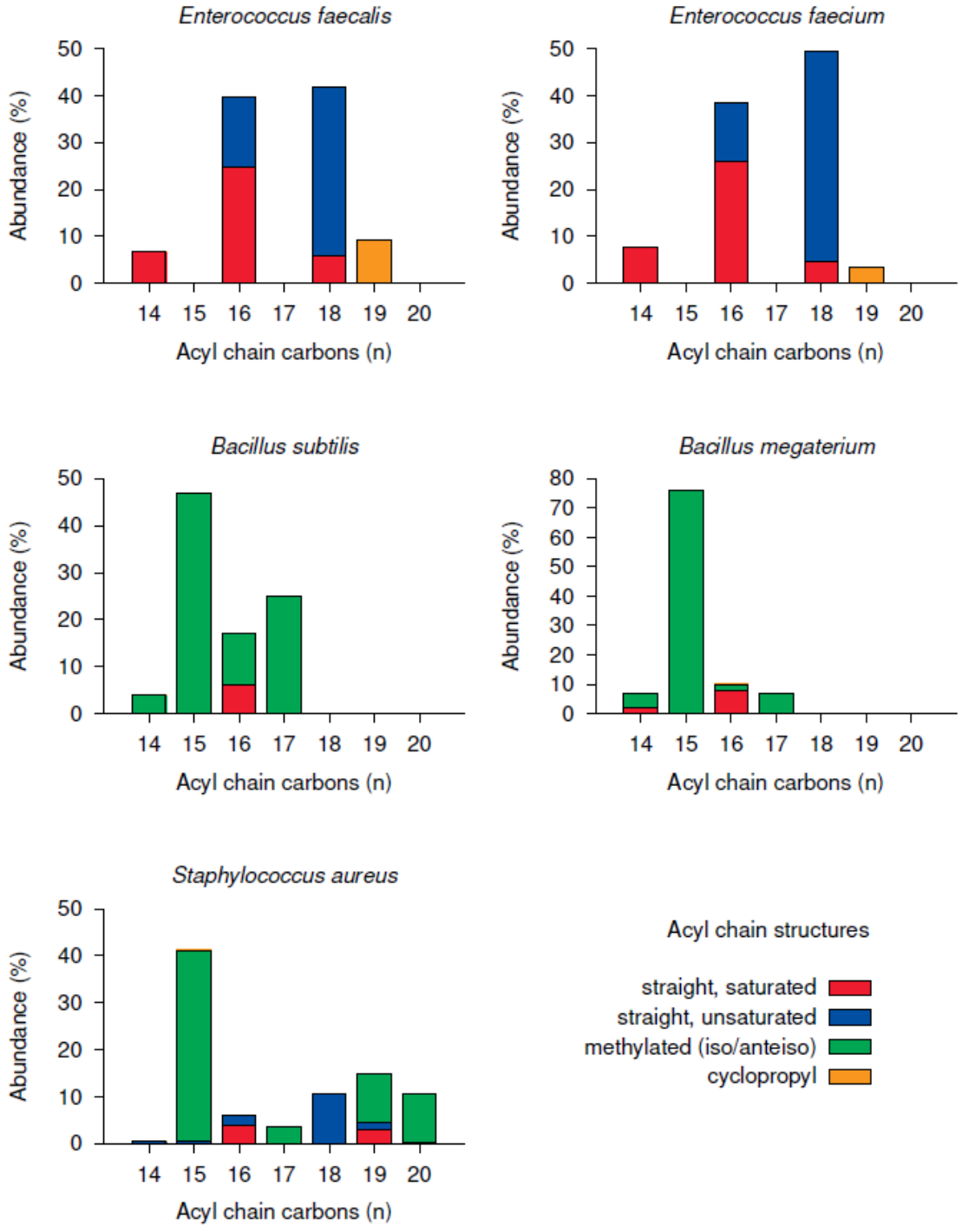

The figure shows a literature overview of the wide variety of phospholipid acyl tails found in the cytoplasmic membranes of Gram-positive bacteria susceptible to treatment by dap.[12,45–47,85]

Appendix B

Figure 1. HPLC trace of NBD-dap - section 3.2.1

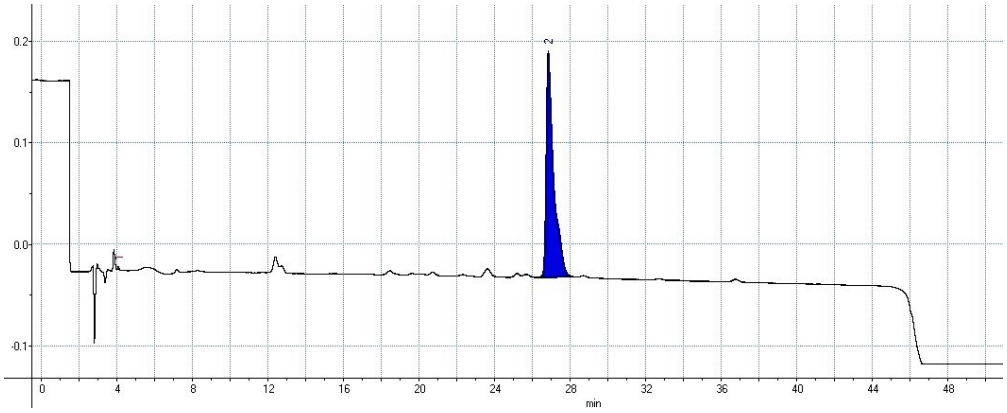

Figure 2. High resolution MS of NBD-dap – section 3.2.1

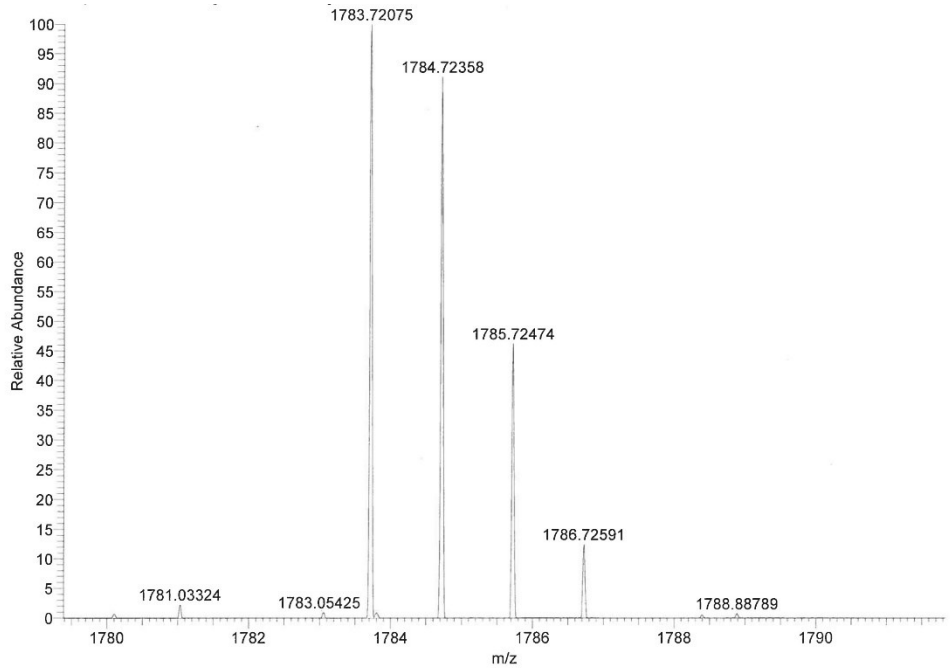

Figure 3. HPLC trace of C_{14}-dap - section 3.2.2

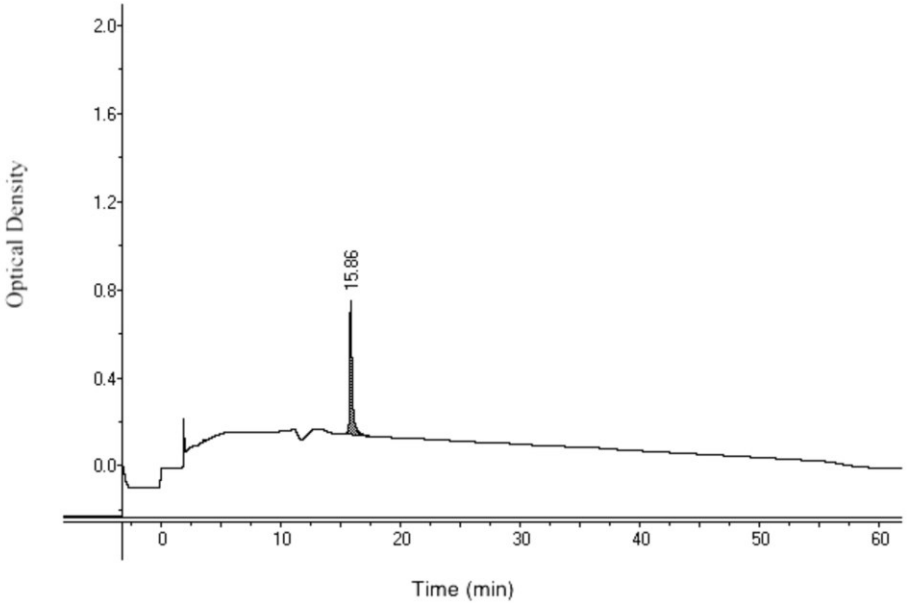

Figure 4. High resolution MS of C_{14}-dap - section 3.2.2

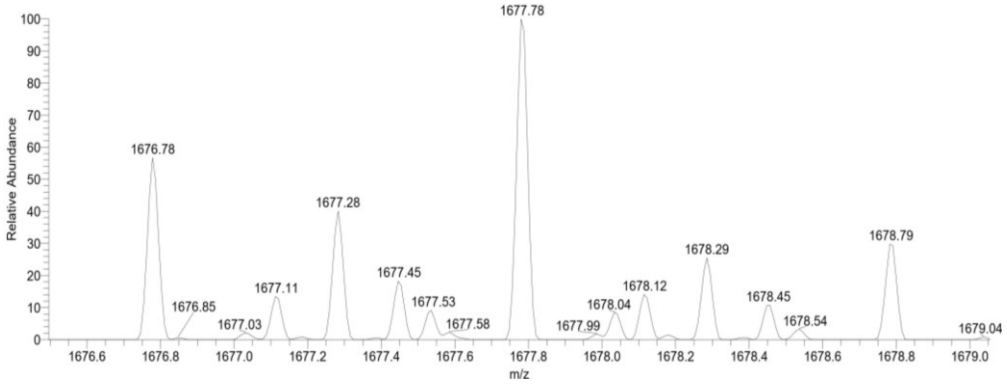

Figure 5. HPLC trance of ante C_{12}-dap - section 3.2.3

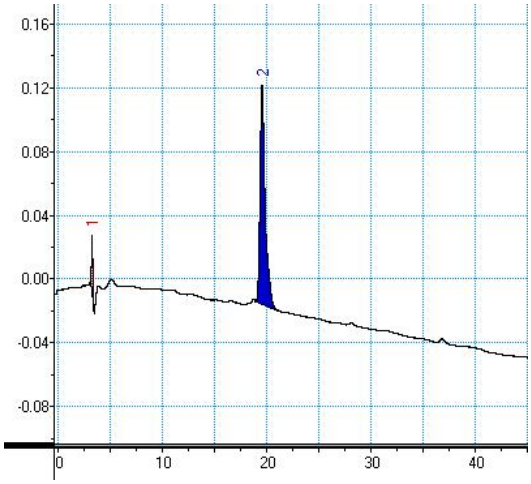

Figure 6. High resolution MS of ante C_{12}-dap - section 3.2.3

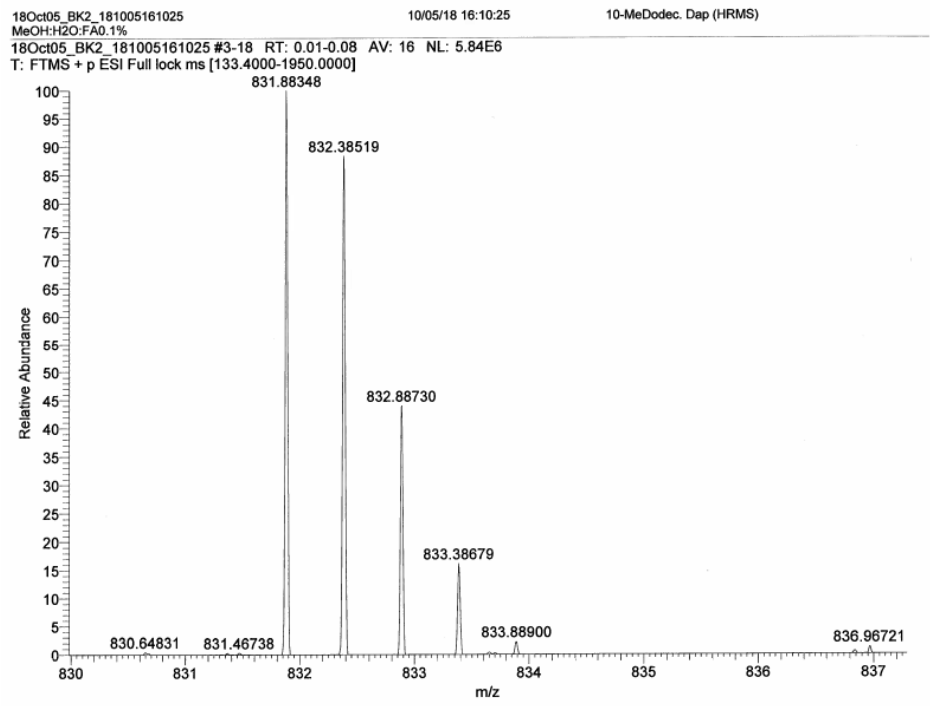

Figure 7. DPH anisotropy membrane fluidity assay

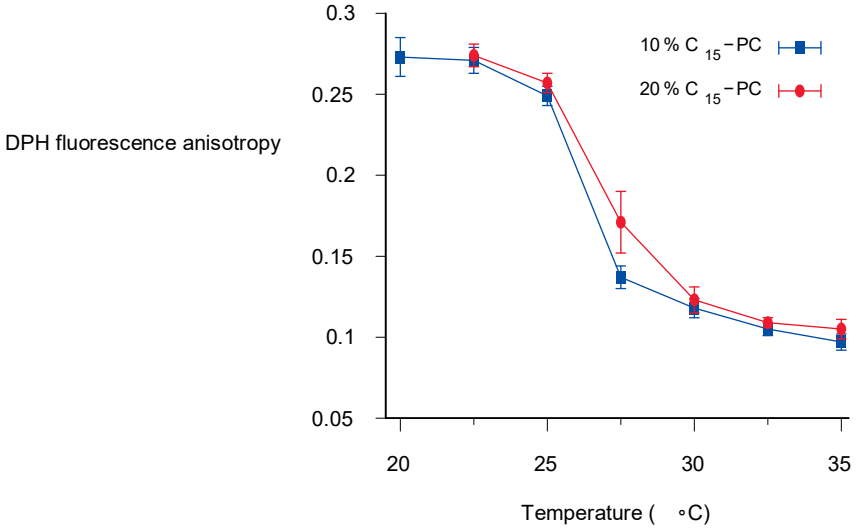

DPH membrane phase transition assay. The phase transition temperature of membrane can be determined by using the fluorescent probe DPH; due to its hydrophobic nature DPH inserts into membranes and as the membrane transitions from the gel phase to the liquid crystalline the fluorescence anisotropy of DPH decreases. This data can then be used to discern the phase transition temperature of the membrane. Figure 7. shows that liposomes containing up to 20% DPDPC reach the fluid state by 32.5ºC. Refer to section 3.3.5.

Appendix C

Figure 1. Dependence of ^{31}P NMR signal intensity on lipid concentration

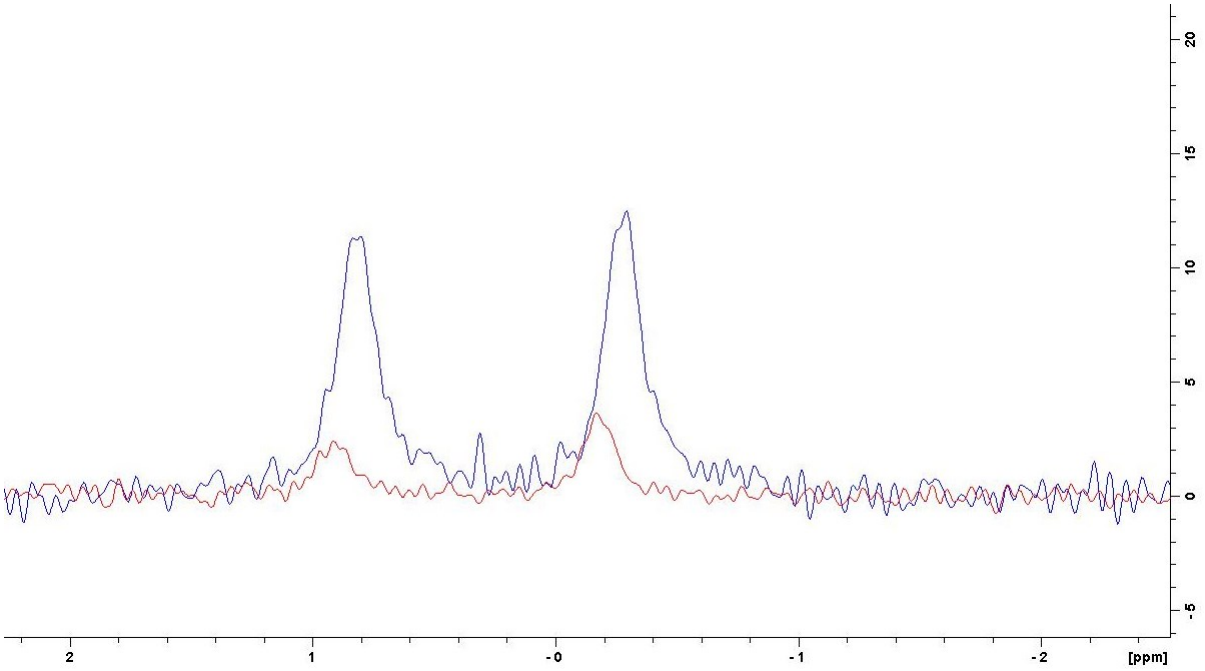

The red line is from a sample containing 1.25 mM equal part DMPG: DMPC containing nanodiscs stabilized by addition of nine polymer equivalents. The red line is from a sample containing 5 mM equal part DMPG: DMPC containing nanodiscs stabilized by addition of nine polymer equivalents. The 5 mM samples were used because better signal intensity could be obtained with a shorter acquisition time. Refer to section 4.2.3.

Figure 2. Schematic of a SMA stabilized nanodisc

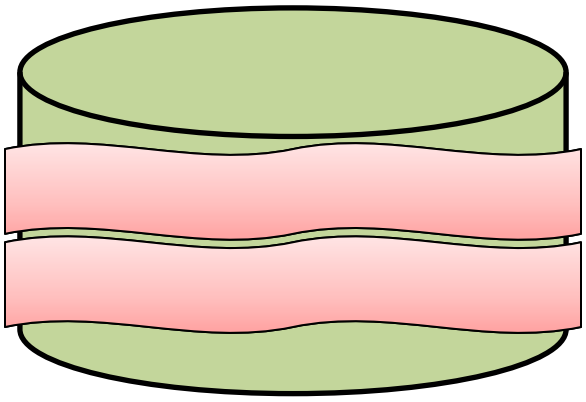

The green cylinder represents the lipid bilayer and the pink bands represent the SMA polymer enveloping the lipid bilayer.

Appendix D

Figure 1. Structure of dap derivatives.

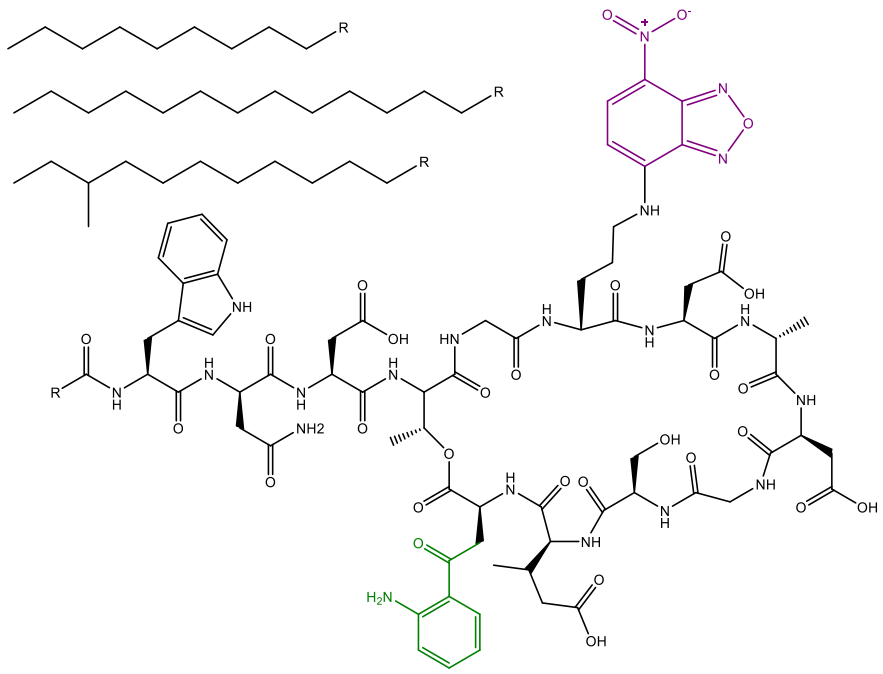

Daptomycin possess a decanoyl moiety. C_{14}-dap has the decanoyl moiety replace with a myristic acyl tail. NBD-dap has an NBD attached (magenta) at the ornithine-6. Kynurenine, whose fluorescence is polarity sensitive is highlighted in green. The anteiso-dodecanoyl dap derivative has the decanoyl moiety replaced with an anteiso-dodecanoyl moiety.

Figure 2. Structures of Lipids

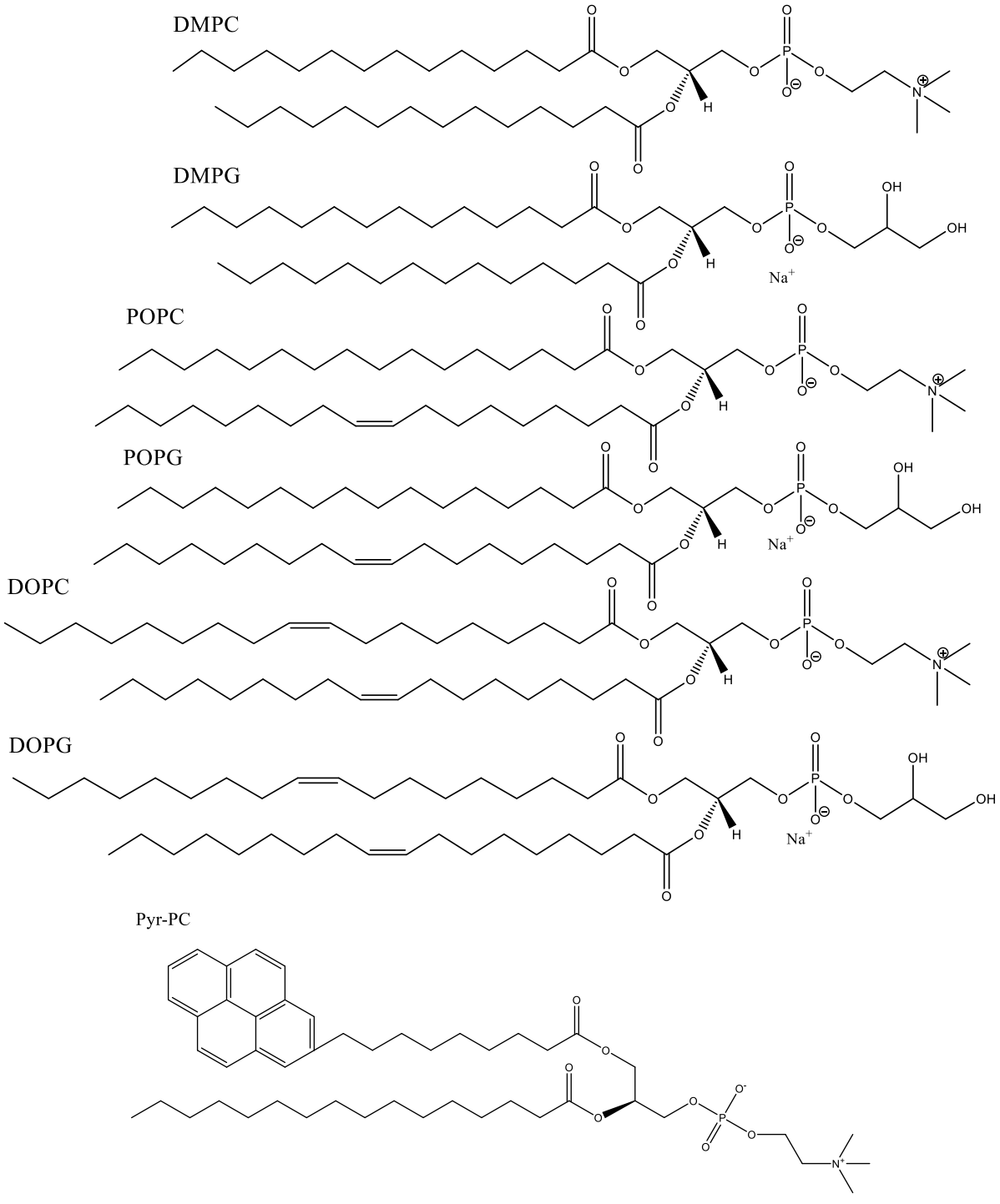

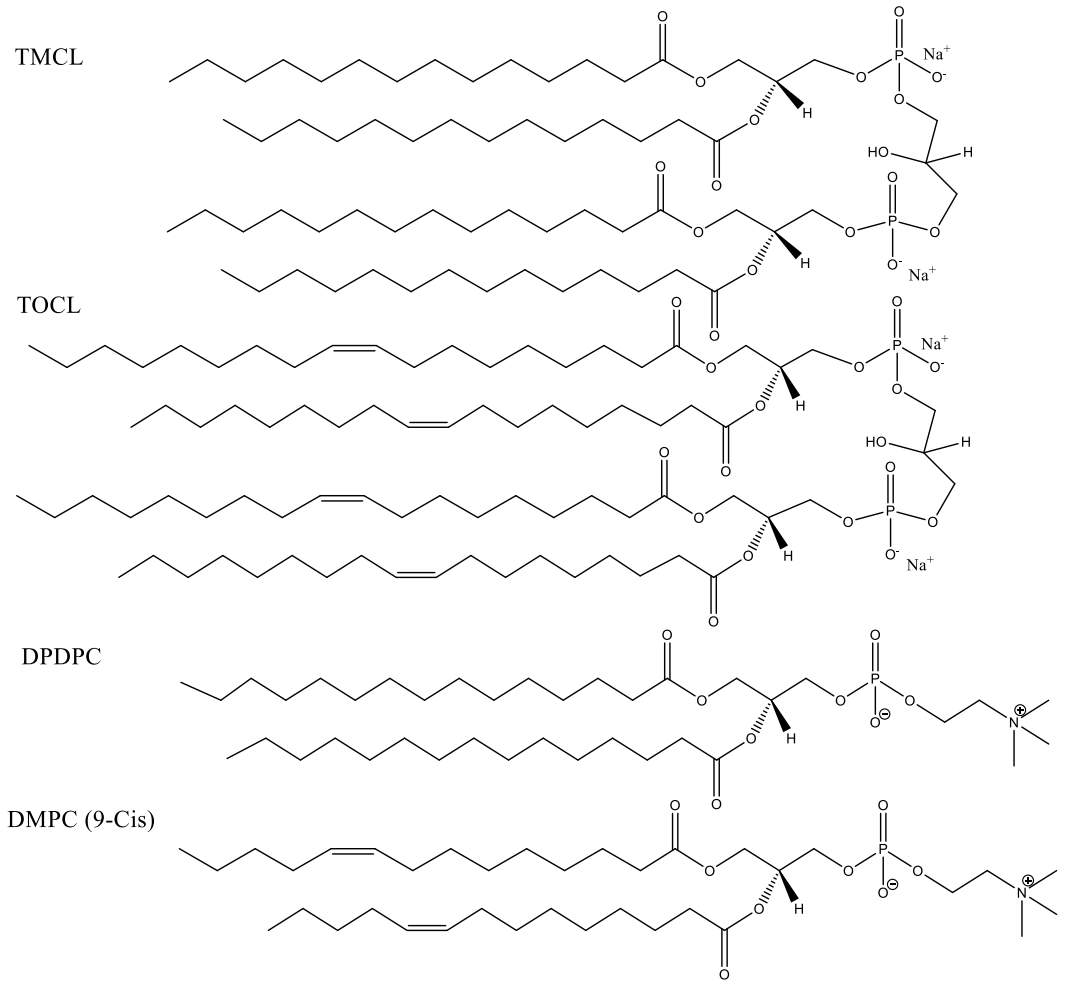

The structures of all lipids used in this study with their acronym:1,2-dimyristoyl-sn-glycero-3-phosphocholine (DMPC), 1,2-dimyristoleoyl-sn-glycero-3-phosphocholine (DMPC Δ9-cis), 1,2-Dimyristoyl-sn-glycero-3-phosphoglycerol (DMPG), 1,2-dioleoyl-sn-glycero-3-phosphocholine (DOPC),1,2-dioleoyl-sn-glycero-3-phospho-(1'-rac-glycerol) (DOPG), 1,2-dipentadecanoyl-sn-glycero-3-phosphocholine (DPDPC), 1-palmitoyl-2-oleoyl-sn-glycero-3-phosphocholine (POPC), 1-palmitoyl-2-oleoyl-sn-glycero-3-phospho-(1'-rac-glycerol) (POPG), , 1-palmitoyl-2-pyrenedecanoyl phosphatidylcholine (pyr-PC), 1',3'-bis[1,2-dimyristoyl-sn-glycero-3-phospho]-glycerol (TMCL), and 1',3'-bis[1,2-dioleoyl-sn-glycero-3-phospho]-glycerol (TOCL).